Studies on Mechanisms of Enhanced Virulence of Oncogenic Marek's Disease Virus

(腫瘍原性マレック病ウイルスの病原性増強機構に関する研究)

Jumpei SATO

CONTENTS

ABBREVIATIONS

A	alanine
AP-1	activator protein-1
APC	allophycocyanin
BAC	bacterial artificial chromosome
BALT	bronchus-associated lymphoid tissue
bcl-2	B-cell lymphoma-2
BP	biological processes
CC	cellular components
cDNA	complementary DNA
CEFs	chicken embryo fibroblasts
cox	cyclooxygenase
D	aspartic acid
DAB	3,3'-Diaminobenzidine Tetrahydrochloride
dpi	days post-infection
E	glutamic acid
EBNA	EBV nuclear antigen
EBV	Epstein–Barr virus
FACS	fluorescence-activated cell sorting
FFE	feather follicle epithelium
FITC	fluorescein isothiocyanate
gB	glycoprotein B
gI	glycoprotein I
GO	Gene Ontology
HSV	herpes simplex virus
i-nos	inducible nitric oxide synthase
icp4	infected-cell protein 4
IFN- γ	interferon-gamma
IHC	immunohistochemical
IRL	internal repeat long
IRS	internal repeat short
K	lysine
KSHV	Kaposi’s sarcoma-associated herpesvirus
L-Meq	long isoform of Meq
mMDV	mild MDV

mAbs	monoclonal antibodies
MD	Marek’s disease
MDV	Marek’s disease virus
MERE	Meq response element
MF	molecular functions
MHC	major histocompatibility complex
mTGF-β	membrane-bound transforming growth factor-β
NK	natural killer
ORFs	open reading frames
PBMCs	peripheral blood mononuclear cells
PBS	phosphate-buffered saline
PD-1	programmed death-1
PD-L1	programmed death-ligand 1
PE	phycoerythrin
PE-Cy7	PE-Cyanine7
PerCP-Cy5.5	PerCP-Cyanine5.5
PFU	plaque-forming units
PGE_2	prostaglandin E_2
pp14	phosphoprotein14
pp38	phosphoprotein38
PRR	proline-rich repeat
RFLP	restriction fragment length polymorphism
rMDV	recombinant Marek’s disease virus
RNA-seq	RNA sequencing
S	serine
S-Meq	short isoform of Meq
SDS-PAGE	sodium dodecyl sulfate-polyacrylamide gel electrophoresis
STING	stimulator of interferon genes
TCR	T-cell receptor
TPM	transcripts per million
Treg	regulatory T
TRL	terminal repeat long
TRS	terminal repeat short
UL	unique long
US	unique short
vMDV	virulent MDV

vvMDV	very virulent MDV
vv+MDV	very virulent plus MDV
Y	tyrosine
ZIP	leucine zipper
γδ	gamma-delta

NOTES

The contents of Chapter I have been published in *Microbiology Spectrum*.

Sato J, Murata S, Motai Y, Win SY, Seo H, Yamagami S, Maekawa N, Okagawa T, Konnai S, Ohashi K. Amino-acid insertion in the Meq protein of Marek's disease virus, an avian oncogenic herpesvirus, accelerates tumorigenesis. *Microbiol Spectr*. 13, e0336824, 2025.

The contents of Chapter II have been published in *Viruses* and are under consideration for publication in *Virology Journal*.

Sato J, Motai Y, Yamagami S, Kurokawa A, Win SY, Horio F, Saeki H, Maekawa N, Okagawa T, Konnai S, Ohashi K, Murata S. Amino acid polymorphisms in the basic region of Meq of vaccine strain CVI988 drastically diminish the virulence of Marek's disease virus. *Viruses* 17, 907, 2025.

Sato J, Kurokawa A, Motai Y, Yamagami S, Win SY, Horio F, Saeki H, Maekawa N, Okagawa T, Kaufer BB, Osterrieder N, Parcells MS, Konnai S, Ohashi K, Murata S. Two distinct polymorphisms in the basic region of Meq protein of Marek's disease virus alter pathological progression and clinical manifestations. *Virol J.* Sep 26;22(1):303. 2025.

The contents of Chapter III have been published in *Pathogens*.

Sato J, Motai Y, Yamagami S, Win SY, Horio F, Saeki H, Maekawa N, Okagawa T, Konnai S, Ohashi K, Murata S. Programmed cell death-1 expression in T-cell subsets in chickens infected with Marek's disease virus. *Pathogens* 14, 431, 2025.

PREFACE

Marek's disease virus (MDV) is an oncogenic avian herpesvirus. Marek's disease (MD) is characterized by malignant lymphomas, immunosuppression, ocular and cerebral inflammation, and peripheral neurological symptoms such as leg paralysis and torticollis (Churchill and Biggs, 1968; Gimeno *et al.*, 2001; Bacon *et al.*, 2001; Faiz *et al.*, 2017). Since MD was first described as generalized polyneuritis in chickens by Hungarian veterinarian József Marek in 1907 (Marek, 1907), MD has caused substantial economic losses in the poultry industry. Although current live-attenuated vaccines have significantly reduced the number of MD onset (Schat, 2016), they primarily suppress clinical signs but fail to block infection and transmission (Read *et al.*, 2015). Notably, highly virulent strains have been shown to shed higher amounts of virus into the environment, suggesting that vaccine-driven selection may contribute to the emergence of more virulent variants (Read *et al.*, 2015). As a result of ongoing evolution, MDV virulence has been currently categorized into four pathotypes based on its ability to cause clinical signs in vaccinated chickens: mild (m), virulent (v), very virulent (vv), and very virulent plus (vv+) (Witter *et al.,* 2005). Furthermore, sporadic outbreaks still continue to be reported worldwide, even in vaccinated flocks (Kozdruń *et al.*, 2020; Chacón *et al.*, 2024; Patria *et al*., 2024). In Asian countries, recent field isolates have also exhibited high virulence (Teng *et al.*, 2022; Wannaratana *et al.*, 2025). These findings highlight growing concerns regarding the increase in MDV virulence and the decline in the effectiveness of vaccines available, posing a critical threat to poultry health and sustainability of the industry.

MDV is taxonomically assigned to an alphaherpesvirus (subfamily *Alphaherpesvirinae*, genus *Mardivirus*, species *Gallid alphaherpesvirus 2*) (Fukuchi *et al.*, 1984), and accordingly, its genome shares structural features typical of other alphaherpesviruses (Tulman *et al.*, 2000). The MDV genome consists of unique long (UL) and unique short (US) regions, each flanked by inverted repeats: the UL region is bordered by terminal repeat long (TRL) and internal repeat long (IRL), whereas the US region is flanked by internal repeat short (IRS) and terminal repeat short (TRS). Despite these conserved genomic characteristics, MDV displays biological features that are more similar to those of lymphotropic oncogenic gammaherpesviruses such as Epstein–Barr virus (EBV) and Kaposi's sarcoma-associated herpesvirus (KSHV). The pathogenic process of MDV has been conceptualized in the "Cornell model of MDV infection" (Calnek, 2001) (Fig. 1). According to this model, chickens are primarily infected by inhaling cell-free MDV particles within the contaminated dust or dander, which enter the

respiratory tract and initially infect macrophages and B cells residing in the lungs (Abdul-Careem *et al.*, 2009; Baaten *et al.*, 2009). Infected macrophages subsequently deliver the virus to regional lymphoid organs such as the thymus, bursa of Fabricius, and spleen (Calnek, 2001; Barrow *et al.*, 2003; Abdul-Careem *et al.,* 2008). Within these tissues, MDV undergoes cytolytic replication in B cells, T cells, and natural killer (NK) cells, causing transient atrophy of these organs and immunosuppression during early infection stages (Morimura *et al.,* 1996; Berthault *et al*., 2018; Bertzbach *et al.*, 2019). MDV later establishes latency in $CD4^+$ T cells, and a few of these latently infected cells are transformed, leading to aggressive lymphoma development (Nair, 2013). Most tumor tissues found in MD are predominantly composed of clonally or oligoclonally expanded $CD4^+$ T cells (Burgess and Davison, 2002; Mwangi *et al.*, 2011). Furthermore, latently infected T cells migrate to epithelial tissues, where the feather follicle epithelium (FFE) cells are infected with MDV (Baigent *et al.,* 2013; Bavananthasivam *et al*., 2022). The cell-free viral particles produced in the FFE cells are subsequently shed into the environment with dander and dust, facilitating transmission to other naïve individuals.

MDV infection elicits both innate and adaptive immune responses in chickens. Because MDV is a highly cell-associated virus that produces infectious particles exclusively in the FFE cells, cell-mediated immunity is essential for controlling the disease progression. In general, $CD8^+$ T cells play a pivotal role in anti-viral immunity by inducing apoptosis in virus-infected cells and expressing interferon-gamma (IFN-γ). Notably, several studies have shown that $CD8^+$ T cells recognizing MDV antigens such as Meq, phosphoprotein38 (pp38), glycoprotein B (gB), and glycoprotein I (gI) exhibit cytotoxic functions (Markowski-Grimsrud and Schat, 2002; Boodhoo and Behboudi, 2022b). Supporting the importance of these cells in the control of MD, depletion of $CD8^+$ T cells by administration of anti-chicken CD8 antibodies led to increased tumor incidence and reduced vaccine efficacy in MDV-infected chickens (Umthong *et al.*, 2020). Furthermore, booster immunization with the attenuated vaccine strain CVI988 induces rapid $CD8^+$ T cell proliferation and cytokine production, suggesting that memory $CD8^+$ T cells significantly contribute to vaccine-induced protection (Hao *et al.*, 2021).

Gamma-delta (γδ) T cells are also believed to play a crucial role in immunity against MDV. In chickens, γδ T cells constitute the predominant T cell subset among both circulating and tissue-resident lymphocytes (Meijerink *et al.,* 2021). Unlike conventional αβ T cells, γδ T cells recognize a broad spectrum of peptides and non-peptide antigens derived from stressed or infected cells in an major histocompatibility complex (MHC)-independent manner, enabling rapid innate-like immune responses (Bonneville *et al.*, 2010). Experimental infection has demonstrated that γδ T cell-deficient chickens showed

increased mortality after MDV infection, supporting their protective role (Sabsabi *et al.,* 2024). Moreover, vaccination with the CVI988 strain promotes early expansion of IFN-γ-producing γδ T cells in the lung, spleen, and skin (Matsuyama-Kato *et al*., 2022). Additionally, adoptive transfer of peripheral blood mononuclear cells (PBMCs) activated by anti-chicken γδ T-cell receptor (TCR) antibodies significantly reduces tumor development following MDV challenge (Matsuyama-Kato *et al.,* 2023b).

MDV infection induces robust immune responses; however, the virus has evolved several mechanisms to evade host immunity. For example, MDV-transformed cells have been reported to exhibit the phenotype of regulatory T (Treg) cells, characterized by the expression of membrane-bound transforming growth factor-β (mTGF-β) (Gurung *et al.,* 2017). The transformed cells also secrete prostaglandin E_2 (PGE_2), which inhibits T cell proliferation (Kamble *et al.*, 2021). Furthermore, MDV may induce immunosuppression mediated by immune checkpoint molecules such as programmed death-1 (PD-1) and its ligand, programmed death-ligand 1 (PD-L1). The mRNA expression of *pd-1* is elevated during the early lytic phase, whereas *pd-l1* mRNA expression is upregulated during the latency. Moreover, mRNA expressions of both molecules are abundantly expressed in MDV-induced tumor tissues (Matsuyama-Kato *et al.*, 2012). Immunosuppressive mechanisms via the PD-1/PD-L1 pathway have been documented in other herpesviruses. In herpes simplex virus (HSV) infection, virus-specific $CD8^+$ T cells exhibit elevated PD-1 expression, which is associated with diminished effector function (Srivastava *et al.,* 2016). In addition, high expression of PD-L1 has been observed in EBV-positive tumor cells (Lee and Oh, 2024). The expression patterns of PD-1 and PD-L1 on virus-specific $CD8^+$ T cells and cells transformed by herpesvirus suggest immune evasion via T cell exhaustion; however, it remains unclear whether the PD-1/PD-L1 pathway directly contributes to immunosuppression in the context of MDV infection.

MDV harbors a unique oncogene, *meq*, which encodes a 339-amino-acid protein, Meq, and *meq* is expressed during both the lytic and latent stages of infection (Jones *et al.*, 1992; Liu and Kung, 2000). Experimental infection using recombinant MDV (rMDV) lacking *meq* has demonstrated that the deletion of *meq* abolishes its ability to induce lymphomas in chickens, highlighting the indispensable role of Meq in MDV-mediated oncogenesis (Lupiani *et al.*, 2004). Structurally, Meq is a basic leucine zipper (ZIP) transcription factor that regulates the expressions of various viral and host genes associated with the disease progression (Fig. 2). The N-terminal region of Meq comprises a basic region involved in DNA binding and subcellular localization to the nucleus and nucleolus (Liu *et al.*, 1997). The ZIP domain, located adjacent to the basic region, enables homodimerization or heterodimerization with activator protein-1 (AP-1) transcription

factors such as c-Jun, JunB, and Fos, resembling the activity of viral oncoproteins Jun and Fos (Qian *et al.*, 1995). Homodimers of Meq have been shown to repress the promoter activities of *pp38* and *pp14* genes, both of which are lytic antigens of MDV, thereby contributing to the establishment of latency. In contrast, Meq/c-Jun heterodimers have been reported to activate the *meq* promoter as well as the promoters of genes associated with the disease progression (Levy *et al.*, 2003). The C-terminal region contains a transactivation domain characterized by proline-rich repeat (PRR) sequences. The transactivation domain is essential for the transcriptional activity of Meq; deletion of this domain significantly impairs its ability to activate transcription (Qian *et al*., 1995). The tumor suppressor protein WT-1 contains similar PRR sequences, which show strong transcriptional repression (Gessler *et al.*, 1990). The PRR sequences of Meq also exhibit transcriptional repression when the C-terminal 33 amino acids of Meq are deleted (Qian *et al.,* 1995). Moreover, some prolines present in the PRRs of Meq in recent field strains with high virulence are commonly substituted with other amino acid residues (Shamblin *et al.*, 2004; Murata *et al.*, 2013). Based on these findings, it was proposed that the number of PRRs is inversely correlated with MDV virulence. In DF-1, a chicken fibroblast cell line, transformed by Meq, downstream target genes of the v-Jun pathway, including *jtap-1*, *jac*, and *hb-egf*, are activated. In addition, Meq enhances the expression of anti-apoptotic genes, such as *B-cell lymphoma-2* (*bcl-2*) and *ski*, and suppresses the expression of pro-apoptotic factors, such as *dap5* and *fas*, supporting its role in cell survival (Levy *et al.*, 2005). Furthermore, Meq interacts with host tumor suppressors and immune sensors such as p53 and stimulator of interferon genes (STING) and has the potential to inhibit their functions, thereby facilitating both tumorigenesis and immune evasion (Deng *et al*., 2010; Li *et al*., 2020). Collectively, Meq exerts pleiotropic effects by targeting multiple cellular pathways involved in oncogenesis and immune regulation.

Polymorphisms in Meq are shared among field strains according to their pathotypes (Table 1) (Shamblin *et al.*, 2004). Differences in amino acid sequences in Meq have been shown to influence the transactivation activity, and the introduction of amino acid substitutions into Meq has shown to alter its transactivation activity (Ajithdoss *et al*., 2009; Murata *et al.*, 2011, 2013). Furthermore, experimental infection using rMDVs encoding Meq derived from MDV strains with different pathotypes demonstrated that the amino acid sequence of Meq is highly associated with MDV virulence. In this experiment, rMDVs expressing Meq from vv/vv+MDV strains induced higher virulence compared to those expressing Meq from m/v MDV strains (Conradie *et al.*, 2020). Furthermore, the amino acid sequence of Meq influences the cellular composition of MDV-induced tumor tissues (Kumar *et al.*, 2012). These findings suggest a potent association between

polymorphisms in Meq and MDV virulence; therefore, the key polymorphisms affecting the virulence and their molecular mechanisms are warranted.

In particular, characteristic polymorphisms are commonly observed in the basic region and PRRs in Meq of vv/vv+MDV strains isolated in the US (Table 1; Shamblin *et al.*, 2004). Regarding the polymorphisms in the basic region, vvMDV strains, such as RB-1B and MD-5, and vv+MDV strains, such as N and New, possess alanine (A) at position 71, lysine (K) at position 77, and aspartic acid (D) at position 80 in the basic region. In contrast, the combination of serine (S) and glutamic acid (E) at positions 71 and 77 was found in ancient MDV strains obtained from 19th-century chicken remains as well as in m/vMDV strains isolated in the 1960s (Shamblin *et al*., 2004; Fiddaman *et al.*, 2023). Furthermore, several vMDV strains, such as 567 and 617A, harbor glutamic acid (E) and tyrosine (Y) at positions 77 and 80, respectively. Thus, polymorphisms in the basic region appear to be involved in MDV virulence. However, the amino acid sequences in the basic region of Meq in low-virulence vMDV strains from the US (77E and 80Y) has been observed in Meq in recent isolates from Asia, including Japan, and highly virulent strains from Europe and Nigeria (Trimpert *et al.,* 2017; Patria *et al*., 2024; Yamagami *et al*., 2025). The polymorphisms in the basic region, which is responsible for binding to genomic DNA (Liu and Kung, 2000), are presumed to affect Meq function and MDV virulence; however, their impact has not yet been evaluated.

In highly virulent strains in the US and recent isolates in Asia, the second prolines of the four consecutive prolines present in PRRs are frequently substituted with other amino acids (Table 1) (Shamblin *et al.*, 2004; Yu *et al*., 2013; Teng *et al.*, 2022). PRRs are thought to be involved in the transcriptional regulation; therefore, these amino acid substitutions are reminiscent of changes in the transcriptome regulated by Meq and their impact on the pathogenicity. In addition to polymorphisms, insertions and deletions in the transactivation domain of Meq have been identified in various field strains. A short isoform of Meq (S-Meq), characterized by a deletion of 41 or more amino acids, has recently been identified in virulent MDV strains from Asia and Europe (Wajid *et al.*, 2013; Mescolini *et al*., 2019; Murata *et al*., 2021; Ghalyanchilangeroudi *et al.*, 2022; Motai *et al*., 2024). In contrast, a long isoform of Meq (L-Meq) containing a 59/60-amino-acid insertion in the transactivation domain has been detected in the vaccine strain CVI988, as well as in low-virulent field strains such as JM and BC-1 isolated in the US during the 1960s (Lee *et al*., 2000a; Shamblin *et al*., 2004). This insertion encodes PRR sequences, possibly arising from domain duplication (Spatz *et al.,* 2007). The increased number of PRRs due to the insertion observed in L-Meq was initially hypothesized to be a factor contributing to low virulence. However, subsequent studies revealed that pathogenic field

strains from Australia and Brazil also encode L-Meq (Renz *et al.*, 2012; Chacón *et al*., 2024). Intriguingly, in contrast to the previously proposed theory that an increase in the number of PRRs is a factor in low virulence, experimental infection have demonstrated that the insertion in Meq enhances the virulence of MDV (Conradie *et al*., 2019; Sato *et al.*, 2022), but the mechanisms by which this insertion increases the virulence remain unknown.

This study aimed to elucidate the mechanisms underlying the enhanced virulence of MDV by focusing on the differences in amino acid sequences of Meq. In Chapter I, the impact of insertion in the transactivation domain of Meq on its protein function and viral pathogenesis was investigated. In Chapter II, the effects of polymorphisms in the basic region of Meq on virulence were examined by the experimental infections using rMDVs with the combination of amino acid sequences at positions 71 and 77 found in the vaccine strain CVI988, or amino acid sequences at positions 77 and 80 identified in recent field isolates. Furthermore, in Chapter III, to elucidate the mechanisms of immunosuppression in MD pathogenesis, the involvement of PD-1 expression in MD-developed chickens was examined by analyzing the functions of $CD8^+$ T cells and γδ T cells. This study provides novel insights into the mechanisms by which MDV virulence is enhanced and could contribute to the development of improved strategies to control MD.

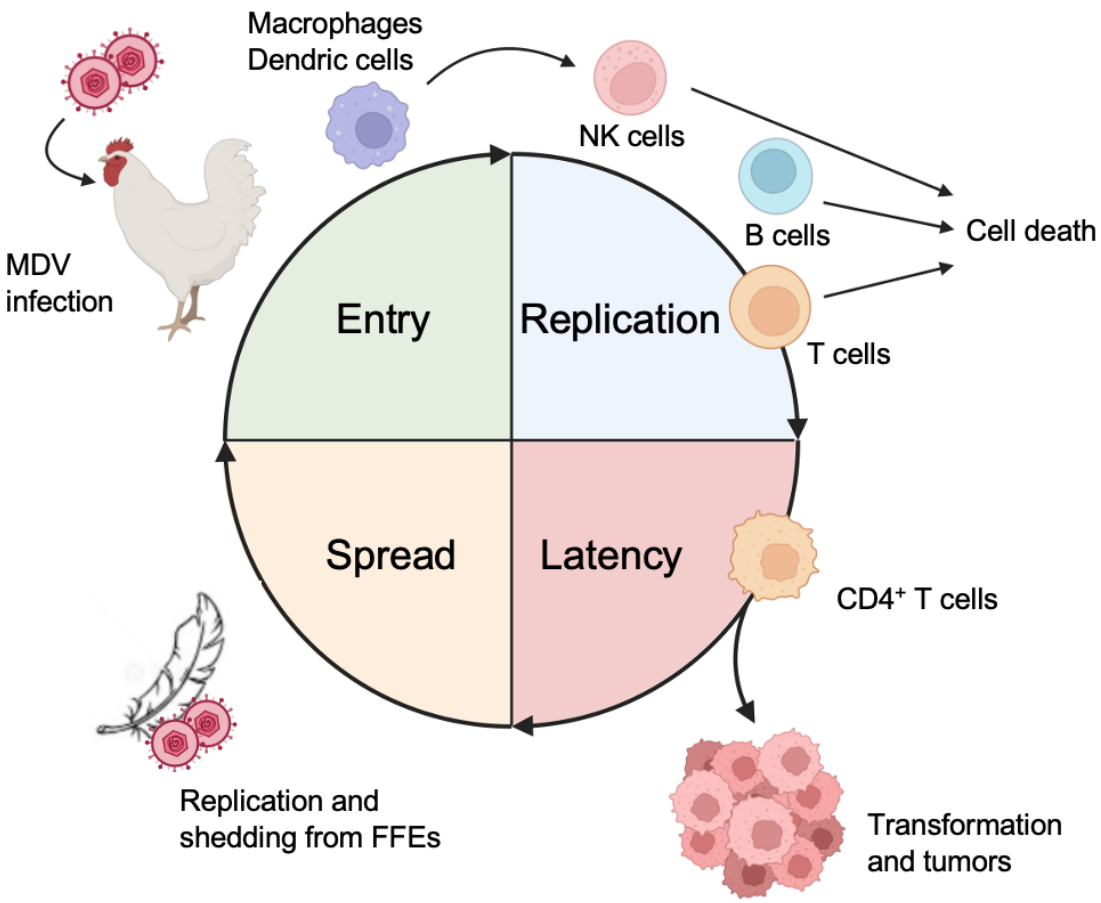

Figure 1. Schematic representation of the "Cornell model of MDV infection"
MDV infection is initiated through the inhalation of infectious dust. Following entry, mononuclear phagocytes, such as macrophages and dendritic cells, transport the virus to lymphoid organs, including the spleen, thymus, and bursa of Fabiricius, where lytic replication occurs in lymphocytes. MDV subsequently establishes latency in $CD4^+$ T cells. These latently infected T cells mediate viral dissemination to the skin and feather follicle epithelium, where cell-free MDV is produced. Furthermore, MDV can transform latently infected T cells, ultimately leading to the development of fatal lymphomas (Adopted from Bertzbach *et al.,* 2020).

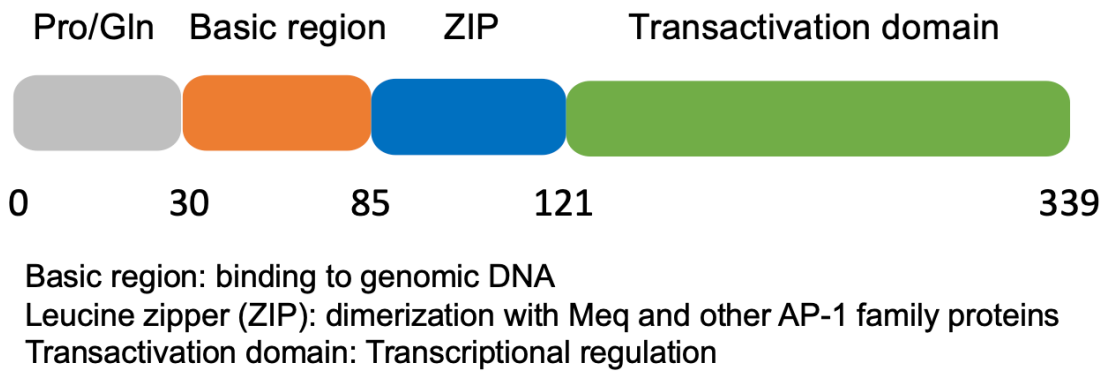

Figure 2. Schematic representation of the structure of Meq protein

Meq comprises a proline/glutamine (Pro/Gln) rich domain followed by a basic region (BR) and leucine zipper (ZIP) at the N-terminal region and a transactivation domain at the C-terminal region.

Table 1. Comparison of the amino acid sequences of Meq in various Marek's disease virus strains.

Strain	Accession No.	Virulence	Country	Position				
				71	77	80	176/217/276	285/326/386
648a	AY362725	vv+	US	A	K	D	A	T
Md5	AY243438	vv	US	A	K	D	A	T
RB-1B	AY243332	vv	US	A	K	D	P	T
BC-1[a]	AY362707	v	US	S	A	D	P	T
Jm[a]	AY243331	v	US	S	A	D	P	T
CVI988[a]	AY243333-8	m	Netherlands	S	E	D	P	I
C12/130	FJ436097	hv	UK	A	E	Y	P	T
HN302	0P897489	vv	China	A	E	Y	A	T
567	AY362709	v	US	A	E	Y	A	T
LEC-LG	OR592064	N.D.	Nigeria	A	E	Y	A	T
Iraq3A[b]	KC243262	N.D.	Iraq	A	E	Y	A	T
855/17[b]	MK139678	N.D.	Italy	A	E	Y	P	T

Adopted from Murata et al., 2020;Yu et al., 2013; Shamblin *et al*., 2004. m, mild MDV; v, virulent MDV; vv, very virulent MDV; vv+, very virulent plus MDV; hv, hypervirulent MDV N.D., Not determined.

a: Strains contain a 59-amino-acid insertion sequence in the transactivation domain

b: Strains contain a 41-amino-acid deletion sequence in the transactivation domain

CHAPTER I

Insertion in the transactivation domain of Meq oncoprotein of Marek's disease virus accelerates tumorigenesis by enhancing its protein stability and transactivation activity

INTRODUCTION

MD is currently controlled using attenuated live vaccines. However, the virulence of field strains of MDV has continued to increase, leading to outbreaks of MD even in vaccinated flocks worldwide. The amino acid sequences of Meq, a major oncoprotein of MDV, vary among MDV strains, depending on their pathotypes (Shamblin *et al.*, 2004). Indeed, experimental infections using rMDVs have demonstrated that differences in the amino acid sequences of Meq influence MDV virulence (Conradie *et al.*, 2020; Sato *et al*., 2022). These findings strongly suggest an association between mutations in Meq and enhanced virulence of MDV field isolates. However, it remains unclear which regions of Meq are responsible for the increased virulence, or how variations in the amino acid sequences of Meq cause differences in MDV virulence.

The attenuated vaccine strain CVI988, developed through serial passages of a low-virulent MDV isolate derived from a seropositive but asymptomatic chicken, currently serves as the global gold-standard vaccine against MD (Rispens *et al*., 1972). CVI988 is a viral strain comprising heterogeneous subpopulations, including at least two subpopulations encoding the 339-amino-acid Meq protein (CVI988-Meq), and the 398/399-amino-acid L-Meq protein (CVI988-L-Meq) (Chang *et al*., 2002). CVI988-L-Meq contains a 59/60-amino-acid insertion in the transactivation domain of CVI988-Meq, resulting in an increase in the number of PRRs. (Lee *et al.*, 2000a; Spatz *et al*., 2007). L-Meq was also identified in low-virulent field isolates from the US (Shamblin *et al.*, 2004), leading to the hypothesis that L-Meq is associated with low virulence. However, this notion was challenged by the subsequent discovery that L-Meq was detected in some recent pathogenic strains (Renz *et al.*, 2012; Wajid *et al.*, 2015; Chacón *et al.*, 2024). Furthermore, experimental infections using the RB-1B-based rMDVs revealed that rMDV encoding CVI988-L-Meq exhibited equivalent or greater virulence than rMDV encoding RB-1B-Meq, although rMDV encoding CVI988-Meq failed to induce clinical signs such as lymphomas or neurologic disorders (Conradie *et al.*, 2019). Compared with the amino acid sequence of Meq of the RB-1B strain, both Meq isoforms in CVI988 differ in three amino acid sequences at positions 71, 77, and 326 (385/386 in CVI988-L-Meq): alanine (A), lysine (K), and threonine (T) in RB-1B-Meq, and serine (S), glutamic acid (D), and isoleucine (I) in the Meq isoforms in CVI988 (Table 1) (Lee *et al*., 2000a). The virulence of rMDV encoding the mutant CVI988-L-Meq, whose amino acid sequence was identical to that of RB-1B-Meq except for the insertion, was significantly increased (Sato *et al.*, 2022). Thus, the insertion in the transactivation domain of Meq contributes to the increased virulence; however, the underlying mechanisms remain unclear.

In this chapter, to clarify the role of the insertion in Meq in the increased virulence of MDV, the impact of insertion on the protein function of Meq, T cell responses in infected chickens, and characteristics of tumor tissues were examined. The effects of insertion in Meq on the protein stability and transcriptional activity were assessed *in vitro*. In addition, the dynamics of tumor cells and major T-cell subsets, as well as the cellular composition and transcriptomic landscape in tumor tissues, in chickens infected with the rMDV encoding mutant CVI988-L-Meq were evaluated.

MATERIALS AND METHODS

Ethics statement

All animal experiments were approved by the Institutional Animal Care and Use Committee of Hokkaido University (Approval Number: 22-0088). All experiments were performed following the relevant guidelines and regulations of the Faculty of Veterinary Medicine of Hokkaido University, which is fully accredited by the Association for Assessment and Accreditation of Laboratory Animal Care International.

Cells

Chicken embryo fibroblasts (CEFs) were isolated from 10-day-old fertilized eggs (Iwamura Hatchery Co. Ltd., Shibata, Japan). Chicken embryos were trypsinized twice for 15 minutes. After the cell suspension was washed with Eagle's minimal essential medium (Nissui Pharmaceutical Co., Ltd., Tokyo, Japan), CEFs were maintained in Eagle's Minimum Essential Medium supplemented with 10% tryptose phosphate broth (Difco Laboratories, Detroit, MI, USA), 0.03% L-glutamine, 100 U/mL penicillin, 100 μg/mL streptomycin, 10% calf serum (Sigma-Aldrich, St. Louis, MO, USA), and 0.1% sodium bicarbonate. DF-1, a continuous chicken fibroblast cell line, was maintained in Dulbecco's Modified Eagle's Medium (FUJIFILM Wako Pure Chemical Corporation, Osaka, Japan) supplemented with 0.03% L-glutamine, 100 U/mL penicillin, 100 μg/mL streptomycin, and 10% fetal bovine serum (MP Biomedicals, Santa Ana, CA, USA). CEFs and DF-1 cells were incubated in a humidified atmosphere containing 5% CO_2 at 37°C and 39 °C, respectively.

Plasmids

Expression plasmids encoding CVI988-L-Meq and RB-1B-Meq were constructed. The open reading frames (ORFs) of L-*meq* from the CVI988 strain (GenBank accession number: AF493555) and *meq* of the RB-1B strain (accession number: HM488349.1) were amplified by PCR using primers containing EcoRI or NotI restriction sites at their 5′ ends. Following digestion with EcoRI (New England Biolabs Inc., MA, USA) and NotI (Toyobo Co., Ltd., Osaka, Japan), the PCR product was ligated into the pCI-neo expression vector (Promega, Madison, WI, USA).

To match the amino acid sequence of CVI988-L-Meq with that of RB-1B-Meq except for the insertion in the transactivation domain, site-directed mutagenesis was employed to introduce amino acid substitutions at positions 71, 77, and 386. The mutations were introduced using the primers listed in Table I-1. The resulting construct

was designated L-Meq (RB-1B). For reporter assays, a c-Jun expression plasmid was constructed (Okada *et al.*, 2007). Additionally, luciferase reporter plasmids containing the promoter regions of *pp38*, *pp14*, *infected-cell protein 4* (*icp4*), *gb*, chicken *cd30*, and chicken *bcl-2* were constructed by inserting each promoter upstream of the firefly luciferase gene in the pGL3-Basic vector (Promega) using the primers listed in Table I-2 The pRL-TK *Renilla* luciferase plasmid (Promega) was utilized as an internal control.

Dual-luciferase reporter assay

DF-1 cells were seeded at 2.0×10^5 cells per well in 24-well plates and incubated for 24 hours at 39 °C with 5% CO_2. For reporter assays using the *icp4*, *gb*, chicken *cd30*, and chicken *bcl-2* promoters, each well was transfected with 300 ng of Meq or L-Meq expression plasmid, 200 ng of c-Jun expression plasmid, 500 ng of reporter plasmid, and 5 ng of the internal control plasmid pRL-TK, using Lipofectamine 2000 (Thermo Fisher Scientific, Waltham, MA, USA) according to the manufacturer's protocol. For assays using the *pp38* and *pp14* promoters, DF-1 cells were transfected with 300 ng of Meq or L-Meq expression plasmid, 500 ng of the reporter plasmid, and 5 ng of pRL-TK. At 24 hours post-transfection, cells were lysed using 1× Passive Lysis Buffer (Promega, Madison, WI, USA). Luciferase activity was quantified with the Dual-Luciferase Reporter Assay System (Promega) on a Luminescencer-JNR AB-2100 luminometer (Atto Corp., Tokyo, Japan). Firefly luciferase activity was normalized to *Renilla* luciferase activity, and the results were expressed relative to those from cells transfected with the empty pCI-neo vector. Three independent experiments were conducted in triplicate. Protein expression levels of each Meq isoform were verified by western blotting in all reporter assays.

Protein stability assay

DF-1 cells were seeded at 2.0×10^5 cells per well in 24-well plates and incubated for 24 hours. Transfections were performed using 150 ng of Meq or L-Meq expression plasmid per well and Lipofectamine 2000 (Thermo Fisher Scientific) following the manufacturer's instructions. At 24 hours post-transfection, cycloheximide (Sigma-Aldrich) was added at a final concentration of 100 μg/mL to inhibit protein synthesis. Cells were collected at 0, 3, 6, 9, 12, and 24 hours after cycloheximide treatment and lysed in Laemmli sample buffer (Bio-Rad, Hercules, CA, USA) containing 5% 2-mercaptoethanol (Sigma-Aldrich).

Western blotting

For western blotting analysis, anti-Meq rabbit polyclonal antiserum was generated by immunizing a rabbit with a synthetic peptide corresponding to amino acid residues between positions 292–309 of RB-1B-Meq, which are conserved among most MDV strains. Protein samples were denatured by heating at 99 °C for 5 minutes and subjected to sodium dodecyl sulfate-polyacrylamide gel electrophoresis (SDS-PAGE). Following the separation on 10% polyacrylamide gel, proteins were transferred onto nitrocellulose membranes (Sigma-Aldrich). Membranes were blocked overnight in 3% skimmed milk and then incubated for 1 hour at room temperature with rabbit anti-Meq antiserum (20 μg/mL) and mouse anti-chicken actin antibody (20 μg/mL) as internal control. After three washes with phosphate-buffered saline (PBS) containing 0.05% Tween 20 (PBS-T), membranes were incubated with either HRP-conjugated anti-rabbit IgG secondary antibody (Promega) or HRP-conjugated anti-mouse IgG_1 secondary antibody (Thermo Fisher Scientific) for 30 minutes at room temperature. Detection was performed using a chemiluminescent substrate (EMD Millipore Co., Burlington, MA, USA). Three independent experiments were conducted in triplicate.

Generation of recombinant viruses

RB-1B-based rMDVs encoding Meq or L-Meq (RB-1B) were generated according to the previously established methods (Conradie *et al*., 2019; Sato *et al*., 2022). The RB-1B genome, in which the IRL region was deleted, cloned as a bacterial artificial chromosome (BAC) plasmid, pRB-1B_ΔIRL (kindly provided by Dr. Benedikt Kaufer, Engel *et al*., 2012), was used to generate mutant recombinant viruses. The native *meq* in the TRL region of pRB-1B_ΔIRL was replaced with RB-1B-*meq* or L-*meq* (RB-1B) using a two-step Red recombination strategy (Tischer *et al.*, 2006; Tischer and Kaufer, 2012).

The resulting BAC plasmids were subjected to restriction fragment length polymorphism (RFLP) analysis to verify that each *meq* was accurately inserted. The BAC plasmids encoding each rMDV genome were digested with BamHI-HF (New England Biolabs Japan Inc., Tokyo, Japan) and screened by electrophoresis on 0.8% agarose gels (Sato *et al*., 2022). Insertion of each *meq* was further validated by PCR and DNA sequencing. rMDVs were reconstituted by transfecting the BAC plasmids into CEFs using the CalPhos Mammalian Transfection Kit (Takara Bio Inc., Kyoto, Japan), and pCAGGS-Cre (Gene Bridges GmbH, Heidelberg, Germany) was co-transfected to excise the BAC sequence. The resulting rMDVs were designated rRB-1B_Meq and rRB-1B_L-Meq, respectively. All reconstituted viruses were passaged several times on CEFs and stored at –80 °C in Cell Banker 1 (Nippon Zenyaku Kogyo Co., Ltd., Fukushima, Japan). Since the IRL region is known to be rapidly restored during virus reconstitution and

several passages (Vychodil *et al*., 2021), restoration of the IRL region and removal of BAC sequences were confirmed by PCR. Viral titers were determined by plaque assays as previously reported (Engel *et al.*, 2012). To exclude the presence of unintended mutations, the whole genomes of reconstituted rMDVs were sequenced using DNA extracted from CEFs infected with each rMDV. Whole genome sequencing was performed by Hokkaido System Science Co., Ltd. (Hokkaido, Japan). No mutations were detected in the ORFs previously associated with MDV virulence, except for the manipulated *meq* (BioSample accessions: LC849254, LC849255).

***In vitro* replication of the recombinant viruses**

Confluent monolayers of CEFs seeded in 12-well plates were infected with 50 plaque-forming unit (PFU) of recombinant virus. Infected cells were collected daily for five days. Total cellular DNA was extracted using the DNeasy Blood and Tissue Kit (Qiagen). Viral loads were quantified by quantitative PCR (qPCR) to evaluate replication kinetics. Primer sets used for qPCR analysis are listed in Table I-3. Viral loads were calculated as the mean of three independent cultures, with all experiments performed in triplicate.

Experimental infection

Fertilized eggs from white leghorn chickens (Iwamura Hatchery Co. Ltd.) were hatched in the laboratory, and the chicks were raised in isolators. PCR screening confirmed the absence of major infectious pathogens, including chicken infectious anemia virus and infectious bursal disease virus. A total of 83 one-day-old chicks were randomly assigned to three groups and housed separately. Chickens were inoculated intraperitoneally with 5,000 PFU of rRB-1B_Meq ($n = 29$), rRB-1B_L-Meq ($n = 34$), or PBS (pH 7.4) as a negative control ($n = 20$). At 7, 14, 28, 35, and 49 days post-infection (dpi), four chickens from each group were euthanized, and samples of blood, spleen, thymus, and gross tumor lesions were collected. Clinical signs associated with MD were monitored daily for eight weeks after virus inoculation. Chickens showing clinical signs during the experimental period were euthanized by collecting heparinized whole blood from the hearts under deep general anesthesia induced by isoflurane inhalation (Zoetis Japan, Tokyo, Japan), and necropsy was performed to assess the presence of gross tumor lesions. All remaining chickens without clinical signs were euthanized at the end of the experimental period (56 dpi), and tumor incidence was assessed (control group; $n = 4$, rRB-1B_Meq-infected group; $n = 7$). Spleen and tumor tissues were dissected with scissors, homogenized, and filtered through 40-μm cell strainers (BD Biosciences, San

Jose, CA, USA) to obtain single-cell suspensions, which were washed twice in PBS. Mononuclear cells from blood and spleen suspensions were isolated by density gradient centrifugation using Percoll (GE Healthcare, Chicago, IL, USA), followed by two additional PBS washes. Isolated cells were preserved in Cell Banker 1 (Nippon Zenyaku Kogyo Co., Ltd.) for subsequent flow cytometric analysis.

DNA extraction and qPCR

Total cellular DNA was extracted from whole blood samples of infected chickens using the DNeasy Blood and Tissue Kit (Qiagen), following the manufacturer's instructions. qPCR was conducted to determine viral loads using primers specific to the *infected-cell protein 4* (*icp4*) of MDV. qPCR was performed with the TB Green Premix DimerEraser (Takara Bio Inc.) on a LightCycler 480 System II (Roche Diagnostics, Mannheim, Germany). The chicken *inducible nitric oxide synthase* (*i-nos*) was used as an internal reference. Viral loads were expressed as the ratio of *icp4* to *i-nos*. Primer sequences used for the qPCR analyses are listed in Table I-3.

Flow cytometric analysis

PBMCs or cells (5×10^5) isolated from the spleen, thymus, or tumor tissues were seeded into 96-well round-bottom plates and washed twice with fluorescence-activated cell sorting (FACS) buffer (PBS supplemented with 1% bovine serum albumin; Sigma-Aldrich). To block nonspecific binding, cells were incubated with PBS containing 10% chicken serum (Thermo Fisher Scientific) at 25 °C for 15 minutes. Staining of cell surface molecules was performed using the following monoclonal antibodies (mAbs): mouse anti-chicken CD3ε conjugated with PerCP-Cyanine5.5 (PerCP-Cy5.5), anti-chicken CD4 conjugated with PE-Cyanine7 (PE-Cy7), anti-chicken CD8β conjugated with fluorescein isothiocyanate (FITC), anti-chicken TCRγδ conjugated with phycoerythrin (PE) (all from Southern Biotech, Birmingham, AL, USA), and anti-TGF-β1,2,3 conjugated with allophycocyanin (APC; R&D Systems, Abingdon, UK) Or mouse IgG isotype control (R&D Systems) at 4 °C for 30 minutes in the dark. The gating strategy for this analysis is shown in Fig. I-1.

To further characterize γδ, $CD4^+$, and $CD8^+$ T cell subsets, additional staining was conducted using anti-chicken CD3ε (PerCP-Cy5.5), CD4 (PE-Cy7), CD8β (FITC), and CD8α (APC) mAbs (Southern Biotech). Cells were incubated under identical staining conditions, and the gating strategy is presented in Fig. I-2. Viable and non-viable cells were discriminated using Fixable Viability Dye eFluor780 (Thermo Fisher Scientific).

Following staining, cells were washed twice with 200 μL of FACS buffer and analyzed using a FACSLyric flow cytometer (BD Biosciences).

RNA sequencing

Total RNA was extracted from tumor tissues collected from two chickens per rMDV-infected group using the RNeasy Plus Mini Kit (Qiagen) according to the manufacturer's instructions. RNA sequencing (RNA-seq) was performed by Hokkaido System Science Co., Ltd..

RNA quality was evaluated using an Agilent 2100 Bioanalyzer (Agilent Technologies, Böblingen, Germany). Complementary DNA (cDNA) libraries were prepared using the NEBNext Ultra Directional RNA Library Prep Kit (New England Biolabs Japan Inc.) following the manufacturer's protocol. Paired-end sequencing was conducted on an Illumina NovaSeq™ system (Illumina, Inc., San Diego, CA, USA) following the manufacturer's instructions. Adapter sequences were trimmed from raw reads using Cutadapt v1.18 (https://cutadapt.readthedocs.io/en/stable). Reads were additionally trimmed at bases with quality values below 20, and only reads longer than 75 base pairs were retained for subsequent analyses. The raw sequence data were deposited in the DDBJ/ENA/GenBank (BioSample accession numbers SAMD00731360, SAMD00731361, SAMD00731362, and SAMD00731363). For transcript quantification, trimmed reads were mapped to the transcript sequences of *Gallus* GRCg6a (Release 105) from the Ensemble Database as the reference sequence, and transcripts per million (TPM) was calculated using Salmon v1.2.1 (https://github.com/COMBINE-lab/salmon). The corresponding chicken genome sequence was used as a decoy to improve mapping specificity. Transcript abundance was expressed as TPM, which was used for correlation analysis among samples. Differential gene expression between groups was assessed by Gene Ontology (GO) analysis using DAVID Bioinformatics Resources (https://davidbioinformatics.nih.gov/summary.jsp), based on the processed reads.

Statistical analyses

Statistical analyses were conducted using R Statistical Software (version 4.0.3; R Foundation for Statistical Computing, Vienna, Austria). Multi-step growth kinetics were analyzed using the Mann–Whitney U test. T cell dynamics up to 35 dpi were analyzed using the Kruskal–Wallis test followed by Dunn's post hoc test. T cell dynamics after 49 dpi were assessed using the Mann–Whitney U test. Tumor incidence was compared between the groups using Fisher's exact test. Transactivation activity was analyzed using Tukey's multiple comparison test. Spearman's rank correlation test was applied to assess

the correlation among TPM values across samples. Results with $p < 0.05$ were considered statistically significant.

Table I-1 Primers used to introduce mutations into the L-*Meq*.

Position in Meq	Substitution	Type	Sequence
71	Serine–to–alanine	Forward	5′-GAATCGTGACGCCGCTCGGAGAAGACG-3′
		Reverse	5′-CGTCTTCTCCGAGCGGCGTCACGATTC-3′
77	Glutamic-acid–to–lysine	Forward	5′-CGGAGAAGACGCAGGAAGCAGACGGACTATGTAGACAAAC-3′
		Reverse	5′-GTTTGTCTACATAGTCCGTCTGCTTCCTGCGTCTTCTCCG-3′
326	Threonine-to- isoleucine	Forward	5′-TTCCCTCGGATATTCAGTCTACGGT-3′
		Reverse	5′-ACCGTAGACTGAATATCCGAGGGAA3′
386	Isoleucine–to–threonine	Forward	5′-GTTTCCCTCGGATACTCAGTCTACGGTCT-3′
		Reverse	5′-AGACCGTAGACTGAGTATCCGAGGGAAAC-3′

Table I-2. Primers used to construct the reporter plasmid

Type	Type	Sequence
pp38	Forward	5′-GCTAGCGGCCGTGCCATTCTGAGAG-3′
	Reverse	5′-AAGCTTCCGTCCGACGAGAGCAAG-3′
pp14	Forward	5′-TAAGAGCTCCTTATCCTATACCGCCGCCTC-3′
	Reverse	5′-AATAAGCTTGAGAGCATCGCGAAGAGAGAA-3′
meq	Forward	5′-GCTAGCCCACGTACTGACGAATTTAGTAC-3′
	Reverse	5′-AAGCTTATTCTTAACATTCCAGCACCAAC-3′
icp4	Forward	5′-TTCGAAGGGTTTAGGAGGGGCGCA -3′
	Reverse	5′-TGGTACCATTAGCCGCGACATCCATCT -3′
gb	Forward	5′-TCAGATCTCAAGTCTCACTCACAAA-3′
	Reverse	5′-TCAGATCTGCTGTTCATAAATTGTGT-3′
cd30	Forward	5′-TAAGAGCTCCTAATTAATAATAGCGTGCTC-3′
	Reverse	5′-TAACTCGAGTCCTGATCTCCCAGCATTGCA-3′
bcl-2	Forward	5′-GCTAGCGACAGCCAGGAGGAAGCG-3′
	Reverse	5′-AAGCTTTGGGAGGGGGAGAGGAAG-3′
il-2	Forward	5′-GAGCTCCGTCTTTGCAAACGATGACAG-3′
	Reverse	5′-AAGCTTAAATACAGCCAAAGATCAGTACT-3′

Underlines indicate the restriction enzyme sites.

Table I-3. Primers used for quantitative polymerase chain reaction and confirmation of generated recombinant viruses.

Primer	Purpose	Type	Sequence
icp4	To qualify viral load	Forward	5′-GCATCGACAAGCACTTACGG-3′
		Reverse	5′-CGAGAGCGTCGTATTGTTTGG-3′
i-nos	Endogenous control for viral load	Forward	5′-GAGTGGTTTAAGGAGTTGGATCTGA-3′
		Reverse	5′-TTCCAGACCTCCCACCTCAA-3′
meq	To quantify transcripts of *meq*	Forward	5′-GTCCCCCCTCGATCTTTCTC-3′
		Reverse	5′-CGTCTGCTTCCTGCGTCTTC-3′
β-actin	Endogenous control for *meq* expression	Forward	5′-GAGAAATTGTGCGTGACATCA-3′
		Reverse	5′-CCTGAACCTCTCATTGCCA-3′
IRL inner	To confirm the restoration of the IRL region	Forward	5′-AGCTACCCCTTTCGGTTTGT-3′
		Reverse	5′-CACCCCCTTGTGGAAGTAGA-3′
IRL outer	To confirm the restoration of the IRL region	Forward	5′-CGAACGGAATGTACAACAGCTTGC-3′
		Reverse	5′-GATAAGACACTTTCCCACTCATAC-3′

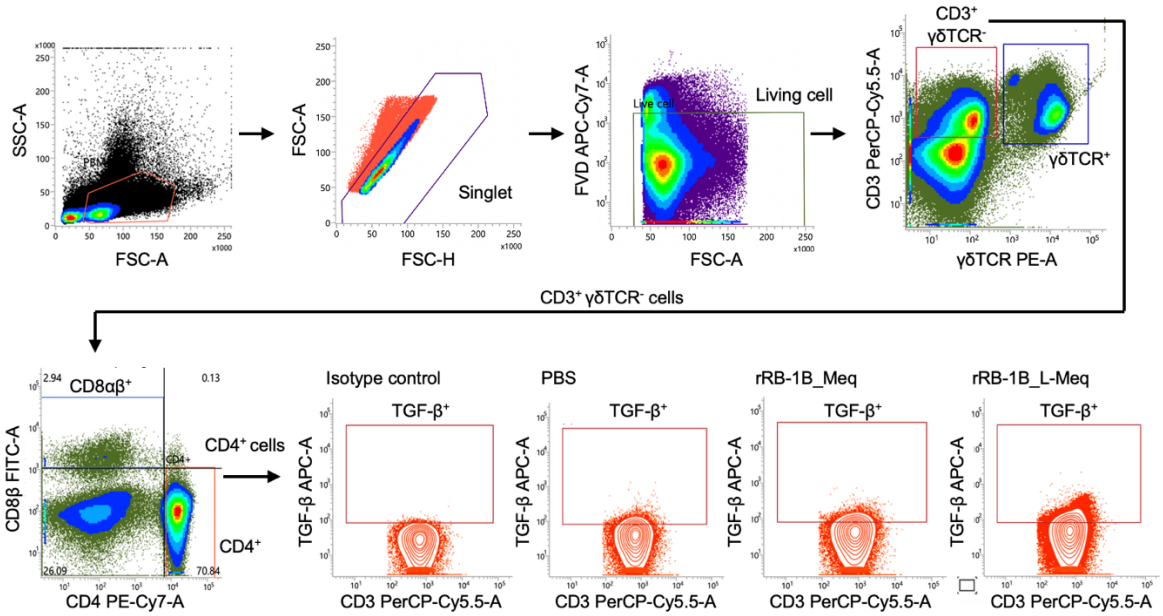

Figure I-1. Gating strategy for the analysis of the dynamics of major T cell subsets in chickens infected with rMDVs

A representative gating strategy is shown for analyzing the dynamics of γδ T cells, CD8αβ$^+$ T cells, CD4$^+$ T cells, and mTGF-β$^+$ CD4$^+$ T cells. Dead cells were excluded using Fixable Viability Dye eFluor780 (Thermo Fisher Scientific).

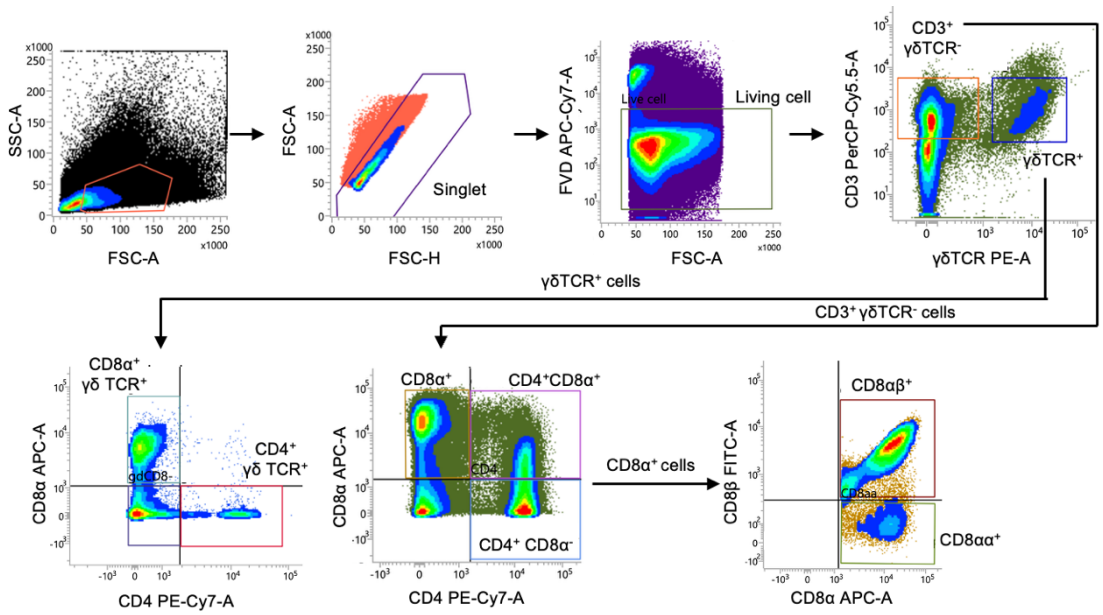

Figure I-2. Gating strategy for the analysis of the dynamics of T cell subsets involved in immune response in chickens infected with rMDVs

A representative gating strategy is shown for analyzing the dynamics of $CD8\alpha^+$ γδ T cells, $CD4^+$ γδ T cells, $CD4^+CD8\alpha^-$ T cells, and $CD8\alpha\alpha^+$ T cells. Dead cells were excluded using Fixable Viability Dye eFluor780 (Thermo Fisher Scientific).

RESULTS

Amino acid insertion in Meq enhances its transactivation activity

A previous study demonstrated that the insertion in the transactivation domain of Meq enhanced the transcriptional activity of the *meq* promoter (Sato *et al.*, 2022). To further elucidate the functional impact of this insertion, its effect on the transcriptional regulation of other Meq-responsive promoters was investigated. Mutations were introduced into the CVI988-L-*meq* to generate a variant identical to the sequence of RB-1B-*meq* except for the insertion (Fig. I-3A). The resulting constructs were designated Meq (RB-1B), L-Meq (wild-type), and L-Meq (RB-1B).

The effects of these Meq isoforms were evaluated on the activities of *pp38*, *pp14*, *icp4*, and *gb* promoters in the MDV genome, as well as the *bcl-2* and *cd30* promoters in the chicken genome. Given that Meq homodimers are known to suppress the *pp38* and *pp14* promoter activities (Levy *et al*., 2003), the transrepression by Meq and L-Meq constructs was compared. All Meq isoforms showed transcriptional repression on the *pp38* promoter, but L-Meq (wild-type) exhibited significantly weaker transrepression compared to Meq (RB-1B) and L-Meq (RB-1B), both of which showed comparable suppression levels (Fig. I-3B). In addition, a similar trend was observed on the activity of the *pp14* promoter (Fig. I-3C). These results suggest that, while some amino acid polymorphisms influence Meq-mediated transrepression, the insertion in L-Meq does not alter its ability to repress *pp38* or *pp14* promoter activities.

Since Meq forms heterodimers with c-Jun and activates the promoters of viral genes, such as *icp4* and *gb*, and host genes, such as *bcl-2* and *cd30* (Burgess *et al.*, 2004; Levy *et al*., 2005; Okada *et al*., 2007), the transactivation activities of three Meq constructs on these promoters were compared. L-Meq (wild-type) displayed lower transactivation activity than Meq (RB-1B) on most promoters, except the *bcl-2* promoter. In contrast, L-Meq (RB-1B) showed significantly higher activity on the *icp4*, *bcl-2*, and *cd30* promoters than Meq (RB-1B), while they exhibited a similar activity on the *gb* promoter (Figs. I-3D–G). Thus, the insertion in Meq did not affect its transrepression but enhanced the transactivation activities on certain promoters. These data suggest that the insertion enhances Meq function in the context of transcriptional activation, although these effects appear to vary for different promoters.

Effect of insertion in Meq on protein stability

Given that the stability of certain viral proteins is enhanced by the presence of proline-rich sequences (Levitskaya *et al*., 1997), the impact of the insertion in Meq on

protein stability was assessed. In DF-1 cells expressing Meq (RB-1B), signals were detected until 3 hours after the cycloheximide treatment at approximately 50 kDa, perhaps post-translationally modified forms. However, no signals exceeding 50 kDa were observed at 6 hours post-treatment (Fig. I-3H). In contrast, in cells expressing L-Meq (wild-type) and L-Meq (RB-1B), the signals showing the highest molecular weight visible at 0 hours were detectable until 12 hours after the treatment (Fig. I-3H). These results suggest that the insertion in the transactivation domain stabilizes Meq protein and contributes to the enhanced transactivation activity.

Recombinant viruses and their growth kinetics *in vitro*

To investigate the mechanisms of increased virulence by the insertion in Meq, rMDVs based on the RB-1B strain, which encoded RB-1B-Meq or L-Meq (RB-1B), were generated. The *meq* in the TRL region was replaced with RB-1B-*meq* or *L-meq* (RB-1B) in the IRL-deleted RB-1B genome cloned as a BAC (Fig. I-4A). The resulting BAC constructs were transfected into CEFs, and the IRL restoration in reconstituted viruses, designated rRB-1B_Meq and rRB-1B_L-Meq, were confirmed by PCR (data not shown) and whole genome sequencing (BioSample accessions: LC849254 and LC849255). No significant differences were observed in the growth kinetics among the rMDVs *in vitro* (Fig. I-4B).

***In vivo* replication of rMDVs and tumor incidence**

To evaluate the replication kinetics *in vivo* and tumorigenic potential of rMDVs, one-day-old chicks were infected with each rMDV. All the recombinant viruses showed efficient replication in infected chickens, but higher viral loads were significantly observed at 28 and 35 dpi in the rRB-1B_L-Meq-infected group than in the rRB-1B_Meq-infected group (Fig. I-4C). In agreement with a previous study (Sato *et al*., 2022), rRB-1B_L-Meq infection resulted in higher mortality (Fig. I-4D) and exhibited a trend toward higher tumor incidence than rRB-1B_Meq ($p = 0.059$; Fig. I-4E).

Dynamics of major T cell subsets in chickens infected with rMDVs

To assess the disease progression following infection with rMDVs, changes in major T cell subsets were analyzed in PBMCs and spleens in each infected group. The gating strategy employed for the flow cytometric analyses is shown in Fig. I-1. An earlier increase in the proportion of $CD4^+$ T cells within the T cell population was observed in both PBMCs and spleens of rRB-1B_L-Meq-infected chickens, and significant differences were noted 35 dpi (Figs. I-5A and B). Additionally, at 56 dpi, $CD4^+$ T cell

proportions in both PBMCs and spleen of rRB-1B_Meq-infected groups tended to exceed those of the control group ($p = 0.058$ and $p = 0.059$, respectively; Figs. I-5A and B).

Treg-like populations characterized by co-expression of mTGF-β and CD4 expanded along with disease progression (Gurung *et al*., 2017). In this study, the percentage of mTGF-β^+ cells among $CD4^+$ T cells in PBMCs was increased in both rMDV-challenged groups, but this elevation occurred earlier in the rRB-1B_L-Meq group (35 dpi) than in the rRB-1B_Meq group (56 dpi) (Fig. I-5C). On the contrary, no significant differences were detected among the groups in the spleens (Fig. I-5D).

The dynamics of $CD8\alpha\beta^+$ T cells, which play a crucial role in cytotoxic responses against infected cells, also differed between the infected groups. An earlier increase in $CD8\alpha\beta^+$ T cells within the T cell population was observed in PBMCs of rRB-1B_L-Meq-infected chickens at 7 and 14 dpi, but it decreased at 35 dpi (Fig. I-5E). This trend was in contrast to the elevated proportion of $CD4^+$ T cells in the same group (Figs. I-5A and B). In contrast, the percentage of $CD8\alpha\beta^+$ T cells within the T cell population in PBMCs of rRB-1B_Meq-infected chickens was increased with a delay, at 35 and 49 dpi, but did not differ from that of the control group at 56 dpi (Fig. I-5E). In the spleens, both infected groups exhibited an increase in the proportion of $CD8\alpha\beta^+$ T cells at 7 dpi, followed by a decrease at 35 dpi in the rRB-1B_L-Meq group and a tendency to be decreased at 56 dpi in the rRB-1B_Meq group (Fig. I-5F).

Given the potential role of γδ T cells in the protection against MD in CVI988-vaccinated chickens (Matsuyama-Kato *et al*., 2022, 2023b), the dynamics of γδ T cells were also evaluated. A reduction in the percentage of γδ T cells within the T cell population was observed at 28 and 35 dpi in PBMCs of the rRB-1B_L-Meq-infected group, and the percentage of γδ T cells in the rRB-1B_Meq-infected group was consistently lower than that in the control group (Fig. I-5G). Similarly, γδ T cell proportions in the spleens of both infected groups tended to remain lower than that in the control group throughout the experimental period (Fig. I-5H). These results suggest that the response of $CD8^+$ T cells and γδ T cells was insufficient to eliminate the transformed $CD4^+$ T cells. Collectively, while similar dynamics were observed in T cell subsets in the terminal phase of infection in both infected groups, the earlier onset of these changes occurred in the rRB-1B_L-Meq-infected group.

Dynamics of $CD8\alpha^+$ γδ T cell subsets in chickens infected with rMDVs

$CD8\alpha^+$ γδ T cells ($TCR\gamma\delta^+$ $CD3^+$ $CD4^-$ $CD8\alpha^+$) have been reported to increase following vaccination with CVI988 and to express IFN-γ, indicating their potential involvement in Th1 polarization and cell-mediated immunity (Hao *et al.*, 2021;

Matsuyama-Kato *et al*., 2022). Therefore, to examine the response of γδ T cells during MDV infection, the proportion of CD8α$^+$ γδ T cells within the γδ T cell population in the spleen was assessed, based on the gating strategy shown in Figure I-2. The percentage of CD8α$^+$ γδ T cells in the spleens of rRB-1B_Meq-infected chickens was significantly elevated at 28 dpi compared with both the control and rRB-1B_L-Meq-infected groups, but declined markedly at 56 dpi (Fig. I-6A). In contrast, chickens infected with rRB-1B_L-Meq did not exhibit any significant difference in CD8α$^+$ γδ T cell proportions relative to the control group up to 28 dpi. However, a significant reduction in this subset was observed at 35 dpi (Fig. I-6A).

Dynamics of CD8αα$^+$ T cells in chickens infected with rMDVs

CD8αα$^+$ T cells (TCRγδ$^-$ CD3$^+$ CD8α$^+$ CD8β$^-$) have been reported to be more prevalent in MD-resistant chicken lines and to expand during the proliferative phase of infection (Hao *et al*., 2021). In this study, the proportion of CD8αα$^+$ T cells within the CD8α$^+$ T cell population in the spleen was analyzed. At 7 dpi, both rMDV-infected groups exhibited a significant reduction in the percentage of CD8αα$^+$ T cells among CD8α$^+$ T cells compared to the control group (Fig. I-6B). However, at 35 dpi, a marked increase in the proportion of CD8αα$^+$ T cells was observed in the spleens of chickens infected with rRB-1B_L-Meq (Fig. I-6B), suggesting a role of CD8αα$^+$ T cells in the immune response to viral antigens or transformed lymphocytes during the later stage of infection.

Composition of T cell subsets and transcriptome analysis of tumor lesions

A previous study demonstrated that amino acid sequences in Meq influence the cellular composition in MDV-induced tumor lesions (Kumar *et al*., 2012). To assess the impact of the insertion in Meq on cellular composition, five representative solid tumors from chickens infected with rRB-1B_Meq or rRB-1B_L-Meq were analyzed. However, no significant differences in the frequencies of CD3$^+$ T cells, Bu-1$^+$ B cells, or macrophages were observed between the two groups (Figs. I-7A-C). In all tumor samples examined, approximately 95% of the T cell population consisted of CD4$^+$ T cells (Fig. I-7D), some of which was a subpopulation expressing mTGF-β (Fig. I-7E). The frequencies of CD8αβ$^+$ T cells and γδ T cells were below 1% (Figs. I-7F and G). In all the T-cell subsets analyzed, no significant difference was observed between the infected groups (Figs. I-7A–D). These results suggest that the insertion in Meq does not alter the cellular composition of tumor lesions.

To further examine the molecular characteristics, the transcriptome in tumor lesions of rRB-1B_Meq- and rRB-1B_L-Meq-infected chickens was compared using RNA-seq.

Among the 39,088 transcripts detected, 15,967 (40.8%) exhibited detectable expression (log_2 TPM > 0) in both rRB-1B_Meq and rRB-1B_L-Meq-infected groups. Of these, 15,262 and 14,601 transcripts were highly expressed in tumor lesions from rRB-1B_L-Meq- and rRB-1B_Meq-infected chickens, respectively. Scatter plot analysis using Spearman's rank correlation indicated strong positive correlations between all samples (Fig. I-7E), suggesting that the transcriptional profiles were broadly similar in both infected groups. Among genes that showed consistently high expression in both groups, *cyclooxygenase-1* (*cox1*) and *cox2* were selected for further validation for the RNA-seq data. Gene expression analysis using 10 additional tumor samples in each group confirmed no significant differences in *cox1* and *cox2* expression (Figs. I-7F and G), supporting that both recombinant viruses potentially induce transformation of $CD4^+$ T cells by similar pathways or by modulating the expression of similar target genes.

Functional enrichment analysis using GO was conducted on the RNA-seq data. Of the 10,313 transcripts annotated with Entrez Gene IDs and exhibiting detectable expression (log_2 TPM > 0), 2,132 transcripts showed more than 2-fold higher expression intensities in rRB-1B_L-Meq samples, while 906 were more highly expressed (>2-fold) in rRB-1B_Meq samples. Subsequently, GO analysis was conducted on these differentially expressed genes, classified under biological processes (BP), cellular components (CC), and molecular functions (MF). The most significantly enriched GO terms in each category are shown in Tables I-4–I-6, in order of their significance in terms of *p*-value. In the rRB-1B_L-Meq-infected group, genes related to "T cell proliferation", such as *interleukin 15* (*IL15*), *IL21*, and *CD28*, were significantly enriched, suggesting an enhancement of proliferative potential in transformed cells. Genes related to "chemotaxis", such as *CXC chemokine receptor 5* (*cxcr5*), *CC motif chemokine ligand 4* (*ccl4*), *ccl4*, and *ccl13*, were also enriched in both the BP and MF categories of rRB-1B_L-Meq. In contrast, the rRB-1B_Meq-infected group exhibited enriched GO terms associated with metabolic processes, particularly lipid metabolism, including "cellular lipid metabolic process," "cholesterol homeostasis," and "triglyceride homeostasis" in the BP category. Additionally, pathways associated with the biosynthesis of lipid-derived signaling molecules, such as "prostaglandin biosynthetic process" and "estrogen biosynthetic process" were upregulated in the rRB-1B_Meq group. Thus, more gene expression indicating immune activation was observed in tumor lesions in the rRB-1B_L-Meq group, while tumor lesions in the rRB-1B_Meq group showed characteristics displaying metabolic reprogramming. The insertion in Meq appears to cause minor differences in gene expression patterns in tumor lesions.

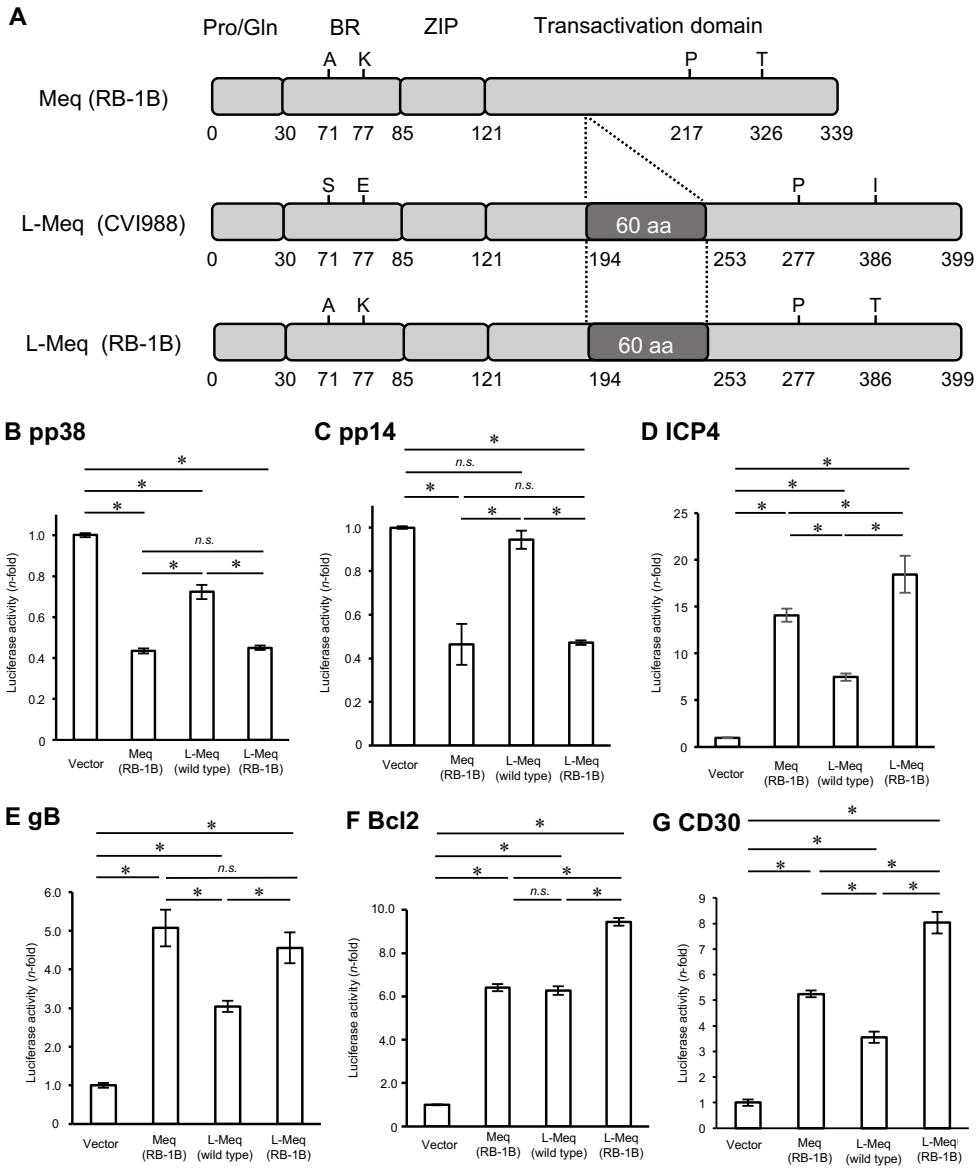
A
Pro/Gln
BR
ZIP
Transactivation domain
Meq (RB-1B)
L-Meq (CVI988)
L-Meq (RB-1B)
60 aa
B pp38
C pp14
D ICP4
E gB
F Bcl2
G CD30
Luciferase activity (n-fold)
Vector
Meq (RB-1B)
L-Meq (wild type)
L-Meq (RB-1B)
n.s.

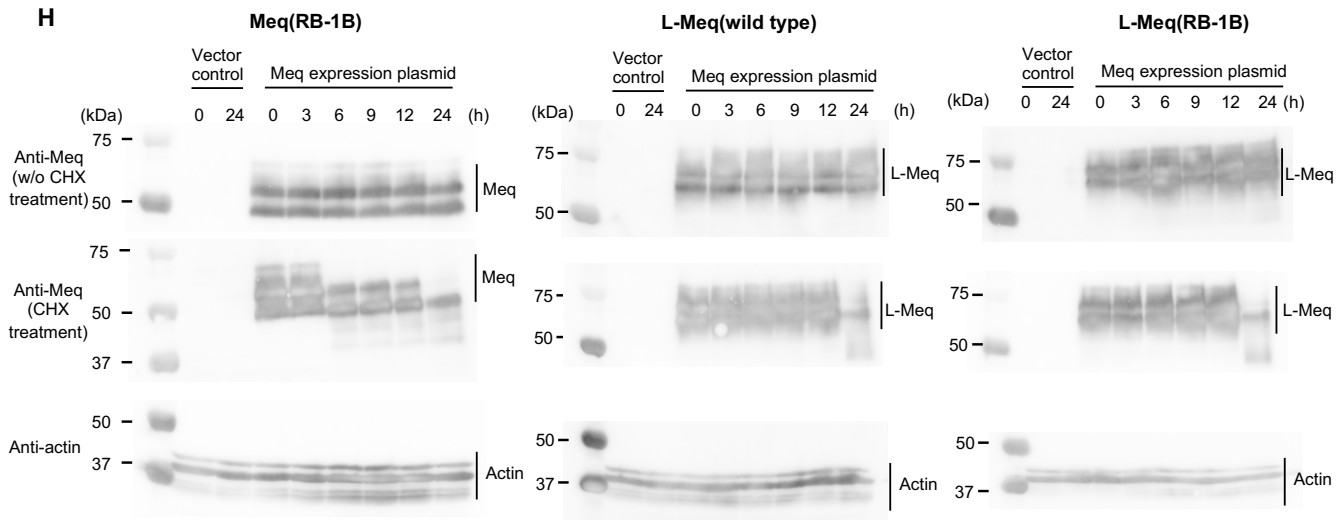
H
Meq(RB-1B)
L-Meq(wild type)
L-Meq(RB-1B)
Vector control
Meq expression plasmid
(kDa)
(h)
Anti-Meq (w/o CHX treatment)
Anti-Meq (CHX treatment)
Anti-actin
Meq
L-Meq
Actin

Figure I-3. Analysis of transcriptional regulation by the Meq and L-Meq proteins

(A) Schematic representation of the Meq isoforms. The structures of Meq from RB-1B, long-Meq isoform (L-Meq) from CVI988, and L-Meq (RB-1B) whose sequences were matched with those of RB-1B-Meq, except for the insertion in the transactivation domain. Pro/Gln, rich domain; BR, basic region; ZIP, leucine zipper. The Meq isoforms include amino-acid polymorphisms in the BR and transactivation domain. L-Meq is characterized by a 60-amino-acid insertion in the transactivation domain. (B and C) Transrepression effects of the Meq isoforms. The transrepression effects of RB-1B-Meq, wild-type L-Meq (CVI988), and L-Meq (RB-1B) on (B) the *pp38* promoter and (C) the *pp14* promoter-driven luciferase activities were compared. DF-1 cells in each well were transfected with 300 ng of expression plasmids for each Meq isoform, 500 ng of reporter plasmid, and 5 ng of control pRL-TK plasmid. Luciferase activities were analyzed 24 h post-transfection. Firefly luciferase activity is expressed relative to the mean basal activity in the presence of pCI-neo after normalization to *Renilla* luciferase activity. (D–G) Transactivation activities of the Meq isoforms. The transactivation activities of RB-1B-Meq, wild-type L-Meq (CVI988), and L-Meq (RB-1B) on (D) the *icp4* promoter, (E) the *gb* promoter, (F) the *bcl-2* promoter, and (G) the *cd30* promoter-driven luciferase activities were compared. DF-1 cells in each well were transfected with 300 ng of expression plasmids for each Meq isoform, 200 ng of c-Jun expression plasmid, 500 ng of reporter plasmid, and 5 ng of control pRL-TK plasmid. Error bars indicate standard deviations. Three independent experiments were performed in triplicate. ** $p<0.01$, Tukey's multiple comparison test. (H) Stability of the Meq isoforms. The stability of RB-1B-Meq, wild-type L-Meq (CVI988), and L-Meq (RB-1B) were compared. DF-1 cells in each well were transfected with 150 ng of expression plasmids for each Meq isoform or pCI-neo vector (negative control). The cells in each well were added 100 μg/ml of cycloheximide 24 hours after transfection. The transfected cells were separated on 10% SDS-PAGE and then transferred onto a nitrocellulose membrane. The membrane was incubated with the rabbit anti-Meq antibody and mouse anti-chicken actin antibody for 1 hour and then incubated with anti-rabbit IgG secondary antibody conjugated with HRP or anti-mouse IgG_1 secondary antibody conjugated with HRP for 30 min, respectively. Three independent experiments were performed in triplicate.

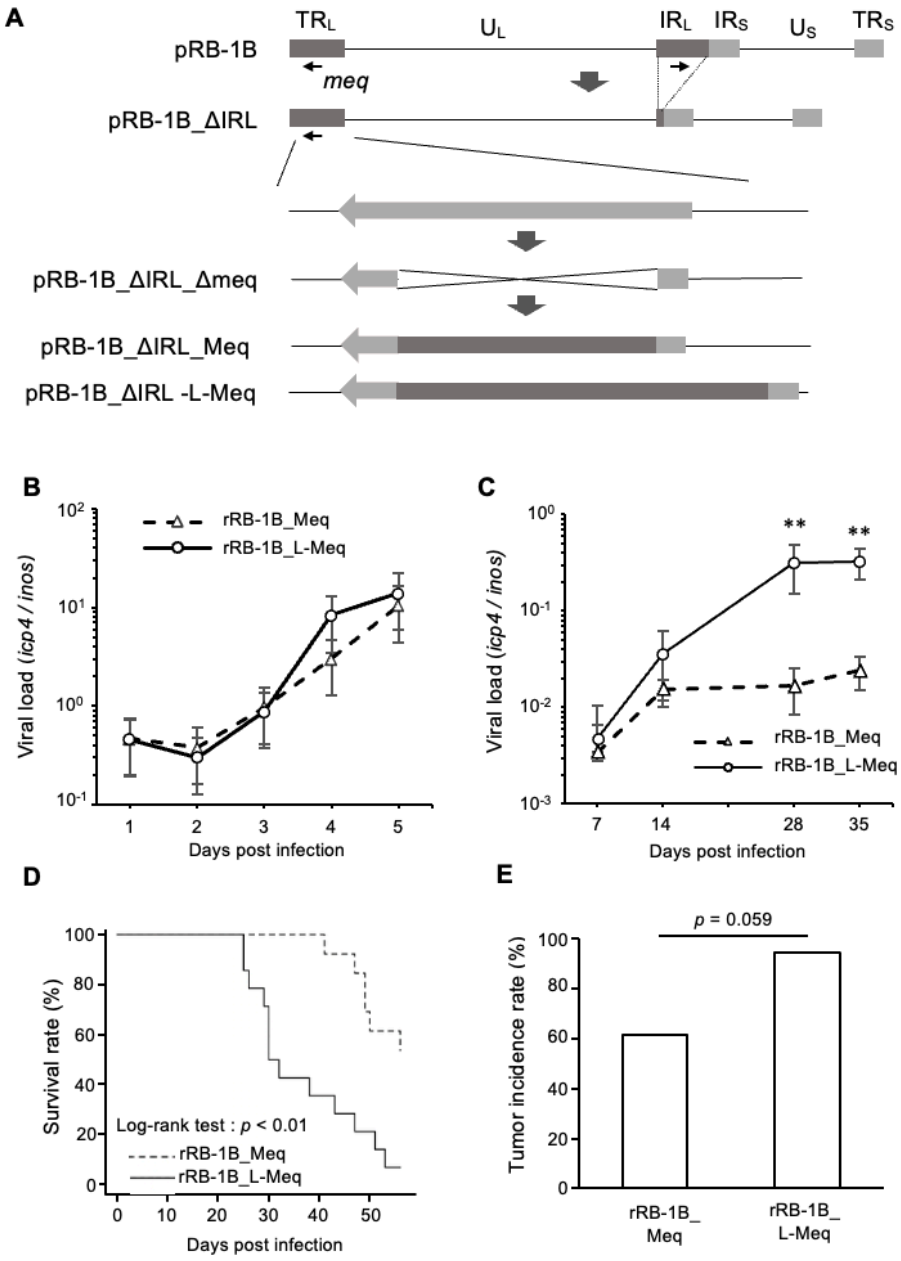

Figure I-4. Reconstitution of recombinant Marek's disease viruses (rMDVs) and their characterization *in vivo*

(A) Schematic diagrams of the constructs cloned using the RB-1B genome in this study. In the RB-1B genome cloned as the bacterial artificial chromosome (BAC) plasmid (pRB-1B); most of the internal repeat long (IRL) regions were deleted in this plasmid, designated as pRB-1B_ΔIRL, and used for mutagenesis. *meq* in the terminal repeat long (TRL) was replaced with RB-1B-*meq* or L-*meq* (RB-1B) (encoding the L-Meq containing the insertion) by two-step red-mediated mutagenesis. (B) CEFs were infected with 50 pfu of rMDVs. The infected cells were collected daily for 6 days. The viral loads in the infected cells were analyzed by quantitative PCR (qPCR) (7–35 dpi: control group: $n = 4$, rRB-1B_Meq-infected group: $n = 4$, rRB-1B_L-Meq-infected group: $n = 4$). Three independent experiments were performed in triplicate. Error bars indicate standard deviations. (C) The viral loads in the whole blood of chickens infected with rRB-1B_Meq and rRB-1B_L-Meq were determined by quantitative polymerase chain reaction (qPCR). Error bars indicate standard deviations. ** $p<0.01$, Mann–Whitney *U* test. (D) Survival rate in chickens infected with rMDVs in the experimental infection. The survival rate among the groups was analyzed using the Log-rank test. (E) Tumor incidence in chickens infected with rMDVs during the study period. * $p<0.05$, Fisher's exact test.

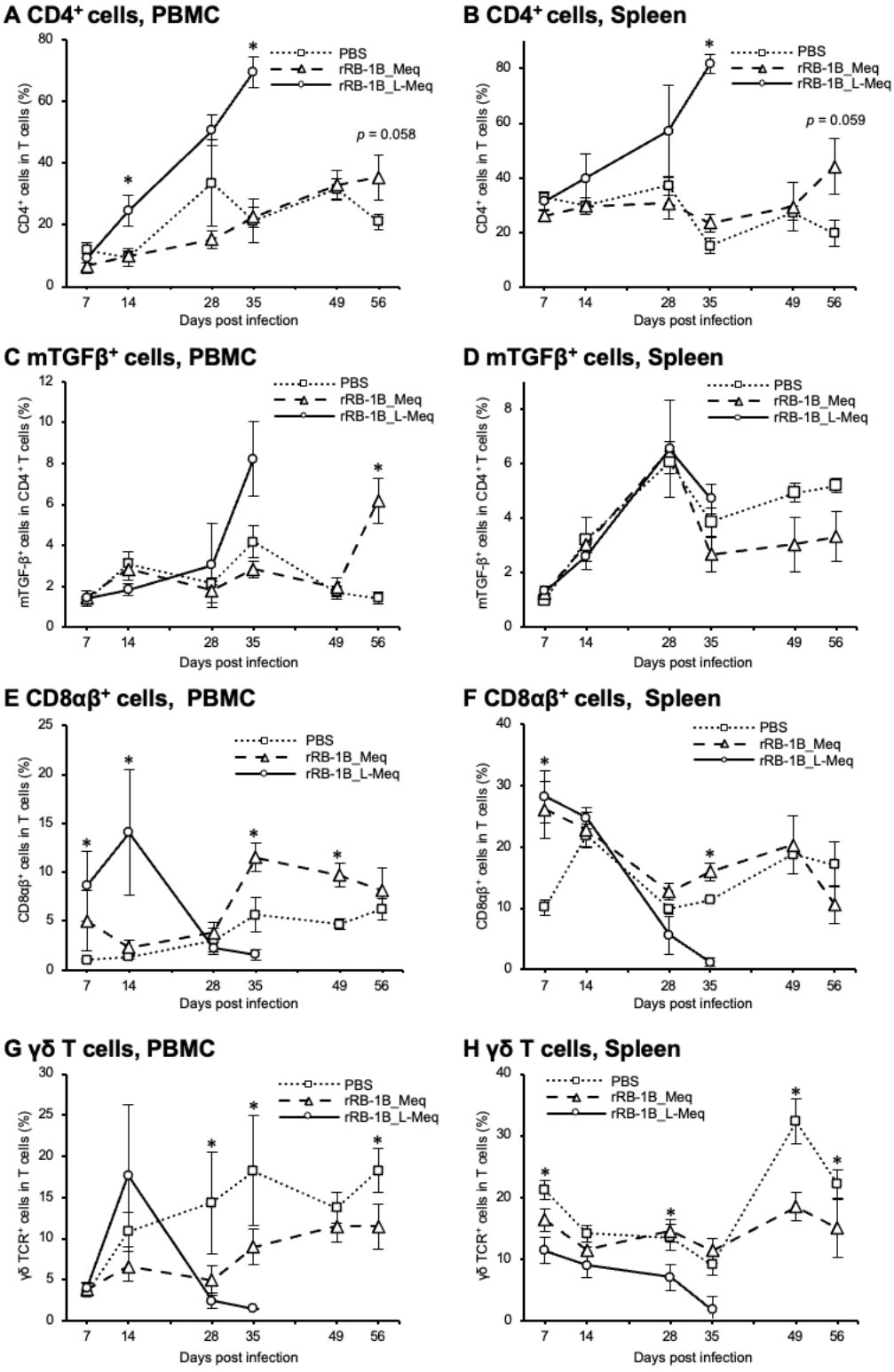

Figure I-5. The dynamics of major T cell subsets in chickens infected with rMDVs
The dynamics of $CD4^+$ cells, mTGF-β^+ $CD4^+$ cells, $CD8\alpha\beta^+$ cells, and γδ T cells in T cells from PBMCs and spleens of chickens infected with rRB-1B-Meq or rRB-1B-L-Meq at each time point during the experimental period (7–49 dpi: control group: $n = 4$, rRB-1B_Meq-infected group: $n = 4$, rRB-1B_L-Meq-infected group: $n = 4$, 56 dpi: control group: $n = 4$, rRB-1B_Meq-infected group: $n = 7$). The percentages of $CD4^+$ cells in the T cell population from (A) PBMCs and (B) spleens, mTGF-β^+ cells in the $CD4^+$ T cell population from (C) PBMCs and (D) spleens, $CD8\alpha\beta^+$ cells in the T cell population from (E) PBMCs and (F) spleens, and γδTCR^+ cells in the T cell population from (G) PBMCs and (H) spleens were analyzed. Error bars indicate standard deviations. * $p<0.05$, Kruskal–Wallis test (7–35 dpi), Mann–Whitney U test (49–56 dpi).

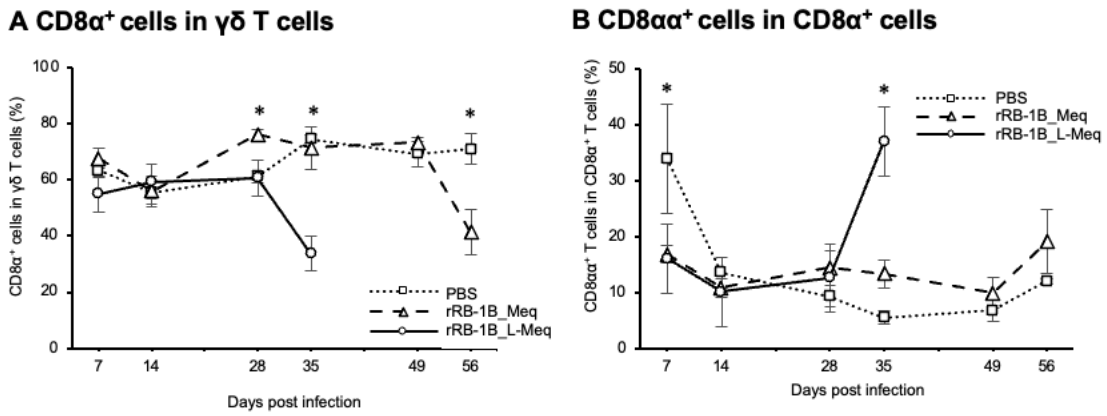

Figure I-6. Dynamics of T cell subsets involved in immune response in chickens infected with rMDVs
The dynamics of $CD8\alpha^+$ γδ T cells, $CD8\alpha\alpha^+$ T cells, and $CD4^+CD8\alpha^-$ T cells from spleens of chickens infected with rRB-1B-Meq or rRB-1B-L-Meq at each time point during the experimental period (7–49 dpi: control group: $n = 4$, rRB-1B_Meq-infected group: $n = 4$, rRB-1B_L-Meq-infected group: $n = 4$, 56 dpi: control group: $n = 4$, rRB-1B_Meq-infected group: $n = 7$). (A) The percentages of $CD8\alpha^+$ T cells in the γδ T cell population from spleens, (B) the percentage of $CD8\alpha\alpha^+$ cells in $CD8\alpha^+$ T cell population from spleens, and (C) the percentage of $CD4^+CD8\alpha^-$ T cells in $CD4^+$ T cell population from spleens were analyzed. Error bars indicate standard deviations. * $p<0.05$, Kruskal–Wallis test (7–35 dpi), Mann–Whitney U test (49–56 dpi).

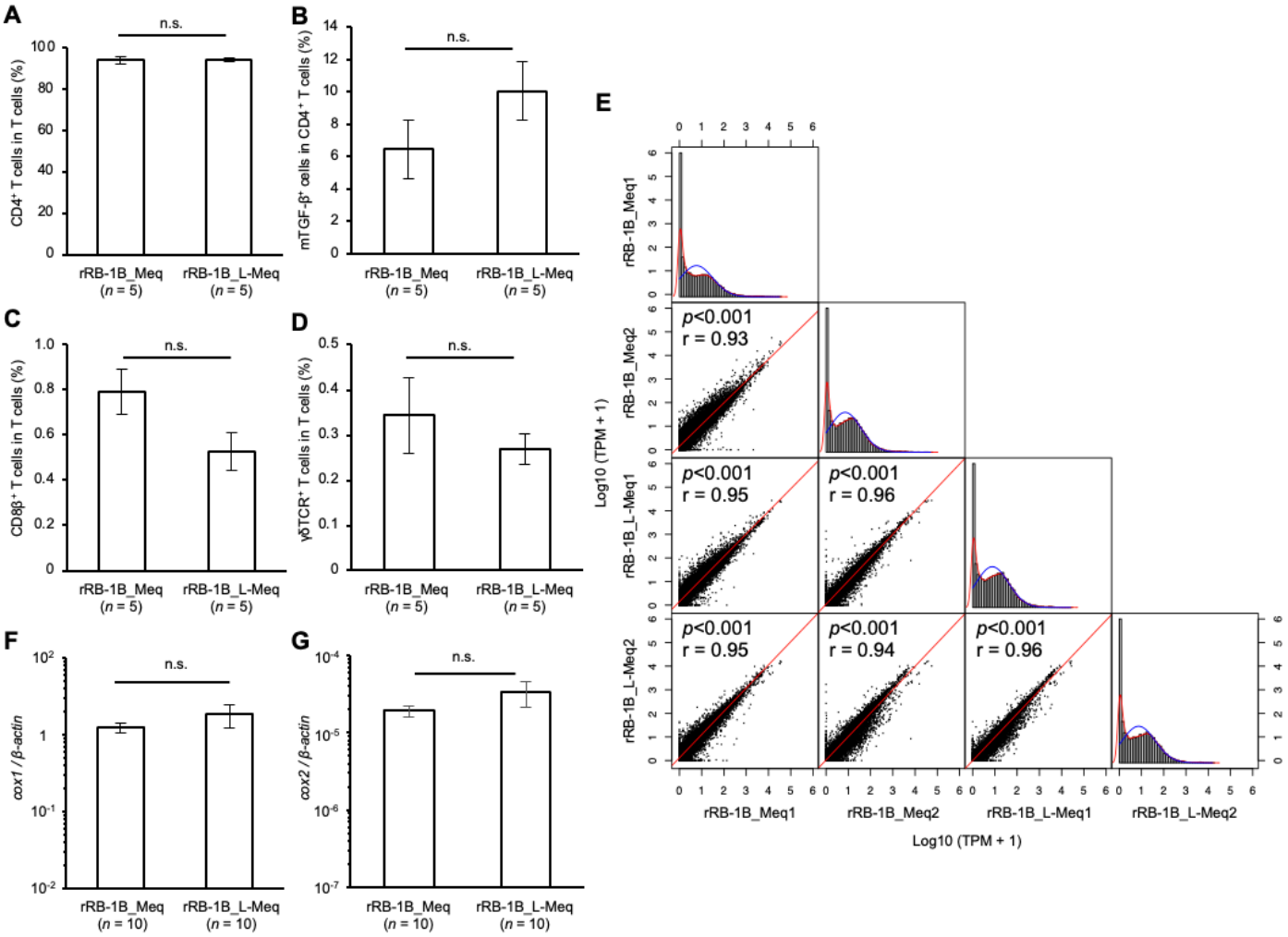

Figure I-7. Composition of T cell subsets and transcriptome analysis of tumor lesions of rMDV-infected chickens

(A–D) The composition of T cell subsets in tumor lesions from chickens that developed tumors in the kidneys or gonads during the experimental period were analyzed by flow cytometry (rRB-1B_Meq-infected group: $n = 5$, rRB-1B_L-Meq-infected group: $n = 5$). (A) The percentages of $CD4^+$ cells in the T cell population, (B) mTGF-β^+ cells in the $CD4^+$ T cell population, (C) $CD8\alpha\beta^+$ cells in the T cell population, and (D) $\gamma\delta TCR^+$ cells in the T cell population were analyzed. (E) The scatter plots show the Spearman rank correlation between each tumor lesion from chickens infected with rRB-1B-Meq and rRB-1B-L-Meq. r: Spearman's rank correlation coefficient. The expression levels of (F) *cox1* and (G) *cox2* in tumor lesions from chickens infected with rRB-1B-Meq or rRB-1B-L-Meq at 7 dpi were determined by qPCR.

Table I-4. Top 20 Gene Ontology categories with respect to "Biological Process"

	L-Meq			Meq		
	p-value	GO term	Functional category	p-value	GO term	Functional category
#1	2.10E-04	GO:0042102	positive regulation of T cell proliferation	3.50E-04	GO:0001516	prostaglandin biosynthetic process
#2	7.30E-04	GO:0006955	immune response	8.10E-03	GO:0045741	positive regulation of epidermal growth factor-activated receptor activity
#3	1.20E-03	GO:0006954	inflammatory response	1.00E-02	GO:1901224	positive regulation of NIK/NF-kappaB signaling
#4	1.40E-03	GO:0071347	cellular response to interleukin 1	1.30E-02	GO:0007173	epidermal growth factor receptor signaling pathway
#5	2.40E-03	GO:0070098	chemokine-mediated signaling pathway	1.30E-02	GO:1903078	positive regulation of protein localization to plasma membrane
#6	2.70E-03	GO:0006915	apoptotic process	1.30E-02	GO:0000226	microtubule cytoskeleton organization
#7	4.20E-03	GO:0071356	cellular response to tumor necrosis factor	1.40E-02	GO:0034145	positive regulation of toll-like receptor 4 signaling pathway
#8	5.70E-03	GO:0030198	extracellular matrix organization	1.40E-02	GO:0006703	estrogen biosynthetic process
#9	7.30E-03	GO:0002755	MyD88-dependent toll-like receptor signaling pathway	1.50E-02	GO:0032722	positive regulation of chemokine production
#10	8.50E-03	GO:0007596	blood coagulation	1.70E-02	GO:0042632	cholesterol homeostasis
#11	1.30E-02	GO:0035556	intracellular signal transduction	2.20E-02	GO:0046628	positive regulation of insulin receptor signaling pathway
#12	1.50E-02	GO:0048247	lymphocyte chemotaxis	2.50E-02	GO:1990830	cellular response to leukemia inhibitory factor
#13	1.50E-02	GO:0009968	negative regulation of signal transduction	3.50E-02	GO:0032731	positive regulation of interleukin-1 beta production
#14	1.60E-02	GO:0007155	cell adhesion	4.40E-02	GO:0070328	triglyceride homeostasis
#15	2.00E-02	GO:0002062	chondrocyte differentiation	4.40E-02	GO:0045840	positive regulation of mitotic nuclear division
#16	2.10E-02	GO:0051491	positive regulation of filopodium assembly	4.40E-02	GO:0061025	membrane fusion
#17	2.10E-02	GO:0002040	sprouting angiogenesis	5.60E-02	GO:0044255	cellular lipid metabolic process
#18	2.10E-02	GO:0001525	angiogenesis	6.50E-02	GO:0050729	positive regulation of inflammatory response
#19	2.50E-02	GO:0002224	toll-like receptor signaling pathway	6.70E-02	GO:0008284	positive regulation of cell proliferation
#20	2.80E-02	GO:0002548	monocyte chemotaxis	7.00E-02	GO:0007098	centrosome cycle

Table I-5. Top 5 Gene Ontology categories with respect to "Cellular component"

	L-Meq			Meq		
	p-value	GO term	Functional category	p-value	GO term	Functional category
#1	9.70E-05	GO:0005615	extracellular space	1.50E-03	GO:0005576	extracellular region
#2	2.50E-03	GO:0031012	extracellular matrix	1.90E-03	GO:0005737	cytoplasm
#3	2.70E-03	GO:0005581	collagen trimer	8.20E-03	GO:0045095	keratin filament
#4	4.00E-03	GO:0009897	external side of plasma membrane	8.70E-03	GO:0005615	extracellular space
#5	7.00E-03	GO:0005737	cytoplasm	1.60E-02	GO:0043235	receptor complex

Table I-6. Top 5 Gene Ontology categories with respect to "Molecular function"

	L-Meq			Meq		
	p-value	GO term	Functional category	p-value	GO term	Functional category
#1	3.30E-04	GO:0008009	chemokine activity	1.40E-03	GO:0005154	epidermal growth factor receptor binding
#2	2.00E-03	GO:0005524	ATP binding	4.90E-03	GO:0004601	peroxidase activity
#3	3.10E-03	GO:0003953	NAD+ nucleosidase activity	1.30E-02	GO:0005080	protein kinase C binding
#4	5.10E-03	GO:0050135	NAD(P)+ nucleosidase activity	1.50E-02	GO:0004862	cAMP-dependent protein kinase inhibitor activity
#5	5.10E-03	GO:0061809	NAD+ nucleotidase, cyclic ADP-ribose generating	1.50E-02	GO:0003953	NAD+ nucleosidase activity

DISCUSSION

In this chapter, the effect of the insertion in Meq on MDV virulence was assessed by evaluating Meq-mediated transcriptional regulation and T-cell dynamics in chickens infected with rMDV. The insertion was found to enhance Meq protein stability and its transactivation activity on the promoters of *bcl-2*, *icp4*, and *cd30*, indicating a potential for increased expression of transformation-related genes in latently infected cells. Consistent with this, an earlier expansion of $CD4^+$ T cells, including an MDV-transformed-cell phenotype (mTGF-β^+ $CD8\alpha^-$), was observed in chickens infected with rRB-1B_L-Meq. These observations suggest that the insertion could facilitate the early transformation of $CD4^+$ T cells through enhanced activation of tumor-associated gene expression, thereby accelerating MDV-induced tumor development.

The insertion in Meq showed the enhanced transactivation activities on *bcl-2*, *cd30*, and *icp4* promoters as well as *meq* promoter (Sato *et al*., 2022); this may be partially attributed to increased protein stability. A proline–alanine repeat sequence in EBV nuclear antigen 1 (EBNA1) inhibits ATP-dependent ubiquitination and subsequent proteasomal degradation, thereby stabilizing the protein (Levitskaya *et al*., 1997). Furthermore, the proteasomal degradation is inhibited by inserting this repeat sequence into a different viral protein, EBNA4. These observations suggest that an increase in the number of PRR sequences in L-Meq may promote the inhibition of proteasomal processing, and thus it potentially induces the enhanced protein stability, resulting in the prolonged activity of Meq on the transcriptional regulation. Alternatively, the insertion may induce conformational changes in the Meq protein structure, enhancing its resistance to degradation. In addition to the role in transcriptional regulation, Meq serves as a target for $CD8^+$ T cell responses, as Meq-derived peptides elicited IFN-γ production from MDV-specific cytotoxic T cells (Boodhoo and Behboudi, 2022a). Therefore, enhanced stability of Meq might impair antigen processing and presentation pathways, allowing transformed cells to evade immune surveillance. Further investigation is required to elucidate whether the number of PRRs influences proteasomal degradation and protein conformation, as well as the contribution of Meq stability to MDV pathogenesis.

In contrast to other promoters examined in this study, the insertion in Meq did not enhance the activity of the *gb* promoter. Meq regulates gene expression by forming heterodimers with AP-1 family proteins and binding to the Meq response element 1 (MERE1) located in the promoter region (Levy *et al.*, 2003). The number of MERE1 sequences present in the *gb* promoter is lower than those in the *meq* and *icp4* promoters, which may account for the difference in the effects of the insertion on each promoter

activity. To elucidate the impact of the insertion on transcriptional regulation of Meq, further comprehensive analyses, including the identification of dimerization partners of Meq and the profiling of their binding regions, are required.

Increased percentages of a Treg-like phenotype expressing mTGF-β and CD4 in PBMCs from MDV-infected chickens were observed, consistent with previous findings (Gurung *et al*., 2017), likely reflecting the expansion of tumor cells. Furthermore, the proportion of $CD4^+$ T cells was elevated from 14 dpi in chickens infected with rRB-1B_L-Meq. Given that MDV-transformed cells can arise as early as 10 dpi (Calnek, 2001), an early increase in $CD4^+$ T cells in rRB-1B_L-Meq-infected chickens may be due to the emergence of transformed cells. Thus, the data form the flow cytometric analysis in the present study suggest that tumor cell expansion occurs earlier in rRB-1B_L-Meq-infected chickens.

An increase in the proportion of $CD8\alpha^+$ γδ T cells following vaccination with CVI988 has been reported (Hao *et al.*, 2021). Additionally, a higher frequency of $CD8\alpha^+$ γδ T cells producing IFN-γ was observed during the early lytic phase in chickens superinfected with RB-1B after vaccination (Matsuyama-Kato *et al.*, 2022), suggesting a role of $CD8\alpha^+$ γδ T cells in the immune response against MDV. In contrast, the present study demonstrated a reduction in $CD8\alpha^+$ γδ T cells in both infected groups, coincident with an expansion of $CD4^+$ T cells, suggesting a reduced response to transformed cells. As MDV-transformed Treg-like cells are thought to suppress T cell proliferation via PGE_2 production and PD-L1 expression (Matsuyama-Kato *et al*., 2012; Gurung *et al.*, 2017; Kamble *et al*., 2021), it is plausible that similar mechanisms also inhibit the proliferation of $CD8\alpha^+$ γδ T cells. Notably, the $CD8\alpha^+$ γδ T cell population was reduced at an earlier time point in chickens infected with rRB-1B_L-Meq, suggesting that the disease progression was accelerated in this group.

An increase in the $CD8\alpha\beta^+$ T cell population within PBMCs was detected at 14 dpi in chickens infected with rRB-1B_L-Meq, and subsequently at 35 and 49 dpi in those infected with rRB-1B_Meq. This elevation could reflect a response to MDV-transformed cells. The expansion of $CD4^+$ T cells was observed after the rise in $CD8\alpha\beta^+$ T cells, occurring at 35 dpi in the rRB-1B_L-Meq-infected group and at 56 dpi in the rRB-1B_Meq-infected group. Moreover, a significant increase in $CD8\alpha\alpha^+$ T cells was observed at 35 dpi in the rRB-1B_L-Meq-infected chickens, potentially showing a response to transformed cells. Previous studies showed a similar increase in $CD8\alpha\alpha^+$ T cells during the proliferative phase of MDV infection (Perumbakkam *et al.*, 2016) and a rapid expansion following secondary CVI988 vaccination (Hao *et al*., 2021), indicating that the $CD8\alpha\alpha^+$ T cell subset may include memory T cells specific to MDV. Therefore,

an increase in CD8αα$^+$ T cells during the late lytic phase may have resulted from the reactivation of memory cells established during the acute phase of infection. Further functional characterization of CD8αα$^+$ T cells is required to elucidate their role in MD pathogenesis.

Previous studies have shown that the cellular composition markedly differs between tumors caused by the RB-1B and Md5 strains (Kumar *et al*., 2012). Tumors induced by a recombinant Md5 strain expressing RB-1B-Meq exhibited an intermediate cellular profile between the two strains, suggesting that differences in amino acid sequences of Meq can influence the cellular composition of tumor lesions. In contrast, the present study found no significant differences in the proportions of total T cells, B cells, macrophages, or each T-cell subset in tumor tissues between rRB-1B_Meq and rRB-1B_L-Meq. These findings suggest that the 60-amino acid insertion in Meq markedly accelerates disease progression without altering the cellular composition in tumor lesions. Moreover, these data imply that Meq polymorphisms may alter virulence through mechanisms distinct from those driven by the insertion.

The RNA-seq analysis indicated that rRB-1B_Meq and rRB-1B_L-Meq modulated similar signaling pathways in the process of cellular transformation. However, GO analysis focusing on differentially expressed genes between the groups revealed distinct transcriptional profiles in tumor lesions from rMDV-infected chickens. In tumor lesions derived from rRB-1B_L-Meq-infected chickens, genes involved in immune responses, including cytokines associated with lymphocyte proliferation, chemokines related to lymphocyte migration, and adhesion-related molecules, were predominantly expressed. The upregulation of these genes may contribute to the proliferation of CD4$^+$ T cells during the transformation phase, as well as the migration and adhesion of tumor cells and immune cells, thereby promoting solid tumor formation in several organs. In contrast, tumor lesions from rRB-1B_Meq-infected chickens showed predominant expression of genes associated with lipid metabolism and cell proliferation. Notably, fatty acids such as palmitic acid play an essential role in MDV replication, and MDV-induced fatty acid biosynthesis has been shown to enhance viral replication (Boodhoo *et al*., 2019). The activation of lipid metabolism observed in the tumor microenvironment of rRB-1B_Meq-infected chickens may facilitate viral reactivation at a high frequency. These findings suggest that the characteristics of transformed cells differ between the rMDVs. Moreover, the accelerated disease progression observed in rRB-1B_L-Meq-infected chickens may contribute to the retention of transcriptional signatures related to immune cells, whereas the relatively slow disease progression in rRB-1B_Meq-infected chickens may more accurately reflect the transcriptional properties of tumor cells. For a more comprehensive

understanding, further studies are required to evaluate the contribution of subtle transcriptional changes to MDV virulence.

Given that CVI988 contains the same insertion in the transactivation domain, the findings in the present study hold field relevance (Lee *et al*., 2000a). Although wild-type CVI988-L-Meq exhibited enhanced protein stability similar to that of L-Meq (RB-1B), its transactivation activity was reduced compared to both L-Meq (RB-1B) and Meq (RB-1B), suggesting that polymorphisms in the basic region could reduce the transcriptional activity of CVI988-L-Meq. However, an RB-1B-based rMDV encoding wild-type CVI988-L-Meq retained virulence comparable to that of rMDV encoding RB-1B-Meq (Conradie *et al.*, 2019), suggesting that the insertion could compensate for the virulence reduced by the polymorphisms in the basic region. Furthermore, additional viral factors may contribute to the attenuated virulence of CVI988. Identification of the molecular mechanisms underlying the attenuated virulence may facilitate the development of more effective vaccines for controlling MD.

SUMMARY

Despite the development of effective vaccines, the virulence of MDV field strains has continued to increase, and sporadic outbreaks still occur. A 59/60-amino acid insertion in the transactivation domain of Meq has been identified not only in the vaccine strain CVI988 but also in several virulent field strains. Previous studies using rMDV demonstrated that the insertion in Meq enhanced viral virulence, but the underlying mechanisms remain unclear. Therefore, in Chapter I, to investigate the effect of the insertion in Meq on MDV pathogenesis, comparative analyses were performed focusing on Meq-mediated transcriptional regulation, the dynamics of transformed T cells and relevant T-cell subsets in infected chickens, and gene expression profiles in tumor lesions.

Reporter assays revealed that the insertion enhanced the transactivation activity on the promoters of a viral gene *icp4* and host genes, *bcl-2* and *cd30*. The insertion increased Meq protein stability; therefore, it could contribute to the enhanced transactivation function. On the other hand, no apparent effect was observed on Meq-mediated transrepression on the *pp38* and *pp14* promoters. The insertion in Meq of an RB-1B-based recombinant MDV resulted in higher mortality and tumor incidence, as well as expansion of $CD4^+$ T cells, including an mTGF-β-expressing subpopulation, an MDV-transformed phenotype, in earlier phase of infection. Additionally, the proportions of $CD8^+$ T cells and γδ T cells were reduced earlier in rRB-1B_L-Meq-infected chickens. In contrast, flow cytometric analysis of tumor lesions revealed no significant differences in cellular composition between the rRB-1B_L-Meq and rRB-1B_-Meq-infected groups. Furthermore, transcriptome analysis showed similar gene expression profiles between the infected groups, but GO enrichment analysis for differentially expressed genes identified distinct biological signatures. In tumor lesions from rRB-1B_L-Meq-infected chickens, immune- and migration-related GO terms, such as “T cell proliferation” and “chemotaxis”, were enriched, whereas tumors from rRB-1B_Meq-infected chickens showed enriched GO terms in lipid metabolism-related pathways, including “cellular lipid metabolic process,” “cholesterol homeostasis,” and “triglyceride homeostasis.” Collectively, these findings suggest that although the insertion in Meq does not alter the transcriptional targets of Meq, it accelerates the process of tumorigenesis by enhancing the protein stability and the transactivation activity

CHAPTER II

Effect of amino acid polymorphisms in the basic region of Meq on its transcriptional regulation activity and the virulence of Marek's disease virus

INTRODUCTION

CVI988 is an attenuated vaccine strain derived from a low-virulence MDV and is globally used as a gold-standard vaccine against MD (Rispens *et al*., 1972; Gimeno, 2008; Schat, 2016). In Chapter I, the insertion in the transactivation domain of Meq, which were first identified in CVI988-L-Meq, accelerated MDV-mediated tumorigenesis, presumably due to the enhanced transcriptional regulatory activity resulting from the increased protein stability. Thus, the insertion in Meq appears to enhance its protein function and to promote disease progression. Indeed, L-Meq, which contains the insertion in the transactivation domain, is not unique to CVI988-L-Meq, but has been identified in pathogenic MDV strains circulating in Australia and Brazil (Renz *et al*., 2012; Chacón *et al*., 2024). These observations suggest that the amino acid sequence in other regions of Meq also play a pivotal role in determining virulence.

The basic region corresponds to positions 30–85 of Meq and is responsible for binding to genomic DNA (Jones *et al*., 1992). The basic region contains two sub-domains: basic region 1 at positions 30–36 and basic region 2 at positions 62–78, the latter of which is associated with nuclear localization and nuclear import of Meq (Liu *et al*., 1997). Compared with vv/vv+MDV strains in the US, the Meq isoforms of CVI988 harbor two amino acid polymorphisms in the basic region (Table 1): Serine and glutamic acid are present at positions 71 and 77 in the Meq isoforms of CVI988, whereas alanine and lysine are present in Meq of vv/vv+MDV strains (Lee *et al*., 2000b). These polymorphisms in the basic region of the CVI988-Meq isoforms have also been found in the ancestral MDV detected in 19th-century chicken skeletal remains, as well as in low-virulence field isolates from the 1960s in the US, such as Jm and BC-1 (Shamblin *et al*., 2004; Fiddaman *et al*., 2023). Therefore, changes in the amino acid residues at positions 71 and 77 are assumed to have played an important role in the evolution of MDV virulence.

In Meq of pathogenic MDV strains recently isolated in Asia, Africa, and Europe, glutamic acid and tyrosine have consistently been identified at positions 77 and 80, respectively (Trimpert *et al*., 2017; Deng *et al*., 2021; Patria *et al*., 2024; Yamagami *et al*., 2025). These polymorphisms are predominant in MDV strains in the Eurasian region, whereas they are found in vMDV strains in the US. On the other hand, the amino acid residues at these positions in vv/vv+MDV strains in the US are lysine and aspartic acid. Thus, the amino acid sequences at positions 77 and 80 show obvious differences depending on the virulence or geographic distribution of MDV strains, but the effects of these polymorphisms in the basic region of Meq on its protein function and MDV virulence remain uncharacterized.

In Chapter II, the effects of amino acid polymorphisms at positions 71, 77, and 80 in the basic region on its function and the virulence were examined. The transcriptional regulatory activity of Meq, in which amino acid substitutions at positions 71, 77, and 80, were introduced, was assessed by reporter assays. In addition, rMDVs were generated by replacing the native *meq* in the RB-1B strain with *meq* genes carrying mutations corresponding to the amino acid sequences at positions 71 and 77, or 77 and 80, and their virulence was assessed by experimental infection. Furthermore, to evaluate the influence of these polymorphisms on MDV pathogenesis, the dynamics of infected cells and major host T cell populations was investigated, and histopathological analyses of the lesions were conducted.

MATERIALS AND METHODS

Ethics statement

All animal experiments were approved by the Institutional Animal Care and Use Committee of Hokkaido University (Approval Number: 22-0088). All experiments were performed following the relevant guidelines and regulations of the Faculty of Veterinary Medicine of Hokkaido University, which is fully accredited by the Association for Assessment and Accreditation of Laboratory Animal Care International.

Cells

CEFs were isolated from chicken embryos of 10-day-old fertilized eggs (Iwamura Hatchery Co. Ltd.) as described in Chapter I. CEFs were maintained in Eagle's Minimum Essential Medium (Nissui Pharmaceutical Co., Ltd.) supplemented with 10% tryptose phosphate broth (Difco Laboratories), 0.03% L-glutamine, 100 U/mL penicillin, 100 μg/mL streptomycin, 10% calf serum (Sigma-Aldrich), and 0.1% sodium bicarbonate. DF-1was maintained in Dulbecco's Modified Eagle's Medium (FUJIFILM Wako Pure Chemical Corporation) supplemented with 0.03% L-glutamine, 100 U/mL penicillin, 100 μg/mL streptomycin, and 10% fetal bovine serum (MP Biomedicals). CEFs and DF-1 cells were incubated in a humidified atmosphere containing 5% CO_2 at 37°C and 39 °C, respectively.

Plasmids

Expression plasmids for each Meq isoform with mutations in the basic region were constructed. The ORF of RB-1B-*meq* (GenBank accession no. HM488349.1) was amplified and ligated into the pCI-neo vector (Promega), as described in Chapter I. Alanine-to-serine, lysine-to-glutamic acid, and aspartic acid-to-tyrosine substitutions were introduced at positions 71, 77, and 80, respectively, using site-directed mutagenesis. The mutations were introduced using primers as listed in Table II-1.

For reporter assays, a c-Jun expression plasmid was constructed (Levy *et al.*, 2003). Additionally, reporter plasmids containing the promoter regions of *pp38*, *meq,* and chicken *bcl-2* were constructed by inserting each promoter upstream of the firefly luciferase gene in the pGL3-Basic vector (Promega) as described in Chapter I. The pRL-TK *Renilla* luciferase plasmid (Promega) was utilized as an internal control.

Dual-luciferase reporter assay

DF-1 cells were seeded at 2.0×10^5 cells per well in 24-well plates and incubated for 24 hours at 39 °C with 5% CO_2. For reporter assays using the *meq* and chicken *bcl-2* promoters, each well was transfected with 300 ng of Meq expression plasmid, 200 ng of c-Jun expression plasmid, 500 ng of reporter plasmid, and 5 ng of pRL-TK, using Lipofectamine 2000 (Thermo Fisher Scientific) according to the manufacturer's protocol. For assays using the *pp38* promoters, DF-1 cells were transfected with 300 ng of Meq expression plasmid, 500 ng of the reporter plasmid, and 5 ng of pRL-TK. At 24 hours post-transfection, cells were lysed and luciferase activity was quantified. Firefly luciferase activity was normalized to *Renilla* luciferase activity, and the results were expressed relative to those from cells transfected with the empty pCI-neo vector. Three independent experiments were conducted in triplicate. Protein expression levels of each Meq isoform were verified by western blotting in all reporter assays.

Generation of recombinant viruses

RB-1B-based rMDVs encoding Meq, Meq71/77, or Meq77/80 were generated as described in Chapter I (Conradie *et al*., 2019; Sato *et al.*, 2022). pRB-1B_ΔIRL (kindly provided by Dr. Benedikt Kaufer; Engel *et al.*, 2012), was used to generate mutant recombinant viruses. The native *meq* in the TRL region of pRB-1B_ΔIRL was replaced with RB-1B-*meq*, *meq* carrying mutations corresponding to the amino acid sequences at positions 71 and 77 (alanine-to-serine and lysine-to-glutamic acid substitution, respectively; *meq71/77*), or *meq* carrying mutations corresponding to the amino acid sequences at positions 77 and 80 (lysine-to-glutamic acid and aspartic acid-to-tyrosine substitution, respectively; *meq77/80*) using a two-step Red recombination strategy (Tischer *et al*., 2006; Tischer and Kaufer, 2012).

The resulting BAC plasmids were subjected to RFLP analysis to verify that each *meq* was accurately inserted. The BAC plasmids encoding each rMDV genome were digested with BamHI-HF (New England Biolabs Japan Inc.) and screened by electrophoresis on 0.8% agarose gels. Insertion of each *meq* was further validated by PCR and DNA sequencing. rMDVs were reconstituted by transfecting the BAC plasmids into CEFs using the CalPhos Mammalian Transfection Kit (Takara Bio Inc.), and pCAGGS-Cre (Gene Bridges GmbH) was co-transfected to excise the BAC sequence. The resulting rMDVs were designated rRB-1B_Meq, rRB-1B_Meq71/77 and rRB-1B_Meq77/80, respectively. All reconstituted viruses were passaged several times on CEFs and stored at –80 °C in Cell Banker 1 (Nippon Zenyaku Kogyo Co., Ltd.). Restoration of the IRL region and removal of BAC sequences were confirmed by PCR. Viral titers were determined by plaque assays as previously reported (Engel *et al.*, 2012). To exclude the

presence of unintended mutations, the whole genomes of reconstituted rMDVs were sequenced using DNA extracted from CEFs infected with each rMDV. Whole genome sequencing was performed by Hokkaido System Science Co., Ltd. No mutations were detected in the ORFs previously associated with MDV virulence, except for the manipulated *meq* (BioSample accessions: LC862891).

In vitro replication of the recombinant viruses

Confluent monolayers of CEFs seeded in 12-well plates were infected with 50 PFU of recombinant virus. Infected cells were collected daily for five days. Total cellular DNA was extracted using the DNeasy Blood and Tissue Kit (Qiagen). Viral loads were quantified by qPCR to evaluate replication kinetics as described in Chapter I. Viral loads were calculated as the mean of three independent cultures, with all experiments performed in triplicate.

Expression of *meq* mRNA in cells infected with recombinant viruses *in vitro*

CEFs were seeded in 12-well plates and infected with 50 PFU of each rMDV. Infected cells were harvested daily for five days. Total RNA was extracted using TRI Reagent (Molecular Research Center, Inc., Cincinnati, OH, USA) in accordance with the manufacturer's protocol, and treated with DNase I (Promega) to remove unwanted genomic DNA. cDNA was synthesized using PrimeScript Reverse Transcriptase (Takara Bio Inc.). Expression levels of each *meq* isoform were quantified by qPCR as described in Chapter I.

Experimental infection

Fertilized eggs from white leghorn chickens (Iwamura Hatchery Co. Ltd.) were hatched in the laboratory, and the chicks were raised in isolators. PCR screening confirmed the absence of major infectious pathogens. In all experimental infections described below, each group of chickens was housed separately in individual isolators following group assignment. Clinical signs associated with MD were monitored daily for eight weeks after virus inoculation. Chickens showing clinical signs during the experimental period were euthanized by collecting heparinized whole blood from the hearts under deep general anesthesia induced by isoflurane inhalation (Zoetis Japan), and necropsy was performed to assess the presence of gross tumor lesions.

(i) First experimental infection with rRB-1B_Meq71/77

This experiment was conducted to evaluate survival rate, tumor incidence, lymphoid organ weight, and lymphocyte proportions in PBMCs, spleen, and thymus in chickens

infected with rRB-1B_Meq71/77. A total of 93 one-day-old chicks were randomly assigned to three groups and housed separately. Chickens were inoculated intraperitoneally with 5,000 PFU of rRB-1B_Meq ($n = 35$), rRB-1B_Meq71/77 ($n = 33$), or PBS (pH 7.4) as a negative control ($n = 25$). At 7, 14, 28, and 35 dpi, five chickens from each group were euthanized, and samples of blood, spleen, and thymus were collected. All remaining chickens without clinical signs at the end of the experimental period (56 dpi) were euthanized, and tumor incidence was assessed (uninfected control group: $n = 5$, rRB-1B_Meq-infected group: $n = 13$, rRB-1B_Meq71/77-infected group: $n = 8$). Spleen and tumor tissues were dissected with scissors, homogenized, and filtered through 40-μm cell strainers (BD Biosciences) to obtain single-cell suspensions, which were washed twice in PBS. Mononuclear cells from blood and spleen suspensions were isolated by density gradient centrifugation using Percoll (GE Healthcare), followed by two additional PBS washes. Isolated cells were preserved in Cell Banker 1 (Nippon Zenyaku Kogyo Co., Ltd.) for subsequent flow cytometric analysis.

(ii) Second experimental infection with rRB-1B_Meq71/77

This experiment was conducted to evaluate survival rate, tumor incidence, and histopathological changes. A total of 45 one-day-old chicks were randomly assigned to three groups and housed separately. Chickens were inoculated intraperitoneally with 10,000 PFU of rRB-1B_Meq ($n = 20$), rRB-1B_Meq71/77 ($n = 20$), or PBS (pH 7.4) as a negative control ($n = 5$). Blood samples were collected from five chickens per group at 7, 14, 28, and 35 dpi to monitor viral loads. All remaining chickens without clinical signs at the end of the experimental period (56 dpi) were euthanized, and tumor incidence was assessed (uninfected control group: $n = 5$, rRB-1B_Meq-infected group: $n = 10$, rRB-1B_Meq71/77-infected group: $n = 20$). For histopathological analysis, the spleen, bursa of Fabricius, and thymus were collected at 56 dpi: control ($n = 2$), rRB-1B_Meq-infected ($n = 3$), and rRB-1B_Meq71/77-infected ($n = 5$). Tissues were fixed in 10% neutral-buffered formalin (FUJIFILM Wako Pure Chemical Corporation) for 24 hours.

(iii) First experimental infection with rRB-1B_Meq77/80

This experiment was conducted to evaluate survival rate, tumor incidence, lymphoid organ weight, and lymphocyte proportions in PBMCs, spleen, bursa of Fabricius, and thymus in chickens infected with rRB-1B_Meq77/80. A total of 103 one-day-old chicks were randomly assigned to three groups and housed separately. Chickens were inoculated intraperitoneally with 5,000 PFU of rRB-1B_Meq ($n = 36$), rRB-1B_Meq77/80 ($n = 42$), or PBS (pH 7.4) as a negative control ($n = 25$). At 7, 14, 28, and 35 dpi, five chickens from each group were euthanized, and samples of blood, spleen, bursa of Fabricius, and thymus were collected. All remaining chickens without clinical signs at the end of the

experimental period (56 dpi) were euthanized, and tumor incidence was assessed (uninfected control group: n = 5, rRB-1B_Meq-infected group: n = 11, rRB-1B_Meq77/80-infected group: n = 14). Mononuclear cells from blood and spleen suspensions were isolated by density gradient centrifugation using Percoll (GE Healthcare), and isolated cells were preserved in Cell Banker 1 (Nippon Zenyaku Kogyo Co., Ltd.).

(iv) Second experimental infection with rRB-1B_Meq77/80

This experiment was conducted to evaluate survival rate, tumor incidence, and histopathological changes. A total of 45 one-day-old chicks were randomly assigned to three groups and housed separately. Chickens were inoculated intraperitoneally with 10,000 PFU of rRB-1B_Meq (n = 22), rRB-1B_Meq71/77 (n = 18), or PBS (pH 7.4) as a negative control (n = 5). Blood samples were collected from five chickens per group at 7, 14, 28, and 35 dpi to monitor viral loads. All remaining chickens without clinical signs at the end of the experimental period (56 dpi) were euthanized, and tumor incidence was assessed (uninfected control group: n = 5, rRB-1B_Meq-infected group: n = 12, rRB-1B_Meq71/77-infected group: n = 18). For histopathological analysis, the spleen, bursa of Fabricius, and thymus were collected at 56 dpi: control (n = 2), rRB-1B_Meq-infected (n = 3), and rRB-1B_Meq71/77-infected (n = 5). Tissues were fixed in 10% neutral-buffered formalin (FUJIFILM Wako Pure Chemical Corporation) for 24 hours.

DNA extraction and qPCR

Total cellular DNA was extracted from whole blood samples of infected chickens using the DNeasy Blood and Tissue Kit (Qiagen), following the manufacturer's instructions. qPCR was conducted to determine viral loads using primers specific to the *icp4* and the chicken *i-nos* as described in Chapter I. Viral loads were expressed as the ratio of *icp4* to *i-nos*.

Flow cytometric analysis

(i) Evaluation of the availability of Meq mAbs for flow cytometric analysis

For flow cytometric analysis, monoclonal antibodies against Meq were used (kindly provided by Dr. Kurokawa, National Agriculture and Food Research Organization, Japan; Kurokawa and Yamamoto, 2022). Anti-Meq mAbs (mouse IgG1 isotype) were purified from the supernatant of cultured hybridomas using Protein G Sepharose 4 Fast Flow (GE Healthcare, IL, USA) according to the protocol of the manufacturer. The purified antibody was conjugated with APC using Zenon Mouse IgG_1 Labeling Kit (Invitrogen, MA, USA).

The availability of anti-Meq mAb for flow cytometric analysis was confirmed by analyzing the expression of Meq in DF-1 cells transfected with the pCI-neo expression plasmid cloned with RB-1B-*meq*. The transfected DF-1 cells were washed twice with FACS buffer, followed by fixation and permeabilization using Cytofix/Cytoperm solution (BD Biosciences) for 30 minutes at 4 °C. Subsequently, cells were washed three times with Perm/Wash buffer (BD Biosciences). For intracellular staining, cells were incubated for 40 min at 4°C in the dark with either APC-conjugated mouse anti-Meq mAb or APC-conjugated mouse IgG_1 isotype control (Southern Biotech), followed by two washes with Perm/Wash buffer. The gating strategy for this analysis is shown in Fig. II-1. Following staining, cells were washed twice with 200 µL of FACS buffer and analyzed using a FACSLyric flow cytometer (BD Biosciences).

(ii) Flow cytometric analysis for PBMCs and mononuclear cells from spleen and thymus

PBMCs and mononuclear cells (5×10^5) isolated from the spleen or thymus were seeded into 96-well round-bottom plates and washed twice with FACS buffer (PBS supplemented with 1% bovine serum albumin; Sigma-Aldrich). To block nonspecific binding, cells were incubated with PBS containing 10% chicken serum (Thermo Fisher Scientific) at 25 °C for 15 minutes. Staining of cell surface molecules was performed using the following mAbs: mouse anti-chicken CD3ε (PerCP-Cy5.5), anti-chicken CD4 (PE-Cy7), anti-chicken CD8β (FITC), anti-chicken TCRγδ (PE) (all from Southern Biotech) at 4 °C for 30 minutes in the dark. Viable and non-viable cells were discriminated using Fixable Viability Dye eFluor780 (Thermo Fisher Scientific). For splenic cells obtained from both experimental infection, thymic cells from experimental infection with rRB-1B_Meq71/77, and PBMCs from experimental infection with rRB-1B_Meq77/80, cells were washed twice with FACS buffer, followed by fixation and permeabilization using Cytofix/Cytoperm solution (BD Biosciences) for 30 minutes at 4 °C. Subsequently, cells were washed three times with Perm/Wash buffer (BD Biosciences). For intracellular staining, cells were incubated for 40 min at 4°C in the dark with either APC-conjugated mouse anti-Meq mAb or APC-conjugated mouse IgG_1 isotype control (Southern Biotech), followed by two washes with Perm/Wash buffer. The gating strategy for this analysis is shown in Fig. II-1. Following staining, cells were washed twice with 200 µL of FACS buffer and analyzed using a FACSLyric flow cytometer (BD Biosciences). The absolute number of each T cell subset was quantified using CountBright™ absolute counting beads (Invitrogen, Waltham, MA, USA) and the following formula:

(Number of T cell subset events / Number of bead events) × Number of beads added

Histopathological analysis of rMDV-infected chickens

Histopathological and immunohistochemical (IHC) analyses were performed by National Agriculture and Food Research Organization. Monoclonal antibodies against Meq and pp38 (kindly provided by Dr. Kurokawa, National Agriculture and Food Research Organization, Japan) were utilized for IHC. Tissues from experimentally infected chickens were fixed in 10% neutral-buffered formalin (FUJIFILM Wako Pure Chemical Corporation) for 48 hours, embedded in paraffin, and sectioned. Sections were deparaffinized, treated with 0.3% hydrogen peroxide in methanol for 20 minutes at room temperature (20–26 °C) to block endogenous peroxidase activity, and blocked with 5% skim milk (FUJIFILM Wako Pure Chemical Corporation) for 20 minutes to reduce nonspecific binding. Primary antibodies (1.4 mg/ml for Meq, 4 μg/ml for pp38) were applied and incubated for 20–24 hours at 4 °C. Following PBS washes, sections were incubated with horseradish peroxidase-conjugated secondary antibody reagent (Histofine Simple Stain MAX PO [M] kit, Nichirei Bioscience) for 45 minutes at room temperature. Antigen-antibody reactions were visualized using a 3,3'-Diaminobenzidine Tetrahydrochloride (DAB) substrate kit (Nichirei Bioscience), and sections were counterstained with Mayer's hematoxylin (Muto Pure Chemicals) and coverslipping.

Two types of negative controls were employed: IHC with culture supernatants lacking anti-Meq antibodies to exclude nonspecific staining from hybridoma media, and IHC without primary antibodies to exclude the possibility of nonspecific reactions with the secondary antibodies. No positive signals were detected in tumor tissues from rRB-1B_Meq77/80-infected chickens in both negative controls. All stained sections were examined under a microscope.

Statistical analyses

Statistical analyses were conducted using R Statistical Software (version 4.0.3; R Foundation for Statistical Computing). Multi-step growth kinetics were analyzed using the Mann–Whitney U test. T cell dynamics were analyzed using the Kruskal–Wallis test followed by Dunn's post hoc test. Tumor incidence was compared between the groups using Fisher's exact test. Transactivation activity was analyzed using Tukey's multiple comparison test. Results with $p < 0.05$ were considered statistically significant.

Table II-1 Primers used to introduce mutations into the RB-1B-*meq*.

Position in Meq	Substitution	Type	Sequence
71	Alanine-to-serine	Forward	5′-AATCGTGACGCCTCTCGGAGAAGAC-3′
		Reverse	5′-GTCTTCTCCGAGAGGCGTCACGATT-3′
77	Lysine-to-glutamic-acid	Forward	5′-AGAAGACGCAGGGAGCAGACGTACT-3′
		Reverse	5′-AGTACGTCTGCTCCCTGCGTCTTCT-3′
80	Tytosine-to-aspartic acid	Forward	5′-AGGAAGCAGACGTACTATGTAGACA-3′
		Reverse	5′-TGTCTACATAGTACGTCTGCTTCCT-3′

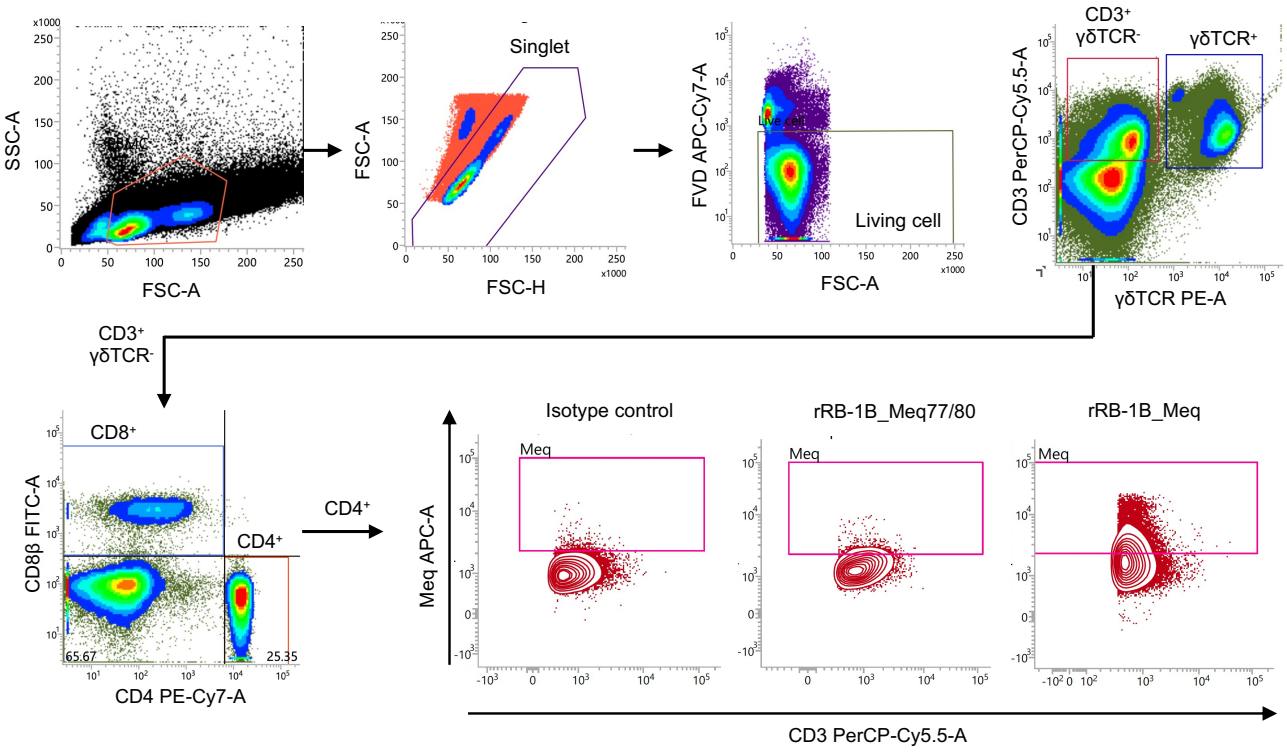

Figure II-1. Gating strategy for the analysis of the dynamics of major T cell subsets in chickens infected with rMDVs

A representative gating strategy is shown to analyze the dynamics of γδ T cells, $CD8^+$ T cells, and $CD4^+$ T cells. Dead cells were excluded using the Fixable Viability Dye eFluor780 (Thermo Fisher Scientific).

RESULTS

Effects of amino acid substitutions in the basic region on its transcriptional regulation activity

The effects of polymorphisms at positions 71, 77, and 80 in the basic region on its transcriptional regulation were evaluated using reporter assays targeting the *pp38*, *meq*, and *bcl-2* promoters. Accordingly, single, double, and triple mutant Meq expression plasmids were generated based on RB-1B-Meq. To compare the transcriptional repression of each Meq mutant, a reporter plasmid containing the *pp38* promoter along with each Meq construct was transfected into DF-1 cells. All Meq isoforms exhibited transcriptional repression on the *pp38* promoter (Fig. II-2A). Although differences were not statistically significant, Meq isoforms with single mutations tended to show reduced transcriptional repression. In contrast, Meq isoforms containing double or triple mutations demonstrated significantly diminished repression compared to the wild-type Meq. These results suggest that polymorphisms in the basic region of Meq in CVI988 and recent strains in Asia, Africa, and Europe impair its ability to repress the *pp38* promoter activity.

Next, the transactivation activity of Meq constructs with mutations in the basic region was assessed using *meq* and chicken *bcl-2* promoters. All Meq isoforms increased *meq* promoter activity, but the Meq isoforms with mutations exhibited significantly lower transactivation levels compared to wild-type Meq (Fig. II-2B). Among them, the Meq isoform carrying mutations at positions 71 and 77, which correspond to the amino acid sequence found in the CVI988 strain, demonstrated the weakest transactivation activity.

Similarly, all Meq isoforms enhanced *bcl-2* promoter activity (Fig. II-2C). However, the isoforms with a single mutation at position 80 or double mutations at positions 77 and 80 displayed transactivation activities comparable to that of the wild-type Meq. These findings suggest that polymorphic combinations in the basic region influence Meq-mediated transcriptional regulation, but the effects appear to vary depending on the combination of mutations and the type of promoter.

Generation and characterization of recombinant viruses *in vitro*

To assess whether combinations of polymorphisms at positions 71 and 77 or at positions 77 and 80 affect MDV virulence, a recombinant RB-1B-based MDV expressing Meq71/77 (rRB-1B_Meq71/77) or Meq77/80 (rRB-1B_Meq77/80) was generated using a two-step Red recombination strategy (Fig. II-3A; Tischer *et al*., 2006; Tischer and Kaufer, 2012), and rMDVs were reconstituted by transfecting the resulting BAC plasmids into CEFs. To verify that the recombination procedure did not affect viral replication or

meq expression *in vitro*, viral loads and *meq* transcription levels were evaluated in CEFs infected with rRB-1B_Meq, rRB-1B_Meq71/77, and rRB-1B_Meq77/80. No significant differences in replication kinetics were detected between rRB-1B_Meq and rRB-1B_Meq71/77, and between rRB-1B_Meq and rRB-1B_Meq77/80 (Figs. II-3B and D). Furthermore, RT-qPCR analysis confirmed no differences in the transcriptional level of *meq* mRNA *in vitro* (Figs. II-3C and E). These observations indicate that the recombination procedure did not impair viral replication or *meq* transcription *in vitro*.

Analysis of the pathogenesis in chickens infected with rRB-1B_Meq71/77

Virulence of rRB-1B_Meq71/77 *in vivo*

To assess the effect of polymorphisms at positions 71 and 77 on MDV virulence and tumorigenesis, one-day-old chickens were infected with 5,000 PFU of either rRB-1B_Meq or rRB-1B_Meq71/77. At 56 dpi, 60.0% of chickens infected with rRB-1B_Meq exhibited clinical signs such as leg paralysis and torticollis, and 56.7% developed solid tumors in visceral organs, including those euthanized at 56 dpi (Figs. II-4A and B). In contrast, no clinical signs or tumor formation were observed in chickens infected with rRB-1B_Meq71/77.

To determine whether rRB-1B_Meq71/77 retained pathogenic potential at a higher dose, the second experimental infection was performed using 10,000 PFU. In this setting, 50.0% of chickens infected with rRB-1B_Meq showed clinical signs, and 55.0% developed solid lymphomas (Figs. II-4C and D). However, even at this higher dose, no clinical signs or tumor formation were observed in the rRB-1B_Meq71/77-infected group. These results indicate that amino acid substitutions at positions 71 and 77 drastically decrease MDV virulence and tumorigenesis.

Changes in lymphoid organ weight in chickens infected with rRB-1B_Meq71/77

Cytolytic replication of MDV induces extensive apoptosis in the thymus and bursa of Fabricius, leading to atrophy of these lymphoid organs (Berthault *et al*., 2018). Additionally, MDV-mediated transformation of $CD4^+$ T cells results in their proliferation and contributes to enlargement in the spleen of infected chickens (Liu *et al*., 2023). To evaluate the impact of amino acid polymorphisms at positions 71 and 77 on these cytolytic replication and transformation induced by rMDV, the weights of the thymus, bursa, and spleen were measured at each time point.

The thymus weight in the rRB-1B_Meq-infected group was significantly lower than that in the control group at 14 dpi, indicating thymic atrophy (Fig. II-5A). Although the rRB-1B_Meq71/77-infected group also showed a trend toward lower thymus weight at 7

and 14 dpi, the differences were not statistically significant. The bursa weight was reduced in rRB-1B_Meq-infected chickens compared to controls at 14 dpi (Fig. II-5B). However, no significant differences in the bursa weight were detected between the rRB-1B_Meq71/77-infected and control groups throughout the experimental period. These results suggest that rRB-1B_Meq71/77 diminished potential to induce atrophy of the thymus and bursa compared to rRB-1B_Meq.

The spleen weights in both rMDV-infected groups tended to be elevated compared to the control group at 7 dpi (Fig. II-5C). From 14 dpi onward, the spleen weight in the rRB-1B_Meq-infected group increased compared to those of the rRB-1B_Meq71/77-infected and control groups and was significantly higher at 56 dpi. In contrast, the spleen weight in the rRB-1B_Meq71/77-infected group did not differ significantly from that of the control group after 14 dpi. Collectively, rRB-1B_Meq71/77 induces only transient pathogenic changes in lymphoid tissues during the early phase of infection, but no significant alterations were observed during the later phase.

Histopathological analysis of chickens infected with rRB-1B_Meq71/77

Histopathological analysis was conducted on chickens at 56 dpi in the second experimental infection (control group: n = 2; rRB-1B_Meq71/77 group: n = 5; rRB-1B_Meq group: n = 3). In the rRB-1B_Meq-infected group, all chickens exhibited extensive infiltration of Meq^+ cells throughout the spleen and macrophage infiltration in the red pulp. In contrast, Meq^+ cells were detected in the spleens of only two out of five chickens in the rRB-1B_Meq71/77-infected group, and no proliferative tumor lesions were observed in any of these chickens (Figs. II-6A and B; Table II-2). Similarly, infiltration of Meq^+ cells was observed in the thymus and bursa of Fabricius in all chickens infected with rRB-1B_Meq. In the rRB-1B_Meq71/77-infected group, Meq^+ cells were also detected in the thymus and bursa in two of five chickens, but no proliferative tumor cell infiltration was found in each organ (Figs. II-6C and D; Table II-2).

Replication of rRB-1B_Meq71/77 *in vivo*

To assess the replication kinetics of rRB-1B_Meq71/77 *in vivo*, viral loads in whole blood, spleen, thymus, and feather tips were quantified by qPCR. In both the first and second experiments, the whole blood of chickens infected with rRB-1B_Meq71/77 showed significantly lower viral loads during the later phase of infection, compared to chickens infected with rRB-1B_Meq (Figs. II-7A and B). Similarly, viral loads in the spleen and thymus were markedly reduced in the rRB-1B_Meq71/77-infected group after

14 dpi (Figs. II-7C and D). In feather tips, a significant reduction in viral load was also observed in the rRB-1B_Meq71/77-infected group at 56 dpi (Figs. II-7E). These results suggest that the replication efficiency of rRB-1B_Meq71/77 *in vivo* is significantly lower than that of rRB-1B_Meq.

Dynamics of $CD4^+$ T and Meq^+ cells in the spleens of chickens infected with rRB-1B_Meq71/77

The anti-Meq mAbs (kindly provided by Dr. Kurokawa, National Agriculture and Food Research Organization, Japan) were subsequently employed to analyze Meq^+ cells. Before flow cytometric analysis, the applicability of this mAbs was validated through intracellular staining of DF-1 cells transfected with a Meq expression plasmid and western blotting (Figs. II-8).

The dynamics of T cell subsets in the spleen of rMDV-infected chickens were analyzed by flow cytometry at each time point in the first experimental infection. The absolute number of $CD4^+$ T cells was significantly elevated in rRB-1B_Meq-infected chickens compared to the control group from 28 dpi onward (Figs. II-9A and B). In the rRB-1B_Meq71/77-infected group, the number of $CD4^+$ T cells also increased at 28 dpi and reached significantly higher levels than those in the control group at 35 dpi. However, by 56 dpi, the number of $CD4^+$ T cells had returned to levels comparable to the control group. Throughout the experimental period from 14 dpi onward, the absolute number of $CD4^+$ T cells in rRB-1B_Meq71/77-infected chickens remained consistently lower than in the rRB-1B_Meq-infected group, with a statistically significant difference at 56 dpi.

To characterize the dynamics of infected cells, the proportion of Meq^+ cells within the $CD4^+$ T cell population was assessed. In rRB-1B_Meq-infected chickens, Meq^+ $CD4^+$ T cells were detected in all individuals, and both the percentage of Meq^+ cells among $CD4^+$ T cells and the absolute number of Meq^+ $CD4^+$ T cells increased progressively throughout the experimental period (Figs. II-9C and D). In contrast, in rRB-1B_Meq71/77-infected chickens, the proportion of Meq^+ $CD4^+$ T cells peaked at 7 dpi (7.1%) and thereafter gradually declined to below 1% (Fig. II-9C). At all-time points, the proportion of Meq^+ cells among $CD4^+$ T cells in the rRB-1B_Meq71/77-infected group was significantly lower than in the rRB-1B_Meq-infected group. Moreover, the absolute number of Meq^+ $CD4^+$ T cells in rRB-1B_Meq71/77-infected chickens did not increase over time and remained significantly lower than in rRB-1B_Meq-infected chickens from 14 dpi onward (Fig. II-9D).

Dynamics of CD8$^+$ T cells and γδ T cells in the spleens of chickens infected with rRB-1B_Meq71/77

The dynamics of CD8$^+$ T cells in rMDV-infected chickens were analyzed. In rRB-1B_Meq-infected chickens, the absolute number of CD8$^+$ T cells tended to increase at 7 dpi compared to the control group. From 14 to 35 dpi, the number of CD8$^+$ T cells was significantly higher in the rRB-1B_Meq group than in the control group (Figs. II-9E and F). In contrast, chickens infected with rRB-1B_Meq71/77 exhibited a significantly higher number of CD8$^+$ T cells than the control group at 7 dpi. At 28 and 35 dpi, although CD8$^+$ T cell numbers in the rRB-1B_Meq71/77 group remained significantly elevated compared to the control group, they tended to be lower than those observed in the rRB-1B_Meq group.

Next, the dynamics of γδ T cells were also evaluated. In rRB-1B_Meq-infected chickens, the absolute number of γδ T cells increased slightly at 28 and 35 dpi compared to the control group (Figs. II-9G and H). In the rRB-1B_Meq71/77 group, the number of γδ T cells was significantly higher than that of the control group at 7 dpi, but this difference was not observed throughout the later phase of infection.

Dynamics of T cell subsets in the thymus of chickens infected with rRB-1B_Meq71/77

The dynamics of T cell subsets in the thymus were also analyzed to evaluate the effects of rRB-1B_Meq71/77 infection. In the rRB-1B_Meq71/77-infected group, the absolute number of CD4$^+$ T cells (TCRγδ$^-$ CD3$^+$ CD4$^+$) was significantly decreased at 7 dpi compared to the control group (Figs. II-10A and B), suggesting that cytolytic infection of CD4$^+$ T cells occurred in the rRB-1B_Meq71/77-infected group during the early phase of infection. After 14 dpi, both infected groups showed an increased number of CD4$^+$ T cells compared to the control group, with statistically significant differences at several time points. Despite the overall increase in CD4$^+$ T cell numbers in the later phase of infection, in the rRB-1B_Meq71/77-infected group, the proportion of Meq$^+$ cells within the CD4$^+$ T cell population and the absolute number of Meq$^+$ CD4$^+$ T cells remained lower than those in the rRB-1B_Meq-infected group from 14 dpi onward (Figs. II-10C and D). These results suggest that although the number of CD4$^+$ T cells increased along with disease progression, transformed T cells did not expand in the thymus of chickens infected with rRB-1B_Meq71/77.

Similar dynamics were observed in CD8$^+$ T cells (TCRγδ$^-$CD3$^+$CD8β$^+$). In both rMDV-infected groups, the number of CD8$^+$ T cells slightly decreased at 7 dpi, followed by a gradual increase relative to the control group. Statistically significant elevations were

observed at 28 and 56 dpi in the rRB-1B_Meq71/77-infected group, and at 35 dpi in the rRB-1B_Meq-infected group (Figs. II-10E and F). In contrast, the absolute number of γδ T cells (TCRγδ$^+$ CD3$^+$) in the thymus declined at 7 dpi in both rMDV-infected groups, with a significant reduction observed in the rRB-1B_Meq-infected group compared to the control group (Figs. II-10G and H). Throughout the experimental period, the number of γδ T cells remained consistently lower in both infected groups than in the control group, suggesting sustained suppression of γδ T cell subset following rMDV infection.

Analysis of the pathogenesis in chickens infected with rRB-1B_Meq77/80

Virulence of rRB-1B_Meq77/80 *in vivo*

To investigate the impact of amino acid substitutions at positions 77 and 80 on the virulence and tumorigenicity of MDV, one-day-old chickens were inoculated intra-abdominally with 5,000 PFU of either rRB-1B_Meq or rRB-1B_Meq77/80. Two independent experimental infections were performed.

In the first experiment, 50% of chickens infected with rRB-1B_Meq developed neurological signs, including leg paralysis and torticollis, by 56 dpi. Solid tumors were observed in visceral organs in half of the rRB-1B_Meq-infected chickens, including those euthanized at 56 dpi (Figs. II-11A and B). On the other hand, the group infected with rRB-1B_Meq77/80 exhibited a significantly reduced mortality rate. However, two chickens in this group developed clinical signs, such as open-mouth breathing and depression. No solid tumors were identified in any individuals.

To further investigate the pathogenic potential of rRB-1B_Meq77/80, an increased viral dose of 10,000 PFU was administered to one-day-old chickens. Throughout the experimental period, no dead chickens were observed in the rRB-1B_Meq77/80-infected group (Fig. II-11C). Although two chickens exhibited transient mild respiratory signs, including open-mouth breathing, both individuals fully recovered without wasting or feeding difficulties. By 56 dpi, solid tumor lesions were detected in two chickens from this group (Fig. II-11D). One chicken developed tumors in the spleen and liver, while the other showed lesions in the lung, kidney, and glandular stomach. These findings suggest that the amino acid substitutions at positions 77 and 80 considerably decrease virulence, although residual oncogenic potential may persist under higher viral challenge conditions.

Changes in lymphoid organ weight in chickens infected with rRB-1B_Meq77/80

To evaluate the effects of amino acid polymorphisms at positions 77 and 80 on lymphoid tissues of infected chickens, the relative weights of the thymus, bursa, and spleen were assessed at each time point. At 14, 28, and 35 dpi, the thymus weight was

significantly reduced in both rMDV-infected groups compared to the control group (Fig. II-12A), indicating thymic atrophy. However, chickens infected with rRB-1B_Meq77/80 displayed milder thymic atrophy than those infected with rRB-1B_Meq, although the difference was not statistically significant. Similarly, bursal atrophy was observed at 28 dpi in both infected groups (Fig. II-12B). These findings indicate that rRB-1B_Meq77/80 also causes lymphoid atrophy, but the severity of atrophy in the lymphoid tissues appears to be milder compared to rRB-1B_Meq. These data suggest that amino acid substitutions in the basic region influence the severity of lymphoid tissue atrophy.

Progressive enlargement of the spleen was observed in both groups infected with rMDVs with significant increases in spleen weights compared to those of control group throughout the experimental period (Fig. II-12C). However, the weight of the spleens of chickens infected with rRB-1B_Meq77/80 was significantly lower than that of the rRB-1B_Meq-infected group at 56 dpi (rRB-1B_Meq77/80 vs. rRB-1B_Meq, $p = 0.042$). These results suggest that the severity of the pathogenesis in the spleen of rRB-1B_Meq77/80 is reduced relative to that of rRB-1B_Meq.

Replication of rRB-1B_Meq77/80 *in vivo*

To investigate the replication kinetics of rMDVs *in vivo*, viral loads in whole blood were quantified using qPCR in the first and second experimental infections. In both experiments, chickens infected with rRB-1B_Meq consistently exhibited higher viral loads than those infected with rRB-1B_Meq77/80, although statistically significant differences were limited to certain time points (Figs. II-13A and B).

Additionally, viral loads were assessed in the spleen, thymus, and feather tips. In the spleen and thymus, viral loads in the rRB-1B_Meq-infected group tended to be elevated at 28 and 35 dpi compared to those in the rRB-1B_Meq77/80 group (Figs. II-13C and D). In contrast, no significant differences in viral load were detected in the feather tips between the two infected groups throughout the experimental period (Fig. II-13E).

Dynamics of $CD4^+$ T cells and Meq^+ cells in the PBMCs and spleens of chickens infected with rRB-1B_Meq77/80

The dynamics of T cell subsets in PBMCs and spleens in the first experimental infection were analyzed. In this experiment, no significant increase in the proportion of $CD4^+$ T cells was observed in the PBMCs of rMDV-infected chickens (Fig. II-14A). However, a significantly higher proportion of Meq^+ cells among $CD4^+$ T cells was detected in the PBMCs of rRB-1B_Meq-infected chickens compared to those infected with rRB-1B_Meq77/80 at 56 dpi, suggesting an expansion of MDV-transformed cells

(Fig. II-14B). In contrast, although a gradual increase in the proportion of Meq^+ cells was observed in rRB-1B_Meq77/80-infected chickens, the rate of increase remained markedly lower than that of the rRB-1B_Meq-infected group.

A significantly higher proportion of $CD4^+$ T cells was detected in the spleens of chickens infected with rRB-1B_Meq compared to those infected with rRB-1B_Meq77/80 at 56 dpi ($p = 0.013$; Fig. II-14C). Consistently, the absolute number of $CD4^+$ T cells in the spleen of the rRB-1B_Meq-infected group was elevated compared to the control group at 35 and 56 dpi. In contrast, the rRB-1B_Meq77/80-infected group exhibited persistently a lower number of $CD4^+$ T cells compared to the rRB-1B_Meq group throughout the experimental period (Figs. II-14D and E).

Although no significant differences in the proportion of Meq^+ cells within the $CD4^+$ T cell population between both infected groups were observed at 28 dpi, the proportion of Meq^+ cells was significantly lower than in the rRB-1B_Meq77/80-infected group than in the rRB-1B_Meq group at 35 and 56 dpi (Fig. II-14F). Interestingly, relatively high proportions of Meq^+ $CD4^+$ T cells were still detected in one individual at 35 dpi and two individuals at 56 dpi in the rRB-1B_Meq77/80-infected group. Additionally, two individuals, in which higher proportions of Meq^+ $CD4^+$ T cells were observed, exhibited open-mouth breathing at 44 dpi (Table II-3). The absolute number of Meq^+ $CD4^+$ T cells gradually increased in both infected groups over time, but the absolute number was significantly lower in the rRB-1B_Meq77/80-infected group than in the rRB-1B_Meq-infected group at 35 and 56 dpi (Fig. II-14G).

Dynamics of $CD8^+$ T cells and γδ T cells in the PBMCs and spleens of chickens infected with rRB-1B_Meq77/80

The dynamics of $CD8^+$ T cells in rMDV-infected chickens were investigated. In PBMCs from chickens infected with both rMDVs, the proportion of $CD8^+$ T cells increased at 7 and 14 dpi, although differences were not statistically significant. Notably, significant elevations in the proportion of $CD8^+$ T cells were observed at 35 and 56 dpi in both infected groups compared to the control group (Fig. II-15A). At 56 dpi, the rRB-1B_Meq77/80-infected group displayed a significantly higher proportion of $CD8^+$ T cells than the rRB-1B_Meq-infected group ($p = 0.039$).

In the spleen, a significant increase in $CD8^+$ T cell proportions was observed in rRB-1B_Meq77/80-infected chickens at 14 dpi compared to the control group (Fig. II-15B). Furthermore, the absolute number of $CD8^+$ T cells was significantly elevated in the spleen of rRB-1B_Meq77/80-infected chickens at 7 and 56 dpi compared to the control group,

and significantly higher than that in the rRB-1B_Meq-infected chickens at 56 dpi (p = 0.047) (Figs.II-15C and D).

The proportion of γδ T cells was also examined. In PBMCs, the percentage of γδ T cells in both rMDV-infected groups tended to be lower than that in the control group at 14 and 28 dpi (Fig. II-15E). Furthermore, the proportion of γδ T cells in the rRB-1B_Meq-infected group was significantly lower than that in both the rRB-1B_Meq77/80-infected and control groups at 35 dpi (p = 0.043). Similarly, the proportion of γδ T cells in the rRB-1B_Meq-infected group was significantly lower than the control group between 28 and 56 dpi. Although the γδ T cell proportion in the spleens of the rRB-1B_Meq77/80-infected group also exhibited a declining trend compared to the control group at 35 and 56 dpi, the γδ T cell proportion remained significantly higher than that of the rRB-1B_Meq-infected group at 56 dpi (p = 0.0016) (Fig. II-15F). Additionally, the absolute number of γδ T cells in the spleen was significantly higher in the rRB-1B_Meq77/80-infected group than in the rRB-1B_Meq group at 56 dpi (p = 0.0049) (Figs. II-15G and H).

Taken together, these data suggest that rRB-1B_Meq77/80 infection did not increase the number of $CD4^+$ T cells in PBMCs and the spleen, whereas rRB-1B_Meq77/80-infected chickens exhibited a higher number of $CD8^+$ T cells in both PBMCs and spleens. Although the number of γδ T cells was reduced in both rMDV-infected groups relative to the control group, the RB-1B_Meq77/80-infected group showed a higher proportion of γδ T cells than the RB-1B_Meq-infected group.

Histopathological analysis of chickens infected with rRB-1B_Meq77/80

Histopathological analysis was conducted using samples collected at 56 dpi in the second experimental infection (control group: n = 2; rRB-1B_Meq77/80-infected group: n = 5; rRB-1B_Meq-infected group: n = 3). In the rRB-1B_Meq-infected group, all chickens exhibited solid tumor formation in the liver, kidneys, and gonads, with extensive infiltration of Meq^+ cells observed across multiple organs (Table II-4). In contrast, only two out of five chickens infected with rRB-1B_Meq77/80 developed small solid tumors in the spleen, lungs, and liver, and the extent of lymphoma cell infiltration in each organ was markedly reduced compared to that in rRB-1B_Meq-infected chickens (Table II-4). Moreover, tumor lesions in the livers of rRB-1B_Meq77/80-infected chickens consisted of Meq^+ cells and infiltrating lymphocytes (Figs.II-16A and B), which were not observed in the rRB-1B_Meq-infected group.

In the rRB-1B_Meq77/80-infected group, four chickens exhibited hyperplasia of bronchus-associated lymphoid tissue (BALT) in the lungs, characterized by marked

infiltration and proliferation of lymphoid cells within both follicular and interfollicular regions (Figs. II-16C and D). Although small numbers of Meq^+ lymphocytes were detected in non-tumor regions of different organs, such as the spleen and thymus of two chickens, the majority of lymphocytes in the BALT were Meq-negative (Table II-4; Fig. II-16E), suggesting inflammatory changes with airway stenosis. IHC detected no pp38-positive cells, a marker of lytic viral replication, in the lungs of rRB-1B_Meq77/80-infected chickens (Fig. II-16F). In contrast, neither the control nor rRB-1B_Meq-infected group exhibited BALT hyperplasia (Figs. II-16G and H). Instead, some lung samples from rRB-1B_Meq-infected chickens showed extensive infiltration of Meq^+ T cells (Table II-4).

Intranuclear inclusion bodies were consistently observed in the skin of all rRB-1B_Meq-infected chickens; in addition, IHC analysis revealed $pp38^+$ cells in most FFE cells (mean proportion of feathers with $pp38^+$ cells: neck skin, 47%; thigh skin, 73%) (Table II-4). In contrast, no intranuclear inclusion bodies were detected in rRB-1B_Meq77/80-infected chickens, and $pp38^+$ cells were significantly fewer (neck skin, 14%; thigh skin, 0%).

Collectively, these results suggest that rRB-1B_Meq77/80 displays markedly reduced tumorigenic potential and milder disease progression compared with rRB-1B_Meq. In contrast, chickens infected with rRB-1B_Meq77/80 seem to exhibit severe lung inflammation, whereas this finding was absent in chickens infected with rRB-1B_Meq.

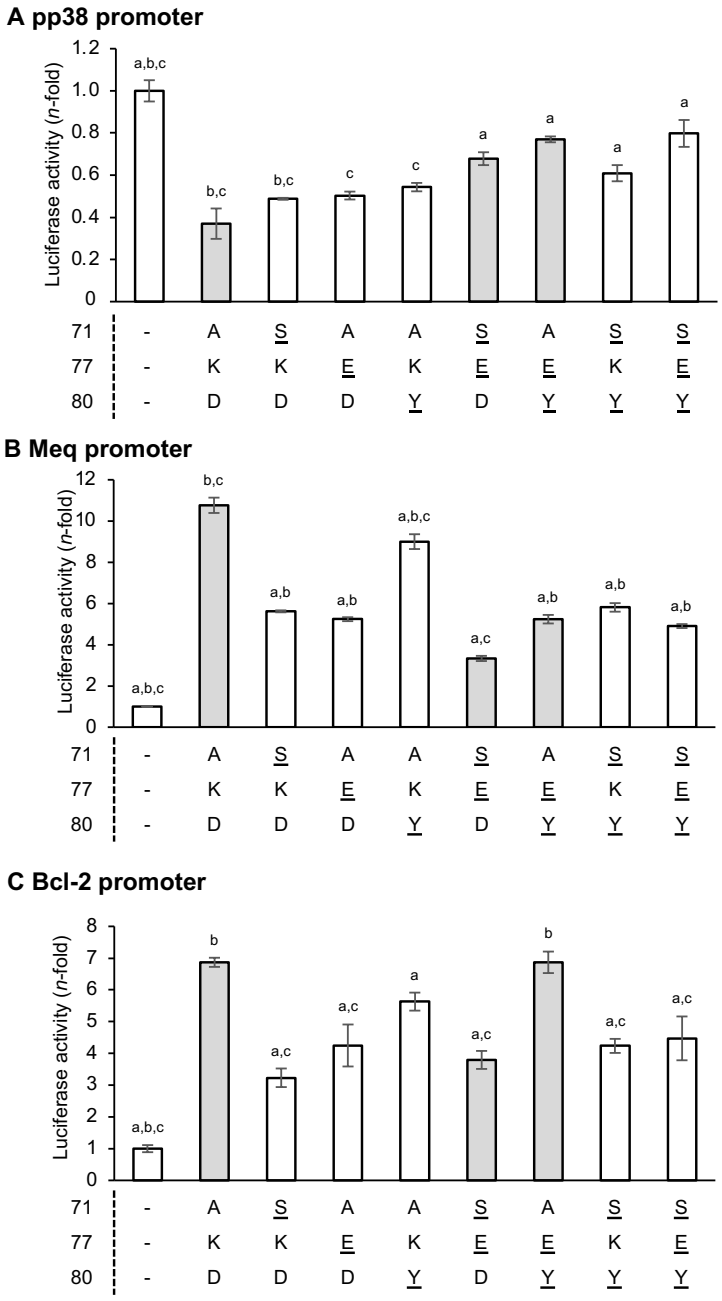

Figure II-2. Analysis of the effect of polymorphisms in the basic region on Meq-induced transcriptional regulation

(A) Transrepression effects of the Meq isoforms. The transrepression effects of each Meq isoform on *pp38* promoter-driven luciferase activities were compared. DF-1 cells in each well were transfected with 300 ng of expression plasmids for each Meq isoform, 500 ng of reporter plasmid, and 5 ng of the control pRL-TK plasmid. Luciferase activities were analyzed 24 h post-transfection. Firefly luciferase activity is expressed relative to the mean basal activity in the presence of pCI-neo after normalization to Renilla luciferase activity. (B and C) Transactivation activities of the Meq isoforms. The transactivation activities of each Meq isoform on the (B) *meq* promoter- and (C) *bcl-2* promoter-driven luciferase activities were compared. DF-1 cells in each well were transfected with 300 ng of expression plasmids for each Meq isoform, 200 ng of c-Jun expression plasmid, 500 ng of reporter plasmid, and 5 ng of the control pRL-TK plasmid. The gray bars indicate Meq isoforms with the amino acid sequences in the basic region found in the field strains. The tables below each graph show the amino acid residues at positions 71, 77, and 80 of each Meq isoform. Error bars indicate the standard deviations. (a: $p < 0.01$, vs. Meq (71A, 77K, 80D); b: $p < 0.01$, vs. Meq (71S, 77E, 80D); c: $p < 0.01$, vs. Meq (71A, 77E, 80Y); Tukey's multiple comparison test)

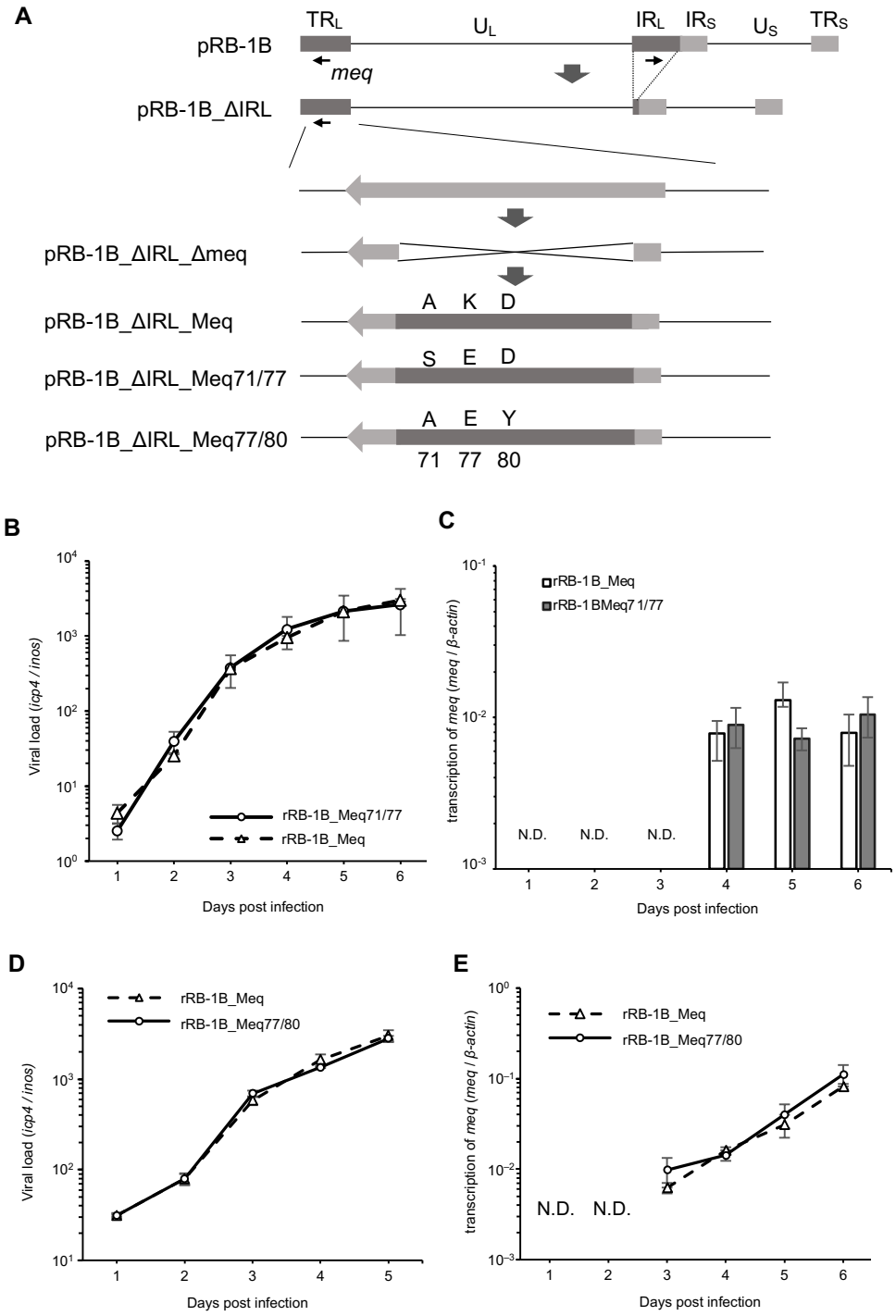

Figure II-3. Reconstitution of rMDVs and their characterization *in vitro*
(A) Schematic diagrams of the constructs cloned using the RB-1B genome in this study. pRB-1B_ΔIRL was used for mutagenesis. *meq* in the TRL was replaced with RB-1B-*meq* or *meq77/80* via two-step Red-mediated mutagenesis. (B and D) Chicken embryo fibroblasts (CEFs) were infected with 50 pfu of rMDVs. The infected cells were collected daily for 6 days, and the viral loads were analyzed using qPCR. (C and E) mRNA expression of each *meq* isoform in CEFs infected with rRB-1B_Meq, rRB-1B_Meq71/77, and rRB-1B_Meq77/80 as confirmed using reverse transcription-qPCR. The growth and gene expression kinetics among the groups were analyzed using the Kruskal–Wallis test. N.D., not determined.

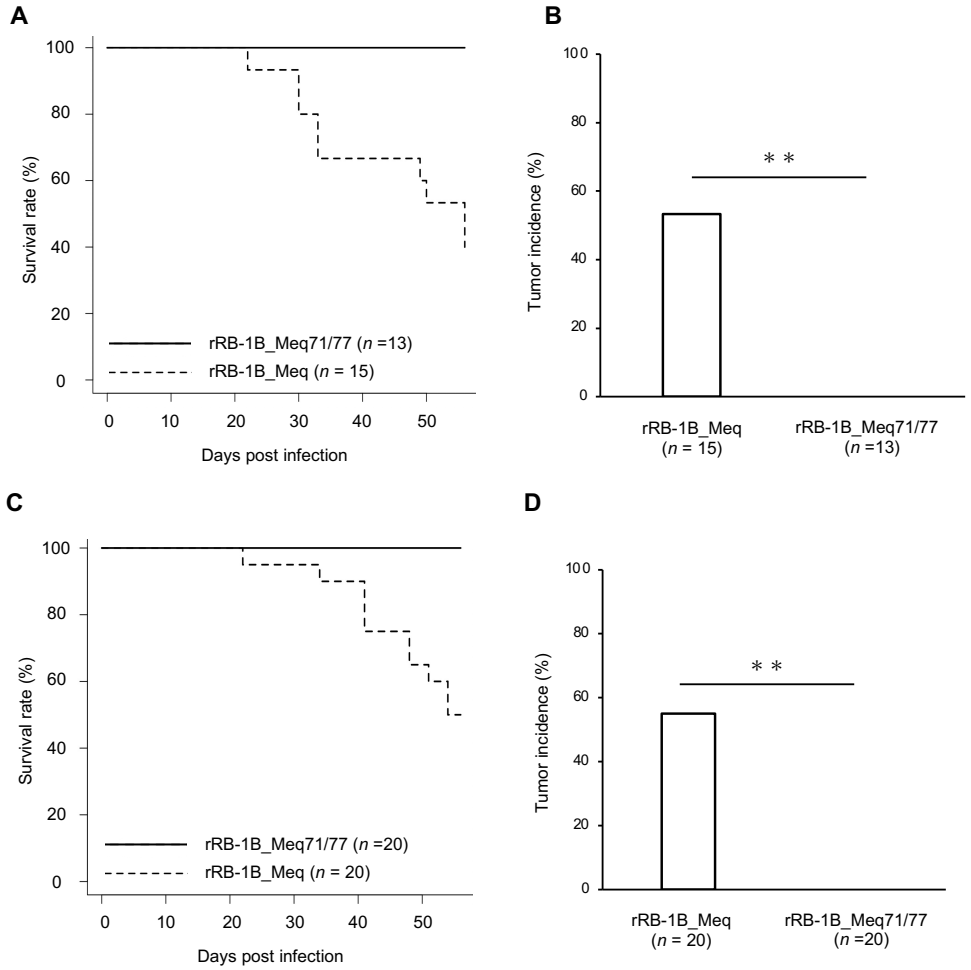

Figure II-4. Mortality and tumor incidence in chickens infected with rRB-1B_Meq71/77
(A and C) Survival rate in chickens infected with rMDVs in (A) the first and (C) the second experimental infections. Survival differences between groups were analyzed using the log-rank test; *p*-values were < 0.01 in both experiments. (B and D) Tumor incidence in chickens infected with rMDVs throughout the experimental period, including those euthanized at 56 dpi. Asterisks indicate significant differences (** $p < 0.01$; Fisher's exact test).

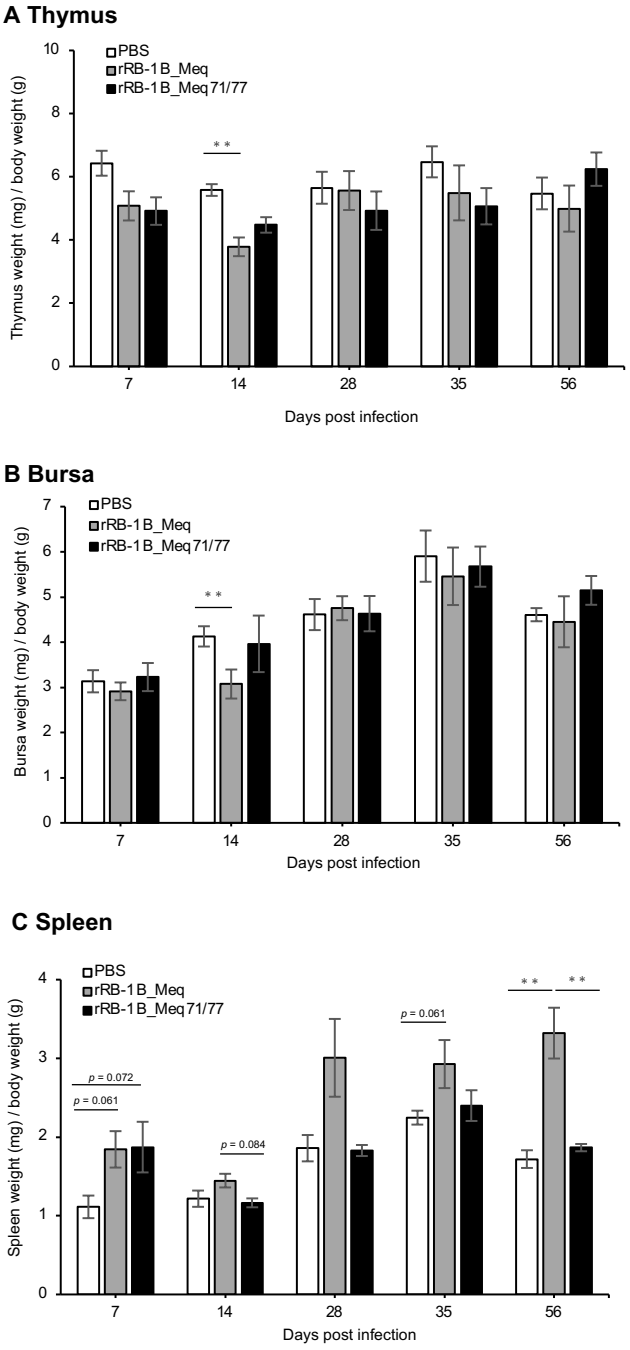

Figure II-5. Change in lymphoid organ weight in chickens infected with rRB-1B_Meq71/77
The dynamics of the lymphoid organ-to-body weight ratios for the (A) thymus, (B) bursa of Fabricius, and (C) spleens in chickens infected with rRB-1B-Meq or rRB-1B-Meq71/77 were analyzed at each time point throughout the experimental period. The spleens, thymuses, and bursas were collected from five chickens per group at 7, 14, 28, and 35 dpi, and from all remaining chickens (uninfected control group: $n = 5$, rRB-1B_Meq-infected group: $n = 13$, rRB-1B_Meq71/77-infected group: $n = 8$) at the termination of the experiment at 56 dpi in the first animal experiment. Statistical significance was determined using Dunn's test. ** $p < 0.01$ and * $p < 0.05$.

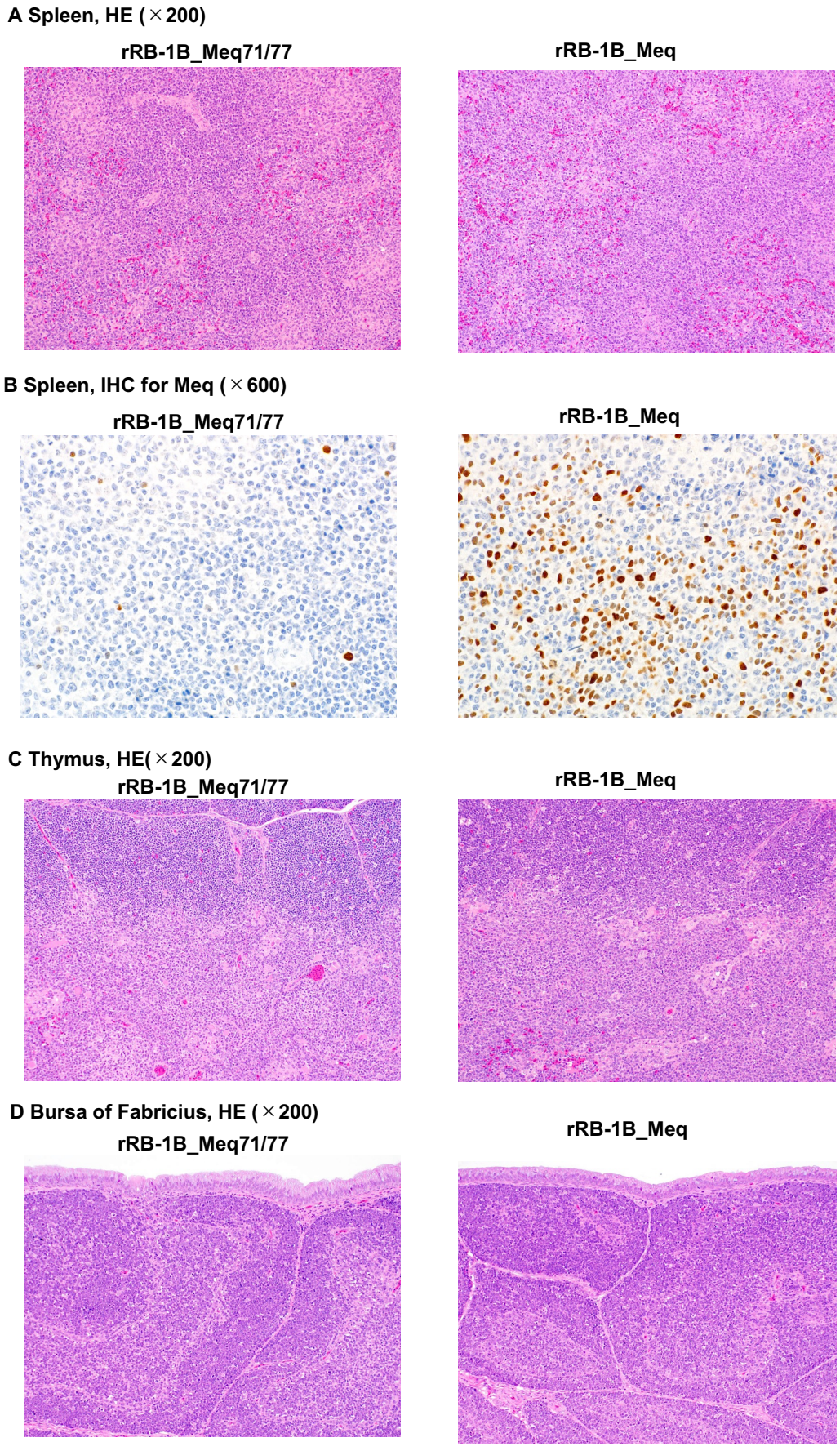

Figure II-6. Histopathological analysis of chickens infected with rRB-1B_Meq71/77
Hematoxylin-eosin staining was performed on the spleen (A), thymus (C), and bursa of Fabricius (D) from chickens in the control, rRB-1B_Meq77/80-infected, and rRB-1B_Meq-infected groups. (B) Immunohistochemical staining for Meq in the spleen of chickens infected with either rRB-1B_Meq or rRB-1B_Meq71/77.

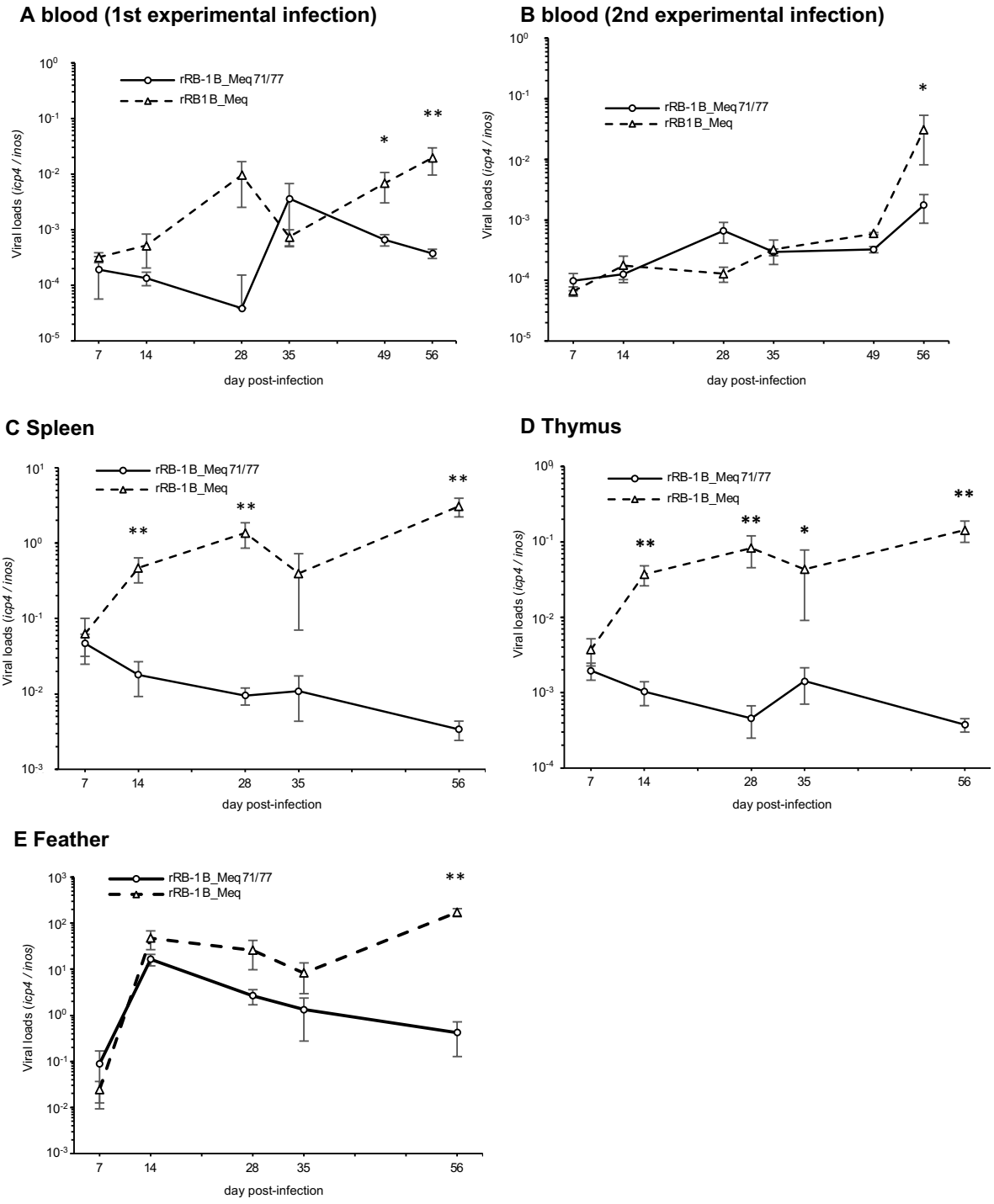

Figure II-7. Replication kinetics of rRB-1B_Meq71/77 *in vivo*

The viral loads in the (A) whole blood in the first experimental infection, (B) whole blood in the second experimental infection, (C) spleens, (D) thymus, and (E) feather tips from chickens infected with rRB-1B_Meq or rRB1B_Meq71/77 were determined by qPCR. Asterisks indicate significant differences (** $p < 0.01$, * $p < 0.05$; the Mann–Whitney U test)

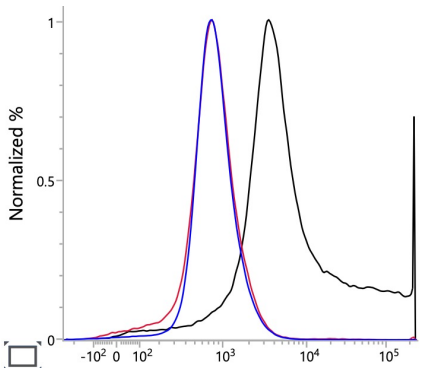

Figure II-8. Verification of binding of anti-Meq monoclonal antibodies
DF-1 cells were transfected with pCI-neo vector inserted with the *meq* gene. Transfected DF-1 cells were incubated with anti-Meq monoclonal antibodies (mAbs) for 30 min. The binding was analyzed using flow cytometry. The red line represents the binding of isotype control antibodies to the transfected DF-1 cells. The blue line represents the binding of anti-Meq mAbs to the DF-1 cells transfected with the pCI-neo vector that was not inserted with the gene.

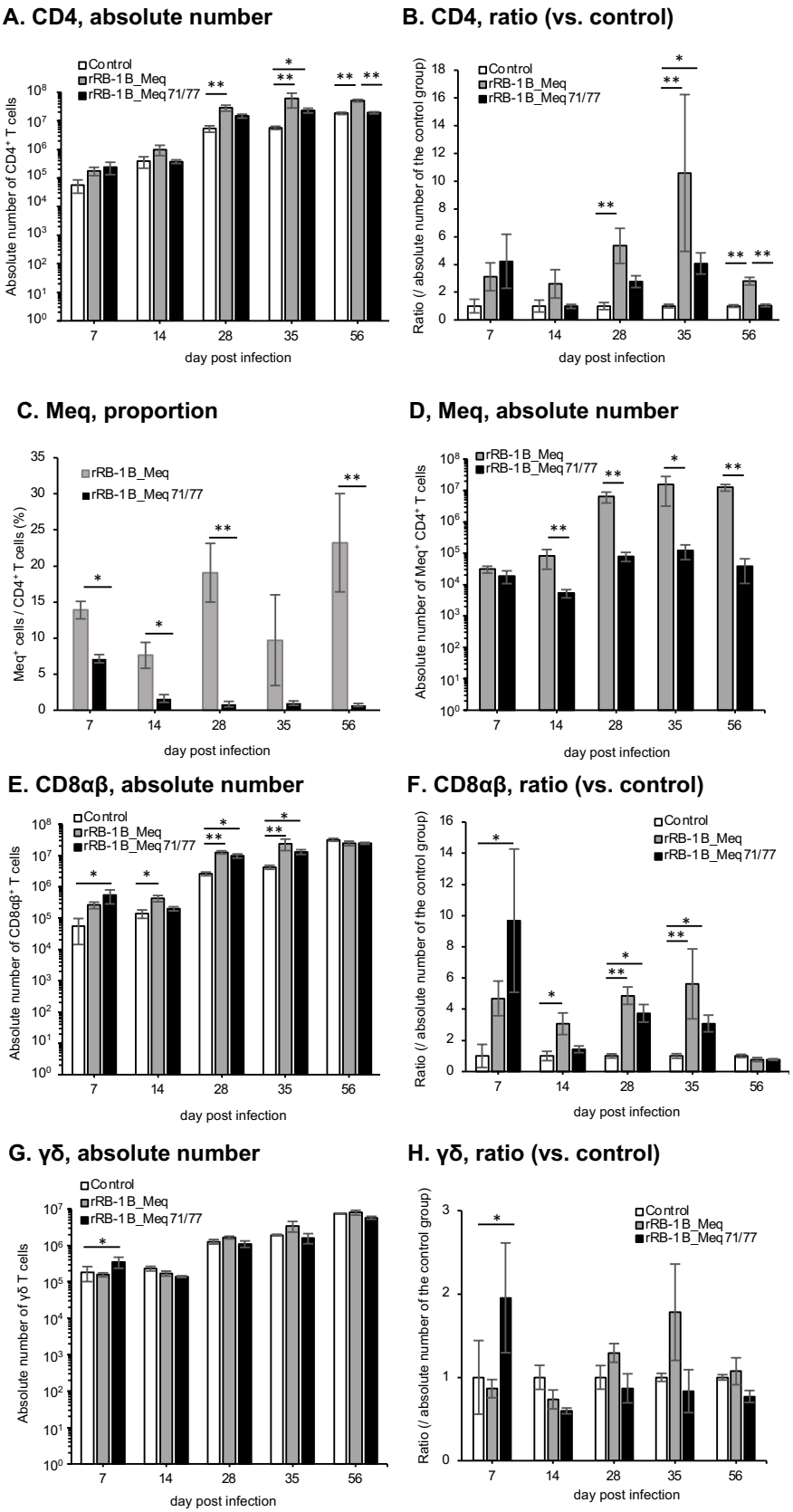

Figure II-9. Dynamics of T cell subsets in the spleen of chickens infected with rRB-1B_Meq71/77
Shown are the dynamics of $CD4^+$ cells, Meq^+ cells, $CD8^+$ cells, and γδ T cells from mononuclear cells isolated from the spleens of chickens infected with rRB-1B-Meq or rRB-1B-Meq71/77 at each time point during the experimental period. Absolute numbers of (A) $CD4^+$ T cells, (D) Meq^+ cells, (E) $CD8\alpha\beta^+$ T cells, and (G) $\gamma\delta TCR^+$ T cells in the spleen were analyzed. The ratios of absolute numbers of (B) $CD4^+$ T cells, (F) $CD8\alpha\beta^+$ T cells, and (H) $\gamma\delta TCR^+$ T cells in the spleen relative to the control group were analyzed. (C) The percentages of Meq^+ cells in the $CD4^+$ T cell population in the spleen were analyzed. Asterisks indicate significant differences (* $p < 0.05$, ** $p < 0.01$; Dunn's test in A, B, E, F,G and H. Mann-Whitney U test in C and D).

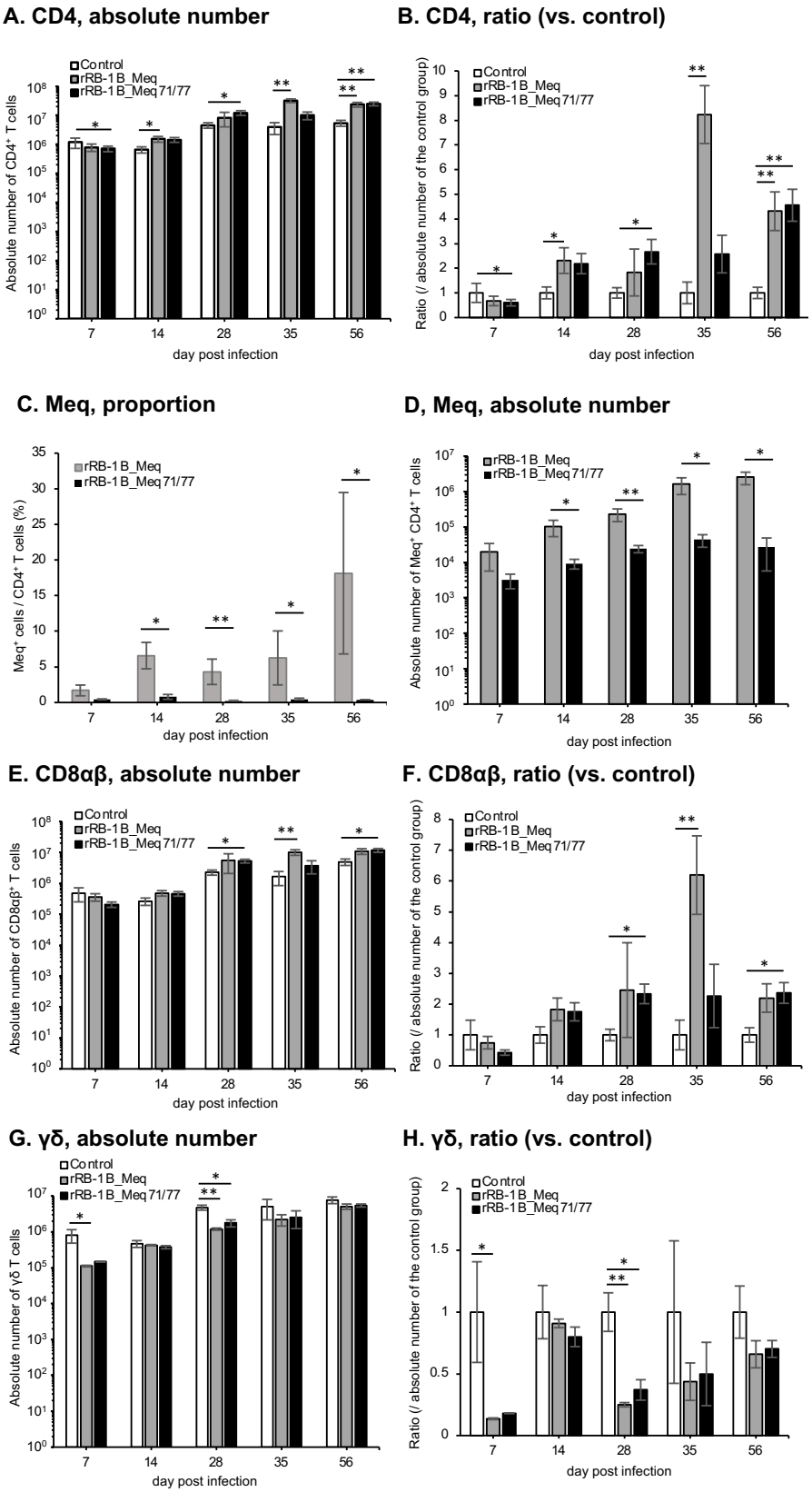

Figure II-10. Dynamics of T cell subsets in the thymus of chickens infected with rRB-1B_Meq71/77
Shown are the dynamics of $CD4^+$ cells, Meq^+ cells, $CD8^+$ cells, and γδ T cells from mononuclear cells isolated from the thymus of chickens infected with rRB-1B-Meq or rRB-1B-Meq71/77 at each time point during the experimental period. Absolute numbers of (A) $CD4^+$ T cells, (D) Meq^+ cells, (E) $CD8\alpha\beta^+$ T cells, and (G) $\gamma\delta TCR^+$ T cells in the thymus were analyzed. The ratios of absolute numbers of (B) $CD4^+$ T cells, (F) $CD8\alpha\beta^+$ T cells, and (H) $\gamma\delta TCR^+$ T cells in the thymus relative to the control group were analyzed. (C) The percentages of Meq^+ cells in the $CD4^+$ T cell population in the thymus were analyzed. Asterisks indicate significant differences (* $p < 0.05$, ** $p < 0.01$; Dunn's test in A, B, E, F,G and H. Mann-Whitney U test in C and D).

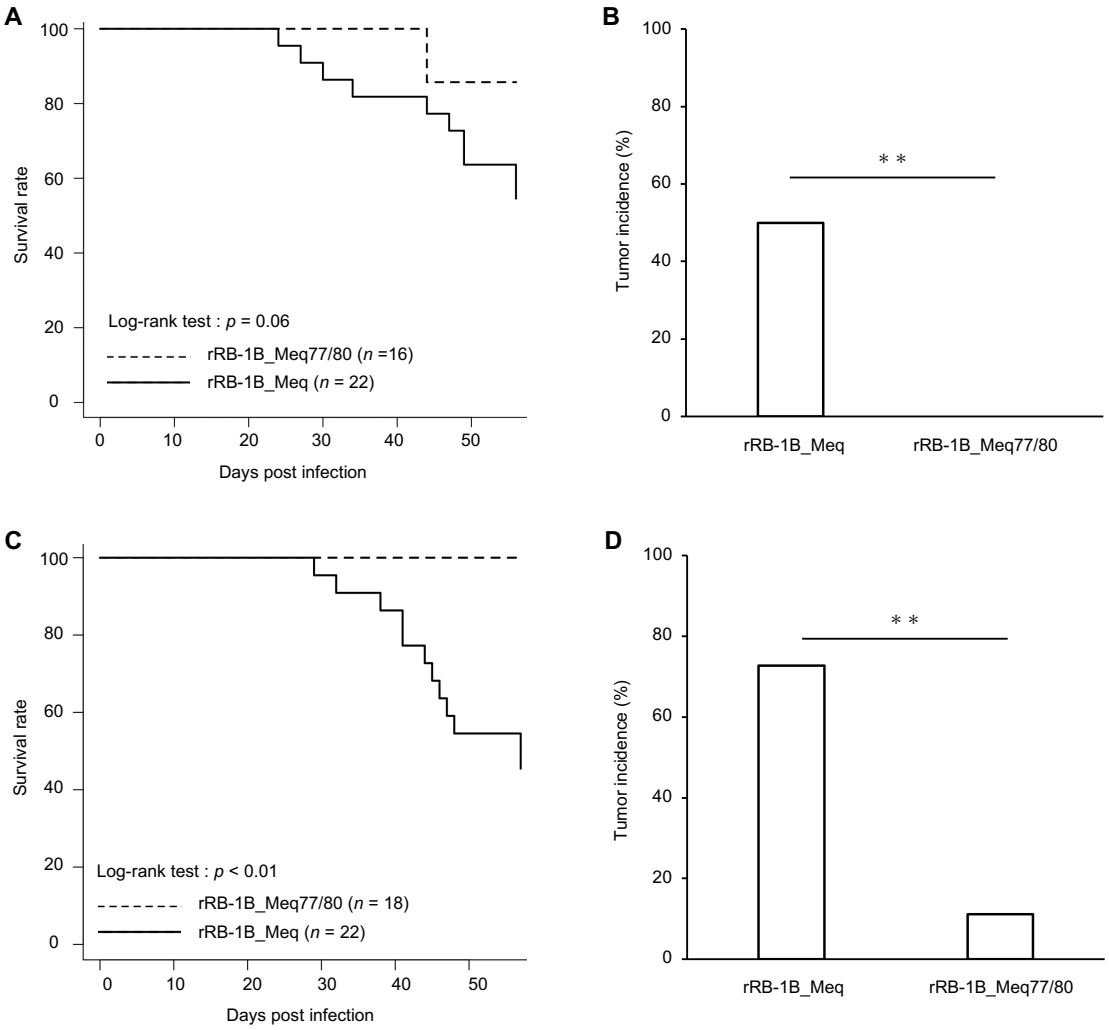

Figure II-11. Mortality and tumor incidence in chickens infected with rRB-1B_Meq77/80
(A and C) Survival rate in chickens infected with rMDVs in (A) the first and (C) the second animal experiments. The survival rates among the groups were analyzed using the Log-rank test. (B and D) Tumor incidence in chickens infected with rMDVs throughout the experimental infection. Asterisks indicate significant differences (** $p < 0.01$; Fisher's exact test).

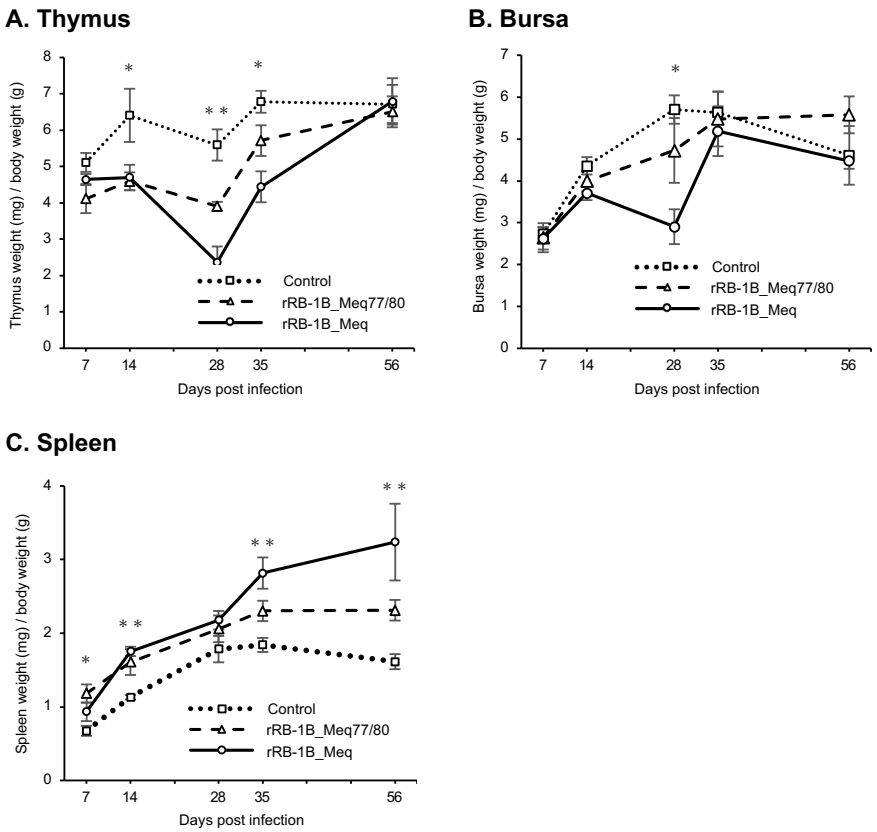

Figure II-12. Change in lymphoid organ weight in chickens infected with rRB-1B_Meq77/80
The dynamics of the lymphoid organ-to-body weight ratios for the (A) thymus, (B) bursa of Fabricius, and (C) spleen in chickens infected with rRB-1B-Meq or rRB-1B-Meq77/80 were analyzed at each time point throughout the experimental period. The spleens, thymii, and bursae were collected from five chickens per group at 7, 14, 28, and 35 dpi, and from all remaining chickens (uninfected control group: $n = 5$, rRB-1B_Meq-infected group: $n = 11$, rRB-1B_Meq77/80-infected group: $n = 14$) at the termination of the experiment at 56 dpi in the first animal experiment, and 35 chickens (control group: $n = 5$, rRB-1B_Meq-infected group: $n = 12$, rRB-1B_Meq77/80-infected group: $n = 18$) at 56 dpi in the second animal experiment. Statistical significance was determined using the Dunn's test. ** $p < 0.01$ and * $p < 0.05$. Significant differences were observed at 14 dpi (rRB-1B_Meq77/80 vs. control, $p = 0.043$; rRB-1B_Meq vs. control, $p = 0.036$), 28 dpi (rRB-1B_Meq vs. control, $p = 0.0008$) and 35dpi (rRB-1B_Meq vs. control, $p = 0.0045$) in (A), at 28 dpi (rRB-1B_Meq vs. control, $p = 0.0164$) in (B), and at 7 dpi (rRB-1B_Meq77/80 vs. control, $p = 0.0087$), 14 dpi (rRB-1B_Meq77/80 vs. control, $p = 0.029$; rRB-1B_Meq vs. control, $p = 0.0045$), 35 dpi (rRB-1B_Meq vs. control, $p = 0.0028$), and 56 dpi (rRB-1B_Meq vs. control, $p = 0.015$; rRB-1B_Meq77/80 vs. rRB-1B_Meq, $p = 0.042$) in (C).

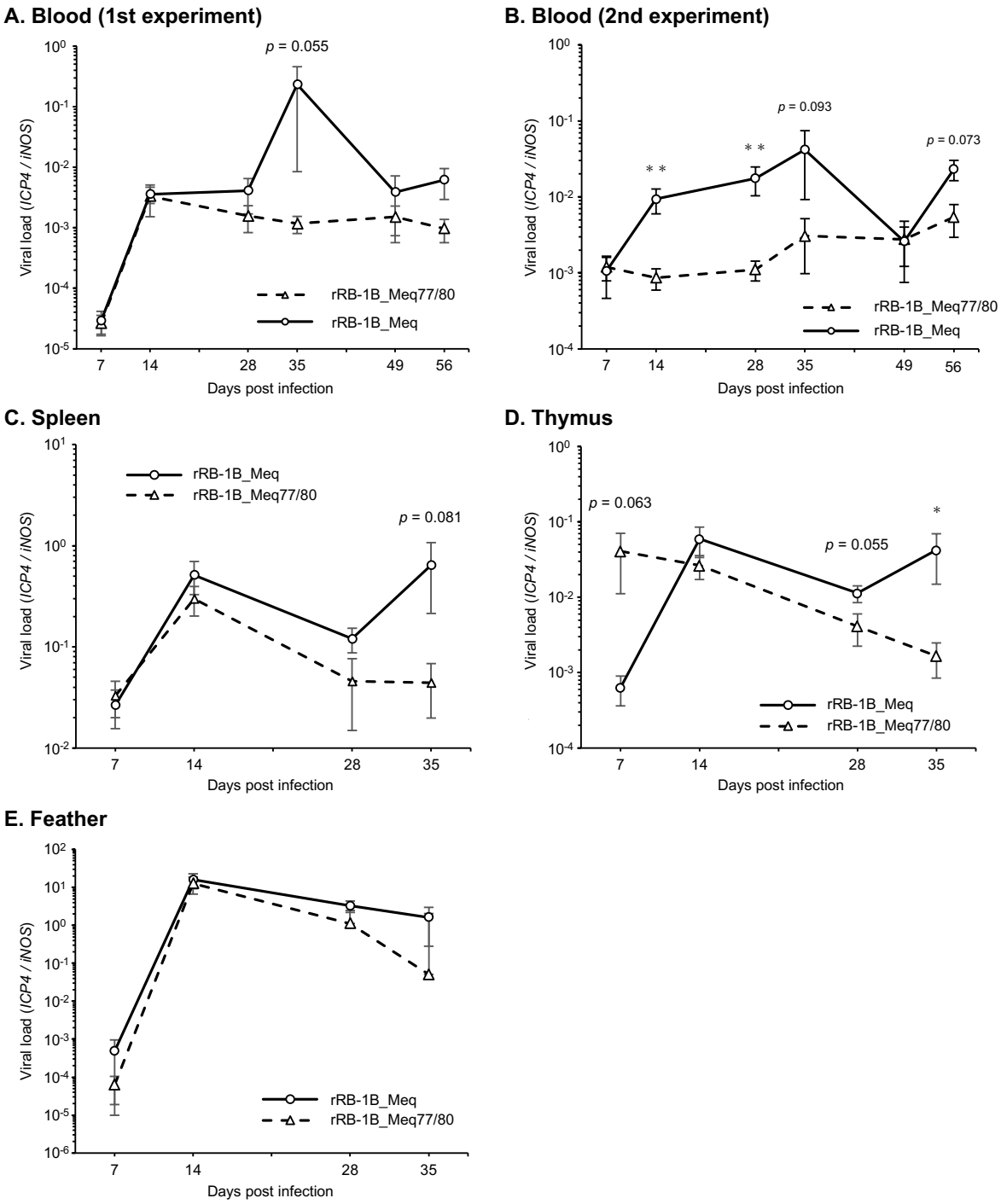

Figure II-13. Replication kinetics of rRB-1B_Meq77/80 *in vivo*

Viral loads in (A) peripheral blood mononuclear cells (PBMCs) in the first experiment, (B) PBMCs in the second experiment, (C) spleen, (D) thymus, and (E) feather tips from chickens infected with rRB-1B_Meq or rRB1B_Meq77/80 were determined using qPCR. Blood samples were collected from five chickens per group at 7, 14, 28, 35, and 49 dpi, and from 25 chickens in the first experiment (rRB-1B_Meq-infected group: $n = 11$, rRB-1B_Meq77/80-infected group: $n = 14$) and 30 chickens in the second experiment (rRB-1B_Meq-infected group: $n = 12$, rRB-1B_Meq77/80-infected group: $n = 18$) at 56 dpi. Asterisks indicate significant differences (* $p < 0.05$; the Mann–Whitney U test).

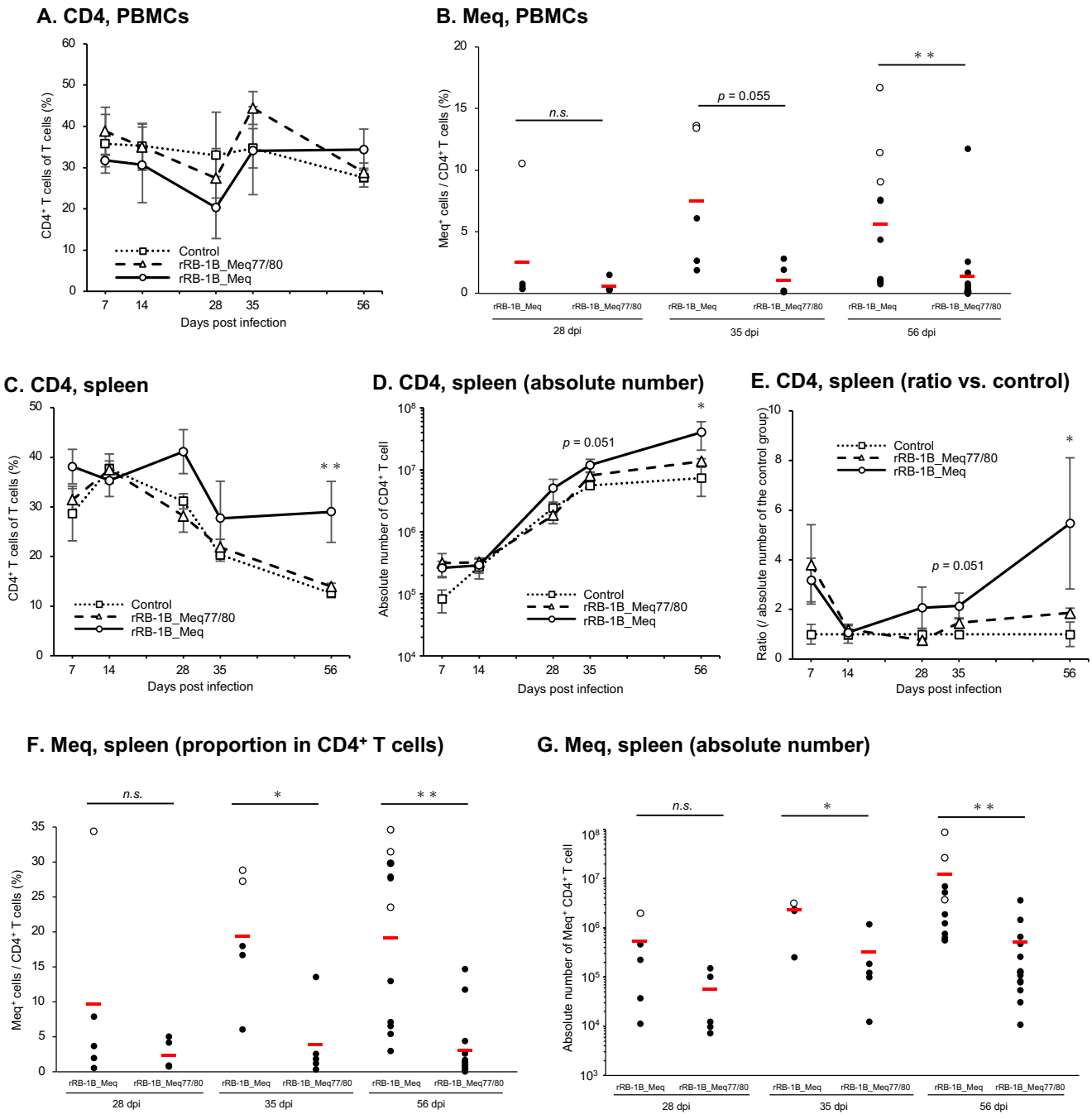

Figure II-14. Dynamics of CD4$^+$ T cells and Meq$^+$ cells in chickens infected with rRB-1B_Meq77/80

Shown are the dynamics of CD4$^+$ cells and Meq$^+$ from the peripheral blood mononuclear cells (PBMCs) and spleens of chickens infected with rRB-1B-Meq or rRB-1B-Meq77/80 at each time point during the experimental period. The percentages of CD4$^+$ T cells in the T cell population from (A) PBMCs and (C) spleens, Meq$^+$ cells in the CD4$^+$ T cell population from (B) PBMCs and (F) spleens were analyzed. White dots in the rRB-1B_Meq-infected group represent chickens with solid tumors in visceral organs. Absolute numbers of (D) CD4$^+$ T cells, (G) Meq$^+$ CD4$^+$ T cells in the spleen were analyzed. The ratios of absolute numbers of (E) CD4$^+$ T cells in the spleen relative to the control group were analyzed. Asterisks indicate significant differences (* $p < 0.05$, ** $p < 0.01$; Dunn's test in A, C, D, and E. Mann-Whitney U test in B, F, and G). Significant differences were observed at 56 dpi (rRB-1B_Meq vs. control, $p = 0.0015$; rRB-1B_Meq77/80 vs. rRB-1B_Meq, $p = 0.013$) in (C), at 56 dpi (rRB-1B_Meq vs. control, $p = 0.018$) in (D and E)

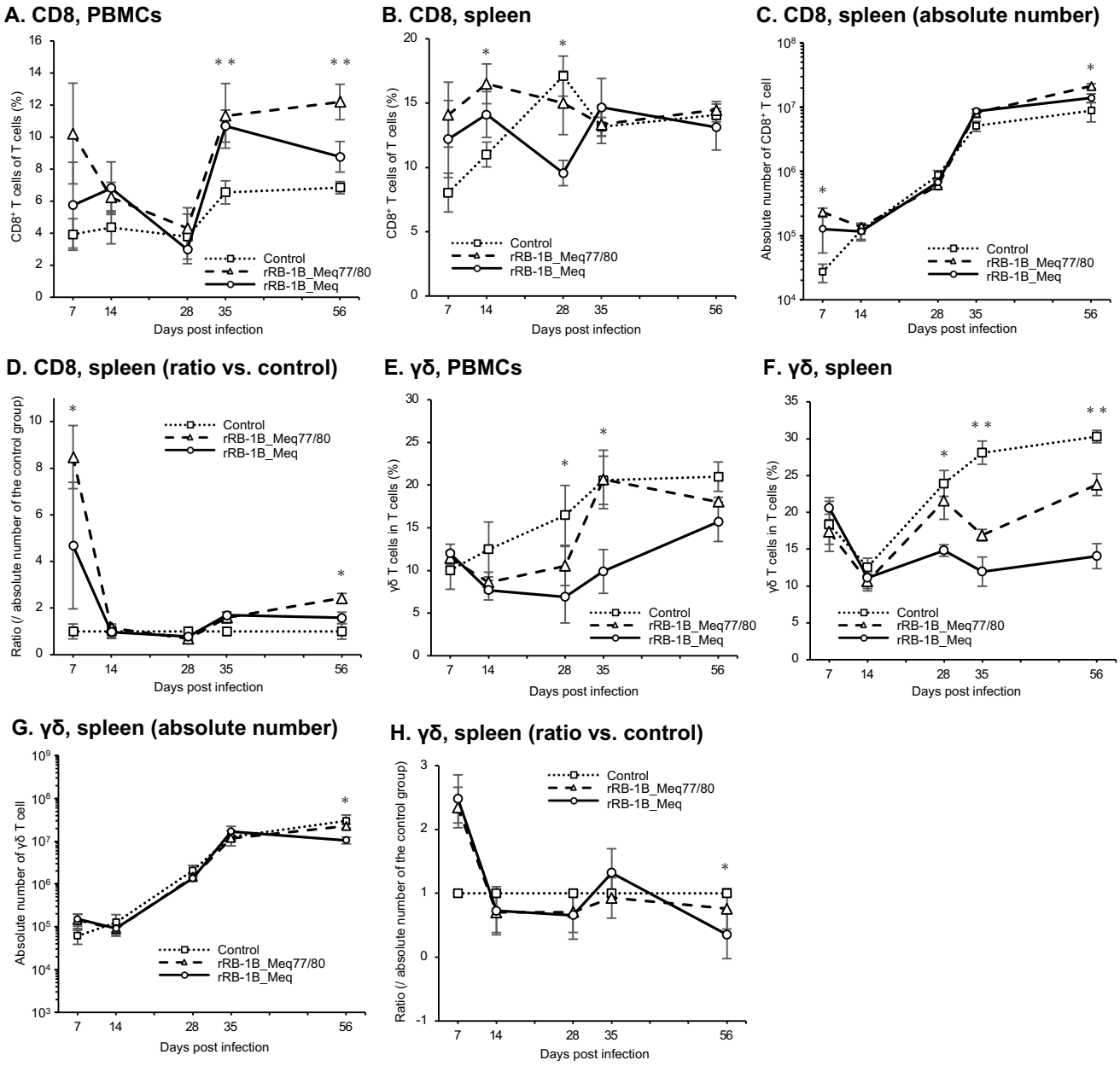

Figure II-15. Dynamics of CD8⁺ T cell and γδ T cells in chickens infected with rRB-1B_Meq77/80

Shown are the dynamics of CD8⁺ cells and γδ T cells from the peripheral blood mononuclear cells (PBMCs) and spleens of chickens infected with rRB-1B-Meq or rRB-1B-Meq77/80 at each time point during the experimental period. The percentages of CD8⁺ T cells in the T cell population from (A) PBMCs and (B) spleens and γδTCR⁺ T cells in the T cell population from (E) PBMCs and (F) spleens were analyzed. Absolute numbers of (C) CD8⁺ T cells and (G) γδTCR ⁺ T cells in the spleen were analyzed. The ratios of absolute numbers of (D) CD8⁺ T cells and (H) γδTCR⁺ T cells in the spleen relative to the control group were analyzed. Asterisks indicate significant differences (* $p < 0.05$, ** $p < 0.01$; Dunn's test).

Significant differences were observed at 35 dpi (rRB-1B_Meq77/80 vs. control, $p = 0.048$; rRB-1B_Meq vs. control, $p = 0.016$) and 56 dpi (rRB-1B_Meq77/80 vs. control, $p = 0.0013$; rRB-1B_Meq77/80 vs. rRB-1B_Meq, $p = 0.039$) in (A), at 14 dpi (rRB-1B_Meq77/80 vs. control, $p = 0.043$) and 28 dpi (rRB-1B_Meq vs. control, $p = 0.011$) in (B), at 7 dpi (rRB-1B_Meq77/80 vs. control, $p = 0.0070$) and 56 dpi (rRB-1B_Meq77/80 vs. control, $p = 0.0091$; rRB-1B_Meq77/80 vs. rRB-1B_Meq, $p = 0.047$) in (C and D), at 28 dpi (rRB-1B_Meq vs. control, $p = 0.043$), 35 dpi (rRB-1B_Meq vs. control, $p = 0.036$; rRB-1B_Meq77/80 vs. rRB-1B_Meq, $p = 0.043$) in (E), at 28 dpi (rRB-1B_Meq vs. control, $p = 0.024$), 35 dpi (rRB-1B_Meq vs. control, $p = 0.017$; rRB-1B_Meq77/80 vs. rRB-1B_Meq, $p = 0.060$), at 56 dpi ((rRB-1B_Meq vs. control, $p = 0.0004$; rRB-1B_Meq77/80 vs. rRB-1B_Meq, $p = 0.0016$) in (F), and at 56dpi (rRB-1B_Meq vs. control, $p = 0.035$; rRB-1BMeq77/80 vs. rRB-1B_Meq, $p = 0.0049$) in (G and H).

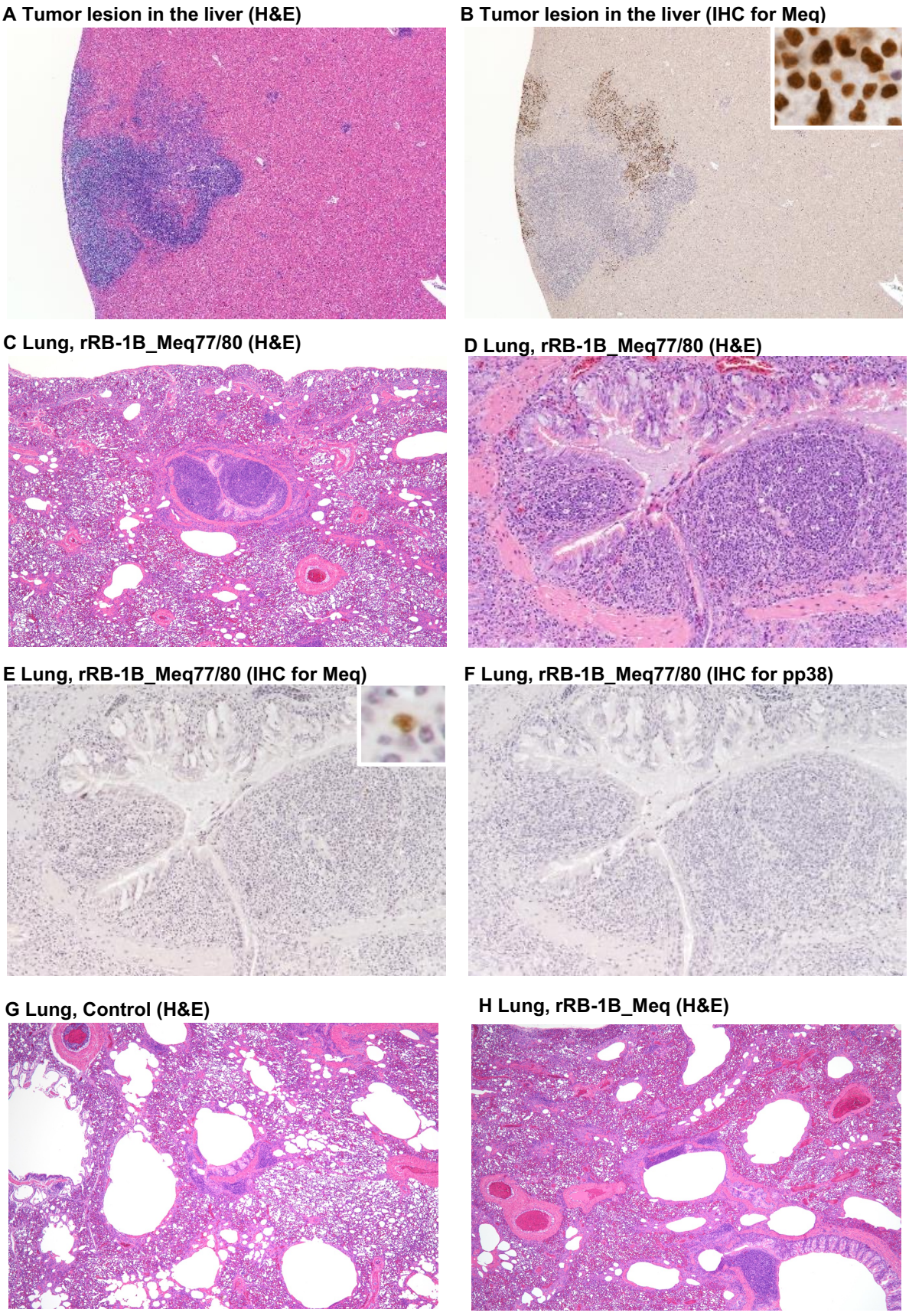

Figure II-16. Histopathological analysis of chickens infected with rRB-1B_Meq77/80
(A) Hematoxylin and eosin (H&E) staining and (B) immunohistochemistry (IHC) staining of a tumor lesion from the liver of an rRB-1B_Meq77/80-infected chicken using anti-Meq monoclonal antibodies. The small panel indicates the presence of Meq-positive cells. (C-D) H&E, (E) IHC staining for Meq, and (F) IHC staining for pp38 in bronchus-associated lymphoid tissue in the lung of an rRB-1B_Meq77/80-infected chicken. (C) shows a low-magnification image, and (D) shows a high-magnification image. H&E in the lung of a chicken in (G) the control group and (D) the rRB-1B_Meq-infected group.

Table II-2. Summary of the results of the histopathological examination of tissues from chickens infected with rRB-1B_Meq71/77.

Virus	Sample number	Lesions	Spleen	Bursa of Fabricius	Thymus	Remarks
rRB-1B_ Meq	#1	Tumor cell infiltration	++	+	++	Solid tumors were developed in the kidneys and ovaries. The spleen was noticeably enlarged. Macrophage infiltration was observed in the red pulp of the spleen.
		Meq+ cells	++	+	++	
	#2	Tumor cell infiltration	++	+	+	Enlargement of the spleen was noted. Macrophage infiltration was observed in the red pulp of the spleen.
		Meq^+ cells	+	+	++	
	#3	Tumor cell infiltration	++	+	+	Enlargement of the spleen was noted. Macrophage infiltration was observed in the red pulp of the spleen.
		Meq^+ cells	+	+	+	
rRB-1B_ Meq71/77	#1	Tumor cell infiltration	−	−	−	-
		Meq^+ cells	−	−	−	
	#2	Tumor cell infiltration	−	−	−	-
		Meq^+ cells	−	−	−	
	#3	Tumor cell infiltration	−	−	−	-
		Meq^+ cells	+	+	+	
	#4	Tumor cell infiltration	−	−	−	-
		Meq^+ cells	−	−	−	
	#5	Tumor cell infiltration	−	−	−	-
		Meq^+ cells	+	+	+	

These results indicate the percentage of infiltrated tumor cells/Meq-positive cells per five fields of view. +, < 30%; ++, 30–80%

Table II-3. Results of flow cytometric analysis of the spleen of rRB-1B_Meq77/80-infected chickens exhibiting open-mouth breathing in the first experimental infection.

	$CD4^+$/T cell ratio	$Meq^+/CD4^+$T cell ratio
rRB-1B_Meq77/80 #1 (44 dpi)	12.2%	4.42%
rRB-1B_Meq77/80 #2 (44 dpi)	12.8%	8.07%
rRB-1B_Meq77/80 (mean, 56 dpi, n = 14)	21.9%	3.02%
rRB-1B_Meq with tumor (mean; 28, 35, and 56 dpi; n = 6)	56.4%	30.0%

TableII-4. Summary of the results of the histopathological examination of tissues from chickens infected with rRB-1B_Meq77/80.

Virus	Sample number	IHC	Spleen	Bursa of Fabricius	Thymus	Proventriculus	Lung	Brain	Cervical peripheral nerves	Cervical skin	Remarks
rRB-1B_ Meq	#1	Meq	++: Tumor lesions	+: Muscular layer, interfollicular region, follicles	++: Medulla +: Adipose tissue	++: Mucosa +: Muscular layer, serous membrane	+: Whole area	++: Perivascular region	++: Nerves	+++: Feather pulp ++: Skin stroma +: Adipose tissue, follicular epithelium	This chicken displayed leg paralysis. Tumor formation was observed in the testis. Enlargement of the sciatic nerve was noted. pp38+ follicular epithelium: 32% (6/19).
		pp38	+: Tumor lesions	+: Follicles	-	-	-	-	-	++: Follicular epithelium	
	#2	Meq	+++: Tumor lesions	+++: Interfollicular regions +: Muscle layer, follicles	+++: Medulla, perivascular lymphocytic clusters +: Adipose tissue	+++: Mucosa, serous membrane +: Muscle layer	+++: Tumor lesions	+++: Tumor lesions +: Meninges, perivascular regions	+: Nerves, adipose tissue	++: Follicular epithelium, skin stroma +: Feather pulp, adipose tissue	This chicken exhibited depression. Tumor formation was noted in the liver, kidneys, and ovaries. The bursa of Fabricius and the thymus were atrophied. pp38+ follicular epithelium: 61% (14/23).
		pp38	+: Tumor lesions	+: Follicles	+: Medulla	+: Serous membrane	+: Tumor lesions	-	-	++: Follicular epithelium	
	#3	Meq	+++: Tumor lesions	+++: Muscle layer, Interfollicular regions +: Follicles	++: Medulla, adipose tissue +: Cortex	+++: Serous membrane ++: Mucosa +: Muscle layer	+++: Tumor lesions ++: Whole area	+: Meninges, perivascular regions	+: Nerves, adipose tissue	++: Follicular epithelium, skin stroma +: Feather pulp, adipose tissue	Tumor formation was observed in the liver, kidneys, ovaries, and intestines. Ascites was present in the abdominal cavity. pp38+ follicular epithelium: 50% (12/24).
		pp38	++: Tumor lesions	+: Follicular medulla	+: Medulla	++: Serous membrane +: Mucosa, muscle layer	++: Tumor lesions +: Whole area	-	-	++: Follicular epithelium +: Feather pulp	
rRB-1B_ Meq77/80	#1	Meq	++: Tumor lesions	++: Tumor lesions	+: Medulla	+: Mucosa	+: Whole area, bronchial follicles	-	+: Nerves	+: Follicular epithelium, skin stroma	Tumor formation was observed in the liver and spleen. Lymphoid cell accumulation and lymphofollicular lesions were observed in the lungs. The body weight was lower than that of other chickens in the same group. pp38+ follicular epithelium: 21% (7/33).
		pp38	+: Tumor lesions	-	+: Medulla	-	+: Whole area (-: Bronchial follicles)	-	-	+: Follicular epithelium	
	#2	Meq	+: Parenchyma	+++: Tumor lesions +: Follicles	+: Medulla	+++: Mucosa, serous membrane ++: Muscle layer	+++: Tumor lesions	+: Meninges, perivascular regions	+++: Tumor lesions in adipose tissue +: Nerves	++: Feather pulp +: Skin stroma	Tumor formation was observed in the kidneys, proventriculus, and lungs. The body weight was lower than that of other chickens in the same group. pp38+ follicular epithelium: 0% (0/10).
		pp38	-	+: Tumor lesions	-	+: Tumor lesions	+: Tumor lesions	-	-	-	
	#3	Meq	+: Parenchyma	+: Follicular cortex, medulla	+: Medulla	+: Mucosa, muscle layer, Serous membrane	+: Whole area, bronchial follicles	-	+: Nerves	+: Follicular epithelium, feather pulp, skin stroma	Tumor formation was observed in the liver. Lymphoid cell accumulations and lymphofollicular lesions were observed in the lungs. pp38+ follicular epithelium: 21% (3/14).
		pp38	-	+: Follicles	-	+: Muscle layer	-	+: Parenchyma	-	+: Follicular epithelium	
	#4	Meq	-	-	+: Medulla	-	-	-	-	+: Skin stroma	Open-mouth breathing, lymphoid cell accumulation, and lymphofollicular lesions in the lungs were observed. pp38+ follicular epithelium: 0% (0/37).
		pp38	-	-	-	-	-	-	-	-	
	#5	Meq	-	-	-	-	-	-	-	-	Open-mouth breathing, lymphoid cell accumulation, and lymphofollicular lesions in the lungs were observed. pp38+ follicular epithelium: 0% (0/10).
		pp38	-	-	-	-	-	-	-	-	

The IHC results indicate the percentage of Meq/pp38-positive cells per five fields of view. +, < 30%; ++, 30–80%; +++, >80%; IHC, immunohistochemistry

DISCUSSION

The amino acid sequences at positions 71, 77, and 80 in the basic region of Meq display distinct differences depending on the virulence or geographic features of MDV strains, but whether these differences in amino acid sequences affect the pathogenicity of MDV remains unclear. Therefore, in Chapter II, the effect of amino acid polymorphisms in the basic region on Meq-mediated transcriptional regulation and MDV virulence was investigated. Introduction of amino acid substitutions found in the Meq isoforms of CVI988 (serine and glutamic acid at positions 71 and 77) or in Meq of low-virulence U.S. strains and recent isolates in Asia, Africa, and Europe (glutamic acid and tyrosine at positions 77 and 80) into RB-1B-Meq markedly reduced transcriptional regulatory activity. Consistent with the decrease in the ability of transcriptional regulation, chickens infected with rRB-1B_Meq71/77 exhibited no clinical signs or solid tumor formation, and showed a significant reduction in Meq^+ cells in the spleen and thymus. Similarly, rRB-1B_Meq77/80 induced lower mortality and tumor incidence than rRB-1B_Meq, but caused distinct clinical manifestations, including open-mouth breathing and depression. Flow cytometric analysis revealed elevated proportions of $CD8^+$ T cells in both PBMCs and spleens of rRB-1B_Meq77/80-infected chickens during the acute and later phase of infection. Histopathological analysis further identified lymphocytic hyperplasia in BALT in this group, suggesting that severe pulmonary inflammation underlie the respiratory symptoms. These findings show that only two distinct polymorphisms in the basic region significantly alter the virulence and influence clinical manifestations.

The amino acid substitutions at positions 71, 77, and 80 were found to reduce transcriptional repression of the *pp38* promoter. While single mutations slightly decreased the transcriptional repression, double or triple mutations led to a significant reduction, indicating a potential synergistic effect of these mutations. Meq71/77 (gray bars in Fig. II-2), corresponding to CVI988-Meq, exhibited lower transcriptional regulation than wild-type RB-1B-Meq. Previous studies showed that the transactivation activity of Meq is correlated with the virulence of several field strains (Murata *et al*., 2011; Sato *et al*., 2022), suggesting that the reduced transcriptional regulatory activity of Meq71/77 is involved in the low virulence of rRB-1B_Meq71/77. Meq77/80 (gray bars in Fig. II-2) also reduced both the transcriptional repression on the *pp38* promoter and the transactivation activity on the *meq* promoter compared with wild-type RB-1B-Meq. In agreement with these observations, rRB-1B_Meq77/80 exhibited lower mortality than rRB-1B_Meq. However, highly virulent strains in Asia, Europe, and Africa also possess glutamic acid and tyrosine at positions 77 and 80 (Trimpert *et al.,* 2017; Teng *et al*., 2022;

Patria *et al*., 2024), and thus, enhanced transactivation activity of Meq may contribute to the increased virulence of MDV, but may not be essential. In highly virulent strains in Asia, Europe, and Africa, enhanced virulence may be mediated by mutations in other viral genes and/or mechanisms independent on the transcriptional regulation.

Furthermore, the amino acid substitutions at positions 77 and 80 did not alter the transactivation activity of the *bcl-2* promoter. These findings suggest that mutations at positions 77 and 80 does not uniformly reduce the binding affinity of Meq for all promoters, but modify promoter specificity, thereby selectively influencing their regulatory functions. Alternatively, mutations at these positions may influence the nuclear and nucleolar localization of Meq due to their proximity to localization signals, or affect the stoichiometry of homo- to heterodimerization (Liu *et al*., 1997; Levy *et al.*, 2003; Anobile *et al*., 2006). Notably, Meq interacts with host proteins such as C-terminal binding protein and p53 through the basic region (Brown *et al*., 2006; Deng *et al*., 2010), and polymorphisms in this domain may influence Meq function by altering these interactions. Therefore, further analyses, such as proximity-dependent biotin labeling and co-immunoprecipitation, are required to identify proteins that interact with Meq.

Although no significant differences in replication kinetics were detected among rMDVs *in vitro*, rRB-1B_Meq-infected chickens exhibited higher viral loads than chickens infected with rRB-1B_Meq71/77 or rRB-1B_Meq77/80. Flow cytometric analyses revealed an increase in Meq^+ $CD4^+$ T cells, which are believed to contain the MDV genome, in the rRB-1B_Meq-infected group, suggesting that the elevated viral loads in this group reflect the proliferation of transformed $CD4^+$ T cells. On the other hand, rRB-1B_Meq71/77-infected chickens did not develop tumors. Furthermore, no histopathological changes were observed in rRB-1B_Meq71/77-infected chickens. These observations show that the transformation potential of rRB-1B_Meq71/77 was markedly reduced due to the amino acid substitutions at positions 71 and 77. Notably, in the flow cytometric analysis, the proportion of Meq^+ $CD4^+$ T cells in the spleens of rRB-1B_Meq71/77-infected chickens was 7.1% at 7 dpi but declined to below 1% after 28 dpi. Similarly, rRB-1B_Meq77/80 demonstrated a significantly lower mortality and tumor incidence compared to rRB-1B_Meq. In addition, the proportion of Meq^+ $CD4^+$ T cells in both PBMCs and spleens of the rRB-1B_Meq77/80-infected group was significantly lower than that of the rRB-1B_Meq-infected group. In the IHC analysis, only a small number of Meq^+ cells were detected in the spleens of rRB-1B_Meq77/80-infected chickens, and these were located at sites distinct from the tumor lesions, unlike those in rRB-1B_Meq-infected chickens (Table II-4). These findings suggest that both rRB-1B_Meq71/77 and rRB-1B_Meq77/80 do not efficiently establish latent infection

effectively or maintain latently infected cells due to impaired function of Meq71/77 and Meq77/80. Moreover, in the spleens of both groups infected with rRB-1B_Meq71/77 or rRB-1B_Meq77/80, the numbers of $CD8^+$ T cells were significantly elevated at 7 dpi, while the viral load gradually decreased over time. These data suggest that a robust cellular immune response is induced in the early phase of infection, leading to the efficient elimination of infected cells. The basic region of Meq is responsible for binding to genomic DNA (Levy *et al.*, 2003), and polymorphisms in this domain may alter the transcriptome regulated by Meq in infected cells. rMDVs encoding distinct Meq variants display differences in the cellular composition of tumor tissues (Kumar *et al*., 2012), suggesting that variation in Meq amino acid sequences influences the expression of genes, including cytokines and chemokines, within tumor cells. Consequently, future studies employing transcriptomic analyses of infected cells, such as single-cell RNA sequencing or enrichment of infected cells using reporter viruses, will be essential to elucidate the underlying molecular mechanisms.

Interestingly, in the rRB-1B_Meq77/80-infected group in the first experiment, one chicken at 35 dpi and two chickens at 56 dpi exhibited relatively high proportions of Meq^+ $CD4^+$ T cells, compared to the other rRB-1B_Meq77/80-infected chickens in the same group. Similarly, high proportion of Meq^+ $CD4^+$ T cells was observed in rRB-1B_Meq77/80-infected chickens that displayed open-mouth breathing. These observations raise the possibility that chickens with high Meq^+ $CD4^+$ T cell proportions in the rRB-1B_Meq77/80-infected group could have developed open-mouth breathing or solid tumors by observing for a longer period.

A previous study demonstrated that recombinant RB-1B expressing wild-type CVI988-Meq completely lost virulence (Conradie *et al.*, 2019). Consistent with the results in the previous study, the introduction of only two amino acid substitutions at positions 71 and 77 found in CVI988-Meq into RB-1B-Meq completely abolished the virulence. These results emphasize the critical role of the basic region of Meq in determining MDV virulence. Intriguingly, a recombinant Md5 strain expressing a chimeric Meq composed of the N-terminal domain of CVI988-Meq and the C-terminal domain of Md5-Meq (rMd5-CVI/Md5-Meq) still caused MD in 37% of infected chickens, despite containing the same polymorphisms at positions 71 and 77 as CVI988-Meq (Ajithdoss *et al*., 2025). These observations suggest that amino acid polymorphisms in the transactivation domain of Meq still influence the virulence of rMd5-CVI/Md5-Meq. Notably, several highly virulent strains, such as N and 648A, share polymorphisms in the PRRs of the transactivation domain, and Md5 also carries a proline-to-alanine substitution at position 217 (P217A) (Shamblin *et al*., 2004). In contrast, although RB-1B does not

have any mutations in the PRRs, and only the P217A substitution significantly enhanced Meq transactivation activity (Murata *et al.*, 2011). Therefore, the alanine at position 217 in rMd5-CVI/Md5-Meq may partially account for its residual virulence.

MDV induces apoptosis in T cells during the acute phase of MDV infection, leading to thymic atrophy (Morimura *et al.*, 1996; Berthault *et al.*, 2018). In the experimental infections, the thymus weight of all rMDV-infected groups tended to be lower than that of the control group during the early phase of infection, indicating thymic atrophy associated with cytolytic infection. Moreover, in the experimental infection with rRB-1B_Meq71/77, the absolute numbers of $CD4^+$ T, $CD8^+$ T, and γδ T cells in the thymus of rMDV-infected chickens were decreased at 7 dpi. Notably, the number of γδ T cells in the infected groups remained consistently lower than in the control group throughout the experimental period, suggesting high susceptibility of γδ T cells to cytolytic infection. In contrast, the numbers of $CD4^+$ and $CD8^+$ T cells were increased after 14 dpi in the rMDV-infected groups. In the rRB-1B_Meq-infected group, this increase in the number of $CD4^+$ T cells coincided with an expansion of Meq^+ cells, implying the proliferation of MDV-transformed cells. However, in the thymus of rRB-1B_Meq71/77-infected chickens, no increase in Meq^+ cells was observed over time, suggesting that early cytolytic infection influences the subsequent cellular composition of the thymus. Further investigation is required to clarify the impact of MDV infection on immune responses in the thymus and on T cell differentiation.

$CD8^+$ T cells play a pivotal role in both antiviral and antitumor immunity during MDV infection (Sharma *et al.*, 1978; Umthong *et al.*, 2020; Hao *et al*., 2021). In rRB-1B_Meq77/80-infected chickens, both the number and proportion of $CD8^+$ T cells increased during the acute and transformation phases compared to rRB-1B_Meq-infected chickens, suggesting a role in eliminating infected and/or transformed cells and contribution to the milder disease progression observed in the rRB-1B_Meq77/80-infected group. However, this increase in the number of $CD8^+$ T cells may also be linked to inflammatory lesions in the lungs, potentially associated with distinct clinical manifestations such as open-mouth breathing. Further studies are needed to clarify the relationship between $CD8^+$ T cell expansion and the clinical manifestations of rRB-1B_Meq77/80 infection.

Tumor incidence was significantly increased in γδ T cell-knockout chickens during experimental infection, highlighting the critical role of γδ T cells in immunity against MDV infection (Sabsabi *et al*., 2024). Consistent with the observation in the thymus in the rRB-1B_Meq-infected chickens, the absolute number of γδ T cells in the spleens of rRB-1B_Meq-infected chickens was lower than that of the control group. The supernatant

of splenocytes from MDV-infected chickens has been reported to impair the function of γδ T cells (Matsuyama-Kato *et al*., 2023a). MDV-transformed cells express PGE_2 and PD-L1, which may contribute to the establishment of an immunosuppressive environment (Matsuyama-Kato *et al*., 2012; Kamble *et al*., 2021), and these immunosuppressive molecules may suppress the proliferation of γδ T cells. Further investigation is warranted to clarify the mechanisms of MDV pathogenesis, particularly the influence of immunosuppressive factors on γδ T cells.

Histopathological analysis revealed hyperplasia in the BALT of the lungs of rRB-1B_Meq77/80-infected chickens; the lesion is absent in both the control and rRB-1B_Meq-infected groups. This observation suggests that the impact of the rRB-1B_Meq77/80 is underestimated because the lesions in the lung were difficult to detect from clinical signs alone. Notably, two chickens that exhibited open-mouth breathing at 44 dpi in the first experimental infection showed elevated proportions of Meq^+ $CD4^+$ T cells, implicating a potential association between increased Meq^+ $CD4^+$ cells and this respiratory manifestation. The lymphocytic hyperplastic bronchitis observed closely resembled the lesions caused by *Mycoplasma* spp. infection, though immunohistochemical staining for *Mycoplasma* was negative in all samples (data not shown). In contrast, minimal Meq^+ lymphocyte infiltration was detected in the proventriculus, gizzard, brain, or vagus nerve, suggesting that open-mouth breathing is not linked to digestive or neurological disorders but rather to lung inflammation.

Although mechanisms underlying rRB-1B_Meq77/80-induced inflammation in the BALT remain unclear, two hypotheses are proposed. First, a small number of transformed cells may drive inflammation. Given the presence of a few Meq^+ lymphocytes within the lymphofollicular lesions in the lung and the reduced transcriptional repression of Meq77/80, which may impair latency or promote viral reactivation, these Meq^+ cells may be insufficient to establish an immunosuppressive environment, thereby resulting in inflammatory responses. This aligns with the observation that inflammatory cells were frequently located adjacent to Meq^+ lymphocytes within tumor lesions in the liver of an rRB-1B_Meq77/80-infected chicken. Second, polymorphisms in the basic region may alter its transcriptional targets. Because this region mediates Meq binding to target regions in the genomic DNA, polymorphisms in the basic region may modify the binding affinity, leading to altered transcriptomic profiles and potentially increased expression of proinflammatory cytokines. To test this hypothesis, comparative analysis of target genes among Meq isoforms using chromatin immunoprecipitation sequencing and electrophoretic mobility shift assays is required. Additionally, direct transcriptomic

comparisons of infected cells via single-cell RNA sequencing may yield critical insights into the molecular basis of these pathological differences.

IHC analysis for Meq revealed that tumor lesions in the livers of rRB-1B_Meq77/80-infected chicken contained a large number of Meq-negative lymphocytes. Given the increased number of $CD8^+$ T cells in the rRB-1B_Meq77/80-infected group, it is possible that effector T cells infiltrated the tumor lesions. A previous study has indicated that differences in the amino acid sequences of Meq are sufficient to alter the cellular composition of tumor tissues (Kumar *et al*., 2012), potentially altering the transcriptome of transformed cells, including the expression of cytokines and chemokines. Consequently, variations in the Meq amino acid sequences may modify the tumor microenvironment. IHC analyses using antibodies against macrophages, NK cells, or other lymphoid populations may clarify whether differences in tumor composition reflect variations in the Meq amino acid sequences.

Observations from the experimental infections suggest that polymorphisms in the basic region of highly virulent strains from the US, such as RB-1B, have contributed to the evolution toward enhanced virulence, whereas MDV isolates from Asia, Africa, and Europe have followed distinct evolutionary pathways, potentially altering clinical manifestations. Recent isolates in Asia have also been reported to contain mutations in PRRs and deletions in the transactivation domain (Murata *et al*., 2013, 2021; Yu *et al.*, 2013; Zhuang *et al*., 2015; Deng *et al*., 2021; Wannaratana *et al.*, 2022; Motai *et al*., 2024). For the comprehensive understanding of the relationship between the amino acid sequence of Meq and MDV virulence, the combined effects of mutations in multiple domains of Meq need to be examined. Notably, even two amino acid substitutions in the basic region unexpectedly altered clinical manifestations, such as open-mouth breathing. Field strains encoding Meq with the same amino acid residues at positions 77 and 80 as Meq77/80 may develop similar respiratory signs. In contrast to typical clinical signs, including lymphomas and neurological disorders, MD cases with respiratory manifestations may be overlooked, potentially leading to underestimation of the impact of MD on the poultry industry. Strengthening MDV field surveillance is essential.

SUMMARY

Although the vaccine strain CVI988 carries an insertion in the transactivation domain of Meq, it remains nonpathogenic despite the accelerated tumorigenesis of MDV due to the insertion in Meq. Accordingly, Chapter II focused on characteristic amino acid polymorphisms in the basic region of Meq, with particular attention to the combination of amino acid residues at positions 71 and 77 present in CVI988 (Meq71/77), and the combination at positions 77 and 80 identified in recent highly virulent isolates in Asia, Africa, and Europe (Meq77/80).

Reporter assays revealed that most amino acid substitutions in the basic region reduced transcriptional regulatory activity. Furthermore, these polymorphisms exhibited synergistic effects in decreasing Meq-mediated transcriptional regulation. In the experimental infection, rRB-1B_Meq71/77-infected chickens exhibited neither clinical signs nor lymphoma development. Flow cytometric analysis revealed no expansion of Meq^+ infected cells in this group, but a significant increase in the numbers of $CD8^+$ T cells and γδ T cells at the early phase of infection. Although IHC analysis identified a few Meq^+ cells in several organs, histopathological analysis confirmed the absence of MD-associated lesions. These results indicate that the polymorphisms at positions 71 and 77 in the CVI988 strain are sufficient to abolish MDV virulence. rRB-1B_Meq77/80 also showed reduced mortality and tumor incidence, while it unexpectedly induced other clinical signs, including open-mouth breathing and depression, in infected chickens. Flow cytometric analysis revealed a decrease in Meq^+ cells, accompanied by a significant increase in $CD8^+$ T cell populations, during the acute phase. Histopathological analysis identified hyperplasia in bronchus-associated lymphoid tissue in the lungs. Furthermore, IHC analysis revealed infiltration of Meq-negative lymphocytes into tumor lesions in the liver of rRB-1B_Meq77/80-infected chickens. Collectively, these findings indicate that only two polymorphisms in the basic region of Meq drastically reduce both Meq-mediated transcriptional regulation and MDV virulence, and thus potentially alter the pathogenesis.

CHAPTER III

Programmed cell death-1 expression in T cell subsets in chickens infected with Marek's disease virus

INTRODUCTION

Previous studies have demonstrated that vv+MDV field strains induce robust immunosuppression in chickens (Faiz *et al*., 2017; Gimeno and Schat, 2018). The MDV-induced immunosuppression is partly attributable to the inhibitory factors released from MDV-transformed cells, such as TGF-β and PGE_2 (Gurung *et al*., 2017; Kamble *et al*., 2021), as well as the cytolytic replication in lymphocytes, leading to atrophy in lymphoid organs (Faiz *et al*., 2018; Berthault *et al*., 2018). In Chapter I, infection with rRB-1B_L-Meq resulted in a decreased proportion of γδ T cells, particularly $CD8\alpha^+$ γδ T cells, in infected chickens, which coincided with an expansion of $CD4^+$ T cells. These findings suggest that MDV-transformed cells suppress the proliferation of $CD8\alpha^+$ γδ T cells. Furthermore, in the experimental infections described in Chapter II, rRB-1B_Meq–infected chickens showed a tendency toward the reduction in absolute numbers of $CD8^+$ T cells in the spleen during the late phase of infection compared with uninfected chickens. Similarly, the absolute numbers of γδ T cells tended to decline in both the spleen and thymus of rRB-1B_Meq-infected chickens. These findings suggest that rRB-1B_Meq infection induced immunosuppression in chickens in the terminal phase of infection.

PD-1 is an immunoinhibitory receptor expressed on the surface of activated T and B cells (Freeman *et al*., 2000). In chickens, both PD-1 and its ligand, PD-L1, have been identified, and their interaction has been shown to suppress IFN-γ production by T cells (Matsuyama-Kato *et al*., 2012). The PD-1/PD-L1 axis plays a crucial role in facilitating immune evasion of tumor cells in a range of human and animal cancers, including melanoma and leukemia (Freeman *et al*., 2000; Ikebuchi *et al*., 2010; Kleffel *et al*., 2015; Maekawa *et al*., 2016). Chronic viral infections are also known to induce exhaustion in T cells. Infections with oncogenic retroviruses, such as human T-cell leukemia virus and bovine leukemia virus, cause an increase in PD-1 expression in $CD4^+$ and $CD8^+$ T cells in accordance with disease progression, resulting in an increase in the number of exhausted T cells, which exhibit impaired effector functions, including reduced cytokine production (Kozako *et al*., 2009; Ikebuchi *et al*., 2010). A similar role for the PD-1/PD-L1 pathway has been proposed in MDV infection. In MDV-infected chickens, *pd-1* mRNA expression in $CD4^+$ and $CD8^+$ T cells increased during the early and secondary cytolytic phases (Parvizi *et al*., 2010). Moreover, mRNA expressions of both *pd-1* and *pd-l1* have been detected in tumor lesions using laser capture microdissection and nested RT-PCR, and the expression level of *pd-1* mRNA showed a positive correlation with *meq* mRNA expression (Matsuyama-Kato *et al*., 2012), suggesting elevated PD-1 expression in MDV-transformed cells. However, the protein expression of PD-1 and PD-L1 in

transformed cells and in infiltrating T cell subsets within tumor lesions remains undefined, and the precise contribution of the PD-1/PD-L1 pathway to immunosuppression during MDV infection is yet to be elucidated.

In Chapter III, to clarify the involvement of PD-1 in MDV pathogenesis, the protein expression of PD-1 in T cell subsets and the effect of PD-1 expression on the effector function of $CD8^+$ T and γδ T cells was examined. Flow cytometric analysis was employed to determine the proportions of PD-1-expressing $CD4^+$, $CD8^+$, and γδ T cells in the spleens and tumor tissues of chickens that developed lymphomas, to elucidate the relationship between PD-1 expression and MDV-induced immunosuppression. The proportions of PD-1-expressing cells in Meq-positive and Meq-negative $CD4^+$ T cells were compared to assess PD-1 expression in MDV-infected cells from chickens with tumors. Additionally, to evaluate the potential impact of PD-1 expression on the function of effector cells, the proportions of IFN-γ-positive cells among PD-1-expressing $CD8^+$ T and γδ T cells were analyzed.

MATERIALS AND METHODS

Ethics statement

All animal experiments were approved by the Institutional Animal Care and Use Committee of Hokkaido University (Approval Number: 22-0088). All experiments were performed following the relevant guidelines and regulations of the Faculty of Veterinary Medicine of Hokkaido University, which is fully accredited by the Association for Assessment and Accreditation of Laboratory Animal Care International.

Cells

CEFs were isolated from 10-day-old fertilized eggs (Iwamura Hatchery Co. Ltd.) as described in Chapter I. CEFs were maintained in Eagle's Minimum Essential Medium supplemented with 10% tryptose phosphate broth (Difco Laboratories), 0.03% L-glutamine, 100 U/mL penicillin, 100 μg/mL streptomycin, 10% calf serum (Sigma-Aldrich), and 0.1% sodium bicarbonate. DF-1, a continuous chicken fibroblast cell line, was maintained in Dulbecco's Modified Eagle's Medium (FUJIFILM Wako Pure Chemical Corporation) supplemented with 0.03% L-glutamine, 100 U/mL penicillin, 100 μg/mL streptomycin, and 10% fetal bovine serum (MP Biomedicals). CEFs and DF-1 cells were incubated in a humidified atmosphere containing 5% CO_2 at 37°C and 39 °C, respectively.

Generation of recombinant viruses

In this experiment, rRB-1B_Meq described in Chapters I and II was used. Briefly, The native *meq* in the TRL region of pRB-1B_ΔIRL was replaced with RB-1B-*meq* using a two-step Red recombination strategy (Tischer *et al*., 2006; Tischer and Kaufer, 2012).rMDVs were reconstituted by transfecting the BAC plasmids and pCAGGS-Cre (Gene Bridges GmbH) into CEFs using the CalPhos Mammalian Transfection Kit (Takara Bio Inc.). Reconstituted rRB-1B_Meq were passaged several times on CEFs and stored at –80 °C in Cell Banker 1 (Nippon Zenyaku Kogyo Co., Ltd.). Restoration of the IRL region and removal of BAC sequences were confirmed by PCR. Viral titers were determined by plaque assays as previously reported (Engel *et al*., 2012).

Experimental infection

Fertilized eggs from white leghorn chickens (Iwamura Hatchery Co. Ltd.) were hatched in the laboratory, and the chicks were raised in isolators. A total of 36 one-day-old chicks were randomly assigned to three groups and housed separately. Chickens were

inoculated intraperitoneally with 5,000 PFU of rRB-1B_Meq ($n = 26$) or PBS (pH 7.4) as a negative control ($n = 10$). During experimental infection, each group of chickens was housed separately in an individual isolator following group assignment. After inoculation with rMDV, chickens were monitored daily for clinical signs of MD for 8 weeks. Chickens exhibiting clinical signs during the experimental period were euthanized by collecting heparinized whole blood from the heart under deep general anesthesia induced by isoflurane inhalation (Zoetis Japan), followed by necropsy to assess the presence of gross tumor lesions. All remaining chickens without clinical signs at the end of the experimental period (56 dpi) were euthanized (rRB-1B_Meq-infected group: $n = 13$). In addition, spleens from the control group were collected at 35 and 56 dpi for flow cytometric analysis. Mononuclear cells from spleen suspensions were isolated by density gradient centrifugation using Percoll (GE Healthcare) and preserved in Cell Banker 1 (Nippon Zenyaku Kogyo Co., Ltd.) for subsequent flow cytometric analysis.

Flow cytometric analysis

(i) Evaluation of the availability of chicken PD-1 polyclonal antibody for flow cytometric analysis

For generating the anti-chicken PD-1 polyclonal antibody, antisera were obtained from a rabbit immunized with a synthetic peptide corresponding to 114–131 amino acid regions of chicken PD-1 (accession number XP_422723) (Sigma-Aldrich). The open reading frame of chicken PD-1 was amplified and inserted into the pCI-neo vector (Promega, Madison). DF-1 cells were transfected with 300 ng of the PD-1 expression plasmid using Lipofectamine 2000 (Thermo Fisher Scientific) according to the manufacturer's protocol. At 24 hours after transfection, the availability of the anti-PD-1 polyclonal antibody in flow cytometric analysis was evaluated by detecting PD-1 expression in DF-1 cells using a FACSLyric flow cytometer (BD Biosciences). The anti-chicken PD-1 polyclonal antibodies successfully detected PD-1 expression in DF-1 cells transfected with the PD-1 expression plasmid (Fig.III-1).

(ii) $CD4^+$ T Cell Staining

Mononuclear cells (5×10^5) isolated from the spleen and tumor tissues were placed in 96-well round-bottom plates and washed twice with FACS buffer. Blocking was performed using PBS containing 10% chicken serum (Thermo Fisher Scientific) at 25 °C for 15 min. The cells were incubated with either rabbit anti-chicken PD-1 polyclonal antibodies or negative rabbit antisera (Sigma-Aldrich) for 30 min at 4 °C, followed by two washes with 200 μL of FACS buffer. Surface staining was carried out using mouse anti-chicken CD3ε mAbs conjugated with PerCP-Cy5.5 (Southern Biotech), mouse anti-

chicken CD4 mAbs conjugated with PE-Cy7 (Southern Biotech), and mouse anti-rabbit IgG_1 mAbs conjugated with APC (Thermo Fisher Scientific) for 30 min at 4 °C in the dark. Dead cells were identified using Fixable Viability Dye eFluor780 (Thermo Fisher Scientific). After two washes with FACS buffer, cells were resuspended in 200 μL of Cytofix/Cytoperm solution (BD Biosciences) and incubated for 30 min at 4 °C, followed by three washes with Perm/Wash solution (BD Biosciences). Intracellular staining was then performed using mouse anti-Meq mAbs conjugated with PE or mouse IgG1 isotype mAbs conjugated with PE (Southern Biotech) for 40 min at 4 °C in the dark, with two subsequent washes using Perm/Wash solution. Finally, cells were resuspended in 300 μL of FACS buffer and analyzed on a FACSLyric flow cytometer (BD Biosciences). The gating strategy is presented in Fig. III-2.

(iii) $CD8^+$ T Cell and γδ T Cell Staining

Mononuclear cells (5×10^5) isolated from the spleen and tumor tissues were seeded into 96-well round-bottom plates and incubated in RPMI-1640 medium (Sigma-Aldrich) containing brefeldin A (Sigma-Aldrich) for 4 hours at 41 °C in 5% CO_2 under unstimulated conditions. For stimulated cultures, the cells were incubated in RPMI-1640 medium supplemented with phorbol 12-myristate 13-acetate (PMA) (FUJIFILM Wako Pure Chemical Corporation), ionomycin (Sigma-Aldrich), and brefeldin A for 4 hours at 41 °C in 5% CO_2. Following incubation, cells were washed twice with FACS buffer and blocked with PBS containing 10% chicken serum (Thermo Fisher Scientific) at 25 °C for 15 min. Surface staining was performed with rabbit anti-chicken PD-1 polyclonal antibodies or negative rabbit antisera (Sigma-Aldrich) for 30 min at 4 °C, followed by two washes with 200 μL of FACS buffer. The cells were then stained with mouse anti-chicken CD3ε mAbs conjugated with PerCP-Cy5.5 (Southern Biotech), mouse anti-chicken γδ TCR mAbs conjugated with PE-Cy7 (Southern Biotech), anti-chicken CD8β mAbs conjugated with FITC (Southern Biotech), and mouse anti-rabbit IgG1 mAbs conjugated with APC (Thermo Fisher Scientific) for 30 min at 4 °C in the dark. Dead cells were identified using Fixable Viability Dye eFluor780 (Thermo Fisher Scientific). After two washes with FACS buffer, cells were resuspended in 200 μL of Cytofix/Cytoperm solution (BD Biosciences) and incubated for 30 min at 4 °C, followed by three washes with Perm/Wash solution (BD Biosciences). Intracellular staining was then carried out using mouse anti-chicken IFN-γ mAbs conjugated with biotin (detection antibody from Chicken IFN-γ CytoSet™, Invitrogen) or mouse IgG_1 isotype mAbs conjugated with biotin (BioLegend, San Diego, CA, USA) for 40 min at 4 °C in the dark, followed by two washes with Perm/Wash solution. Subsequently, the cells were incubated with streptavidin conjugated with PE (Invitrogen) for 40 min at room temperature in the

dark and washed twice with Perm/Wash solution. Finally, cells were resuspended in 300 μL of FACS buffer and analyzed using a FACSLyric flow cytometer (BD Biosciences). The gating strategy is shown in Fig. III-3.

Statistical analyses

Statistical analyses were conducted using R Statistical Software (version 4.0.3; R Foundation for Statistical Computing). Differences in the proportion of T cell subsets in chickens were analyzed using the Kruskal–Wallis test followed by Dunn's post hoc test. The proportions of IFN-γ^+ cells within the same individuals were compared using the Wilcoxon signed-rank test. Results with $p < 0.05$ were considered statistically significant.

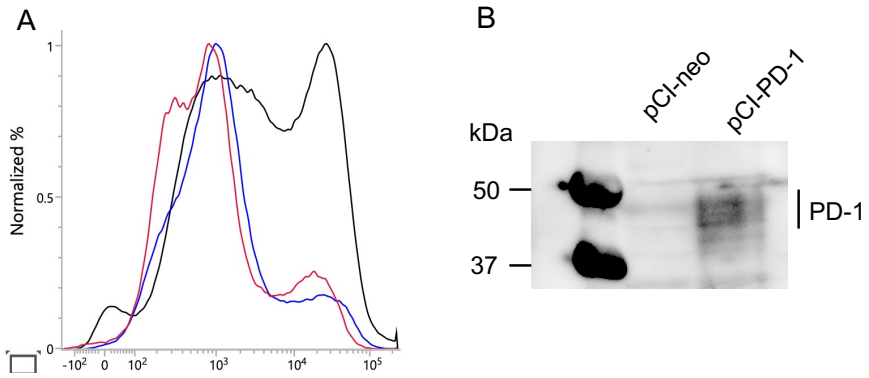

Figure III-1. Verification of binding of anti-chicken programmed cell death 1 (PD-1) polyclonal antibodies

(A) DF-1 cells were transfected with the pCI-neo vector inserted with the chicken *pd-1* gene. Transfected DF-1 cells were incubated with anti-chicken PD-1 polyclonal antibodies for 30 min. The binding to each molecule was analyzed using flow cytometry. The red line represents the binding of isotype control antibodies to the transfected DF-1 cells. The blue line represents the binding of anti-PD-1 polyclonal antibodies to the DF-1 cells transfected with the pCI-neo vector that were not inserted with the gene. (B) Transient expression of the chicken PD-1 construct in DF-1 cells was determined by western blotting using anti-chicken PD-1 polyclonal antibodies.

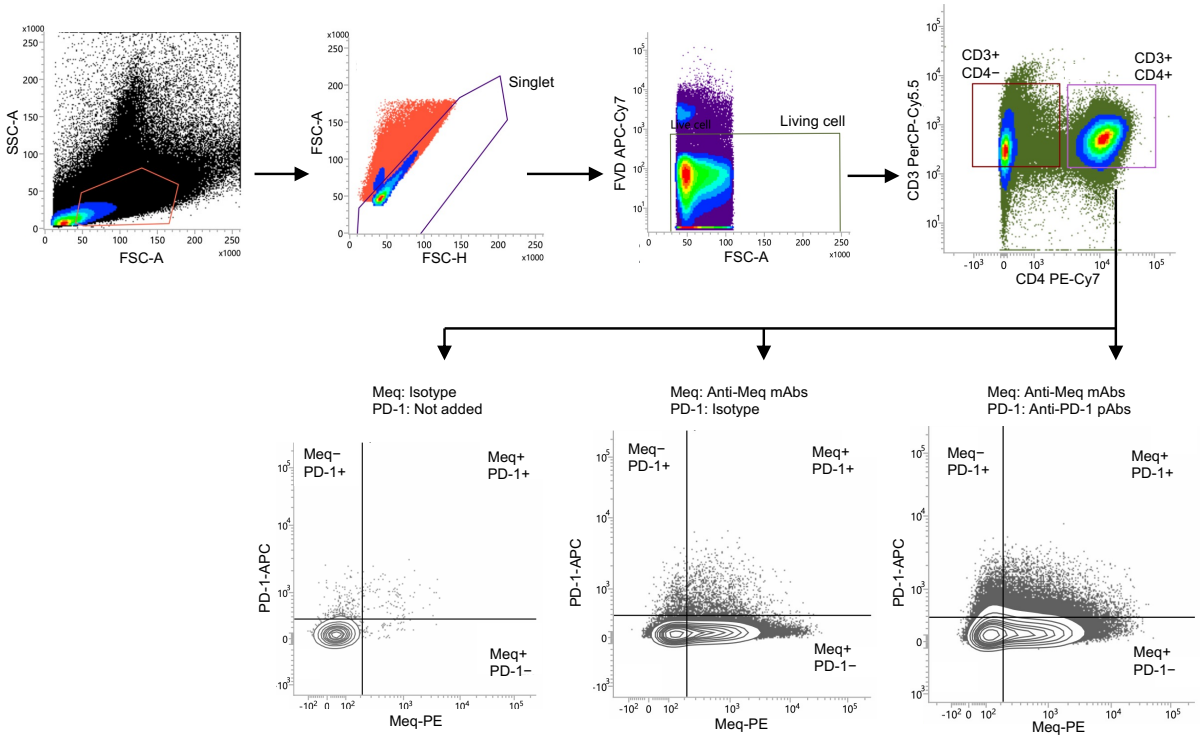

Figure III-2. Gating strategy for analyzing CD4$^+$ T cells.
A representative gating strategy is shown for analyzing CD4$^+$ T cells.

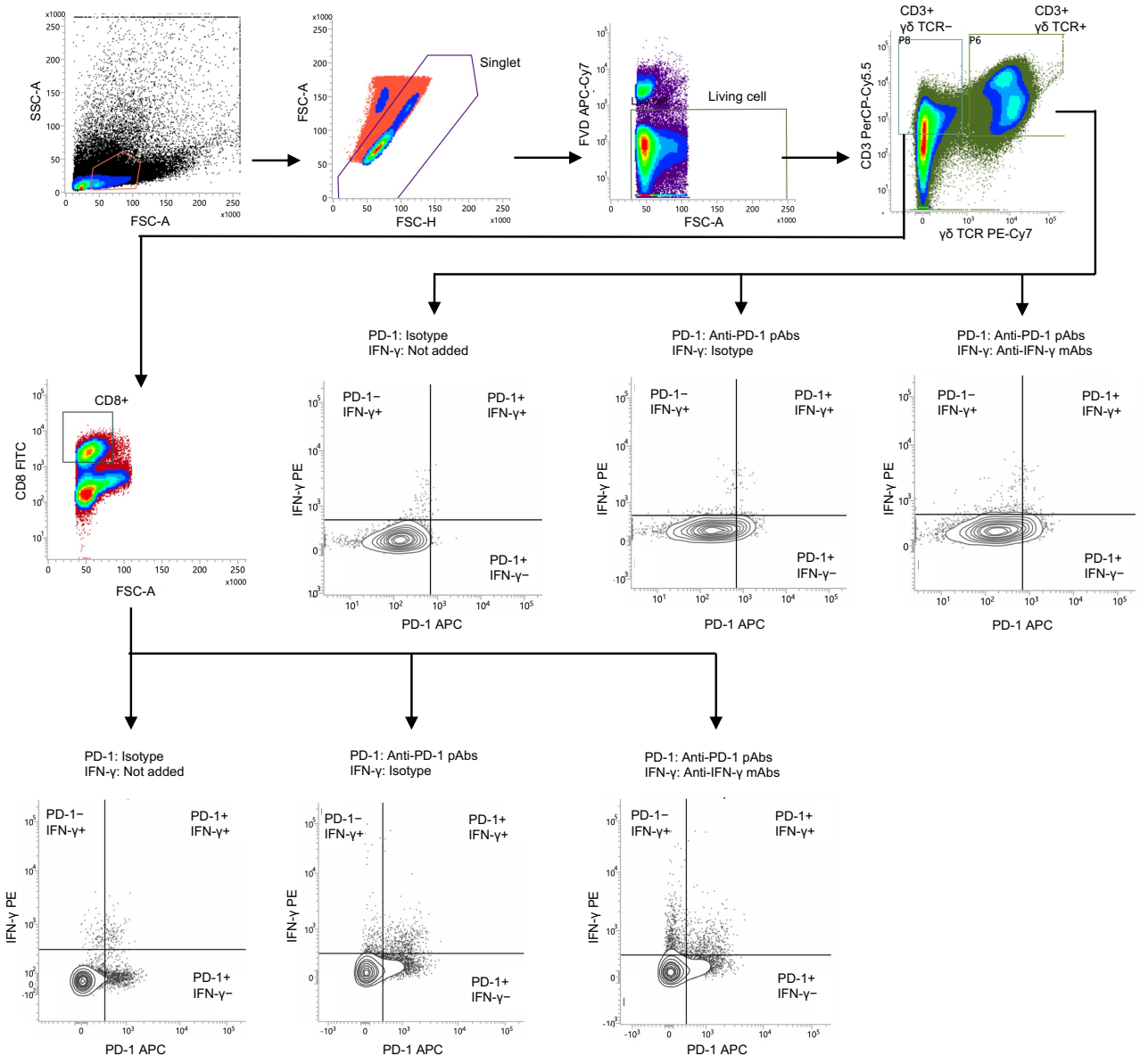

Figure III-3. Gating strategy for analyzing CD8$^+$ T cells and γδ T cells.
A representative gating strategy is shown for analyzing CD8$^+$ T cells and γδ T cells.

RESULTS

CD4$^+$ T cells transformed by MDV exhibit a high proportion of PD-1$^+$ cells

To evaluate PD-1 expression in T cell subsets from chickens that developed MD, chickens were infected with rRB-1B_Meq and monitored for 8 weeks post-infection. Of the 26 rRB-1B_Meq-infected chickens, 13 developed solid tumors in visceral organs. In these chickens with tumors, both the spleen and tumor tissues contained a higher proportion of CD4$^+$ T cells compared to those of the control group (Fig. III-4A).

The anti-Meq mAbs (kindly provided by Dr. Kurokawa, National Agriculture and Food Research Organization, Japan) were subsequently employed to analyze Meq$^+$ cells in the spleen and tumor tissues of chickens with MD. Meq$^+$ CD4$^+$ T cells were detected in both spleens and tumors, with significantly higher proportions observed in tumor tissues compared to spleens (Fig. III-5A). These findings suggest that both the spleen and tumor tissues of chickens with MD contain MDV-transformed CD4$^+$ T cells.

To investigate PD-1 expression in MDV-transformed CD4$^+$ T cells, the proportions of PD-1$^+$ cells within total CD4$^+$ T cells in the spleen and tumor tissues were first analyzed. Compared with the spleen of uninfected chickens, the proportions of PD-1$^+$ CD4$^+$ T cells were significantly higher in both the spleen and tumor tissues of chickens with MD (Figs. III-5B and C). Furthermore, within CD4$^+$ T cells, PD-1$^+$ cell proportions were significantly higher in Meq$^+$ than Meq$^-$ cells in both the spleen and tumor tissues (Figs. III-5B and D). These results show that PD-1 expression is increased in CD4$^+$ T cells, particularly in transformed CD4$^+$ T cells expressing Meq, in chickens with MD.

Expressions of IFN-γ and PD-1 in CD8$^+$ T cells in chickens with MD

The proportion of CD8$^+$ T cells expressing IFN-γ was examined to assess their function in chickens with MD. Compared with the spleen of the control group, the proportion of CD8$^+$ T cells was reduced in the spleen and tumor tissues of chickens with MD (Fig. III-4B), likely due to the expansion of transformed CD4$^+$ T cells. The percentage of IFN-γ$^+$ CD8$^+$ T cells was significantly higher in tumor tissues than in the spleens of both control and infected chickens (Fig. III-6A). In contrast, no significant difference was observed in the proportion of IFN-γ$^+$ CD8$^+$ T cells in the spleens between infected and control groups under unstimulated conditions.

To determine whether CD8$^+$ T cells in chickens with MD retain their ability to produce IFN-γ, isolated cells were stimulated with PMA and ionomycin. In all groups, the stimulation increased the proportion of IFN-γ$^+$ CD8$^+$ T cells compared with unstimulated cells. Notably, after the stimulation, the spleens of chickens with MD

showed a significantly higher proportion of IFN-γ$^+$ CD8$^+$ T cells than the control group, while no significant difference was shown under unstimulated conditions.

PD-1 expression in CD8$^+$ T cells from chickens with MD was subsequently examined. The proportion of PD-1$^+$ CD8$^+$ T cells in the spleens of chickens with MD was significantly higher than that in the control group, while the proportion in tumor tissues tended to be increased compared with that in the control group (p = 0.062; Figs.III-6B and C). To evaluate the cytokine production of PD-1$^+$ CD8$^+$ T cells, the proportion of IFN-γ$^+$ cells was compared between PD-1$^+$ and PD-1$^-$ CD8$^+$ T cell populations in the spleens of uninfected and infected chickens. Within the PD-1$^-$ CD8$^+$ T cell subset, the proportion of IFN-γ$^+$ cells in the infected chickens was elevated relative to that in uninfected controls, while no significant difference was detected in the proportion of IFN-γ$^+$ cells between infected and uninfected groups within the PD-1$^+$ CD8$^+$ T cell subset (Figs. 2B and D). These observations suggest that cytokine production from PD-1$^+$ CD8$^+$ T cells is impaired in chickens with MD.

Expressions of IFN-γ and PD-1 in γδ T cells in chickens with MD

In rRB-1B_Meq-infected chickens, the proportions of γδ T cells in both the spleen and tumor tissues were also significantly reduced compared to those in the control group (Fig. III-4C). The proportion of IFN-γ$^+$ γδ T cells in tumor tissues was significantly higher than in the spleens in both controls and infected chickens (Fig.III-7A). In contrast, the proportion of IFN-γ$^+$ γδ T cells in the spleens of rRB-1B_Meq-infected chickens was comparable to that in the control group (Fig.III-7A). Furthermore, under mitogen stimulation, a significant increase in the proportion of IFN-γ$^+$ γδ T cells was observed in the spleens of both control and infected groups (Fig.III-7A). However, in the tumor tissue of infected chickens, no significant difference was detected between stimulated and unstimulated cultures (Fig.III-7A).

Similar to conventional αβ T cells, γδ T cells may undergo exhaustion after prolonged exposure to pathogen- or tumor-associated antigens (Chen *et al*., 2022). To assess this possibility in MDV infection, the proportion of PD-1$^+$ cells among total γδ T cells was examined in chickens with rRB-1B_Meq. Significantly higher proportions of PD-1$^+$ γδ T cells were detected in the spleens of chickens with MD compared with the control group (Figs. III-7B and C). In tumor tissues, the proportion of PD-1$^+$ γδ T cells was also elevated relative to the control group, although the difference is not significant (p = 0.051, Fig.III- 7C). To investigate the relationship between PD-1 expression and IFN-γ production in γδ T cells, the proportions of IFN-γ$^+$ cells in PD-1$^+$ and PD-1$^-$ γδ T cells were compared in the spleens of uninfected and infected chickens. In the spleens of

the control group, PD-1^{+} γδ T cells displayed a significantly higher proportion of IFN-γ^{+} cells than PD-1^{-} γδ T cells (Figs. III-7B and D). In contrast, no significant difference in the proportion of IFN-γ^{+} cells between PD-1^{+} and PD-1^{-} γδ T cells was detected in the spleens of chickens with MD. Moreover, PD-1^{+} γδ T cells from rRB-1B_Meq-infected chickens exhibited significantly lower proportions of IFN-γ^{+} cells compared with those from controls (Figs.III-7B and D). Collectively, these findings suggest that PD-1^{+} γδ T cells in MDV-infected chickens exhibit impaired effector function.

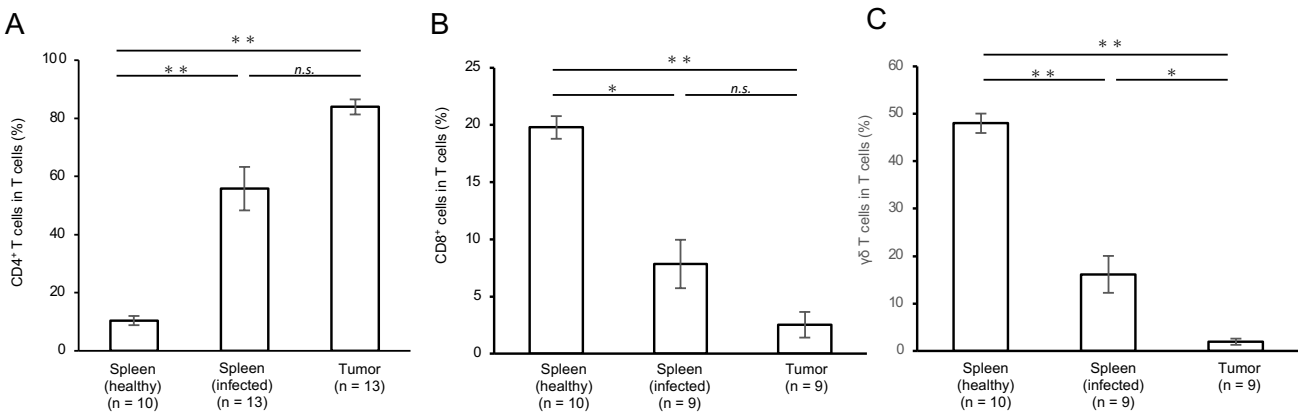

Figure III-4. The percentages of T cell subsets in the spleen and tumor tissue
The percentages of (A) $CD4^+$ T cells, (B) $CD8^+$ T cells, and (C) γδ T cells in the T cell population from spleens and tumor tissues were analyzed.

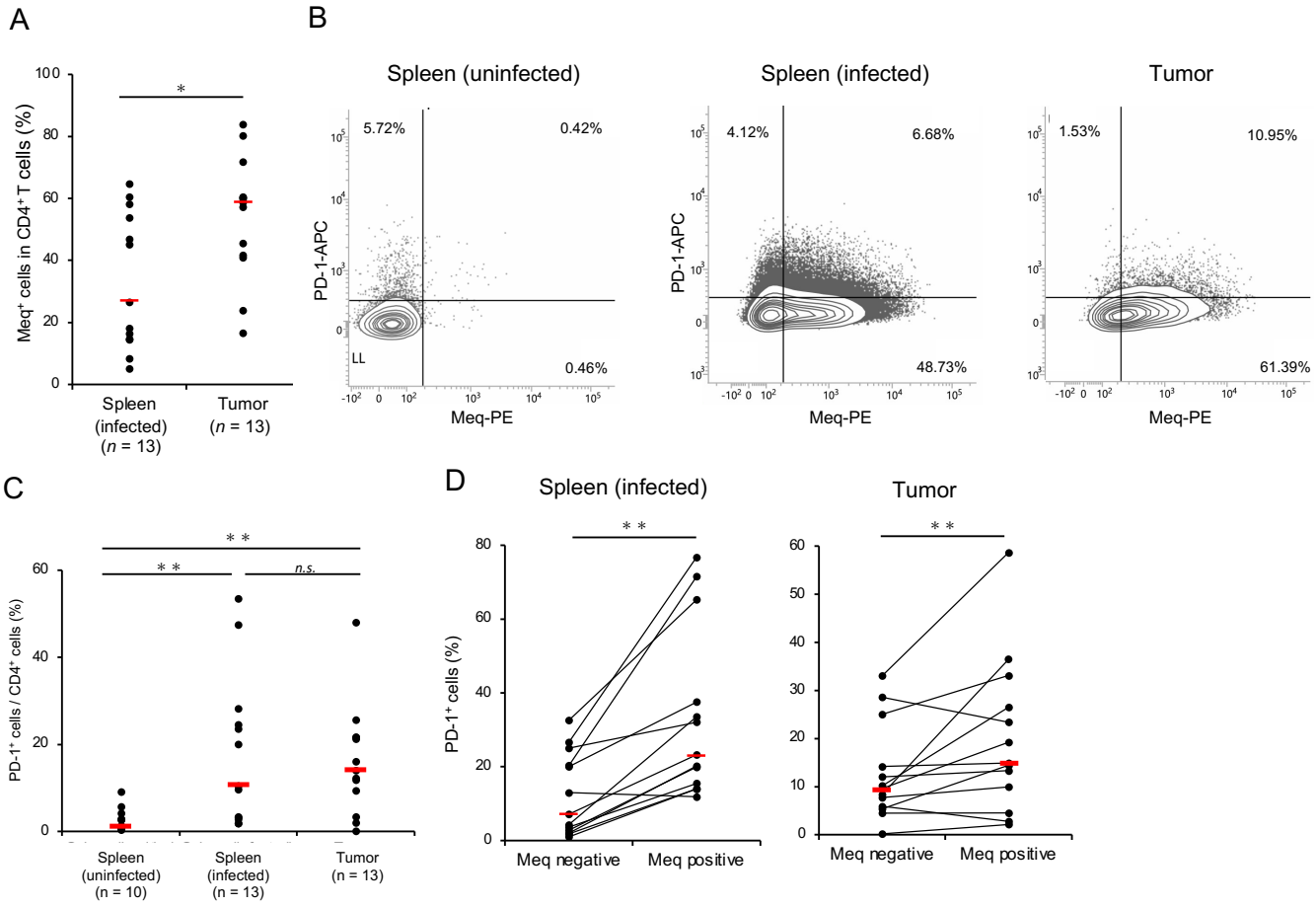

Figure III-5. CD4$^+$ T cells transformed by MDV highly express PD-1
The expression of PD-1 and Meq in the CD4$^+$ T cells was analyzed (control group: n = 10, the spleen of MDV-infected chicken: n = 13, the tumor tissue of MDV-infected chicken: n = 13). (A) A representative gating strategy is shown for analyzing CD4$^+$ T cells. (B) The percentages of PD-1$^+$ CD4$^+$ T cells in the CD4$^+$ T cell population from spleens and tumor tissues were analyzed. (C and D) The percentages of PD-1$^+$ T cells were compared between spleens and tumor tissues in (C) Meq$^+$ CD4$^+$ T cells and (D) Meq$^-$ CD4$^+$ T cells. (E and F) The percentages of PD-1$^+$ CD4$^+$ T cells were compared between Meq$^+$ CD4$^+$ T cells and Meq$^-$ CD4$^+$ T cells in the spleen of (E) the control group and (F) the MDV-infected group. Asterisks indicate significant differences (** $p < 0.01$,* $p < 0.05$; Dunn's test (between the groups), Wilcoxon signed-rank sum (within the same individual)).

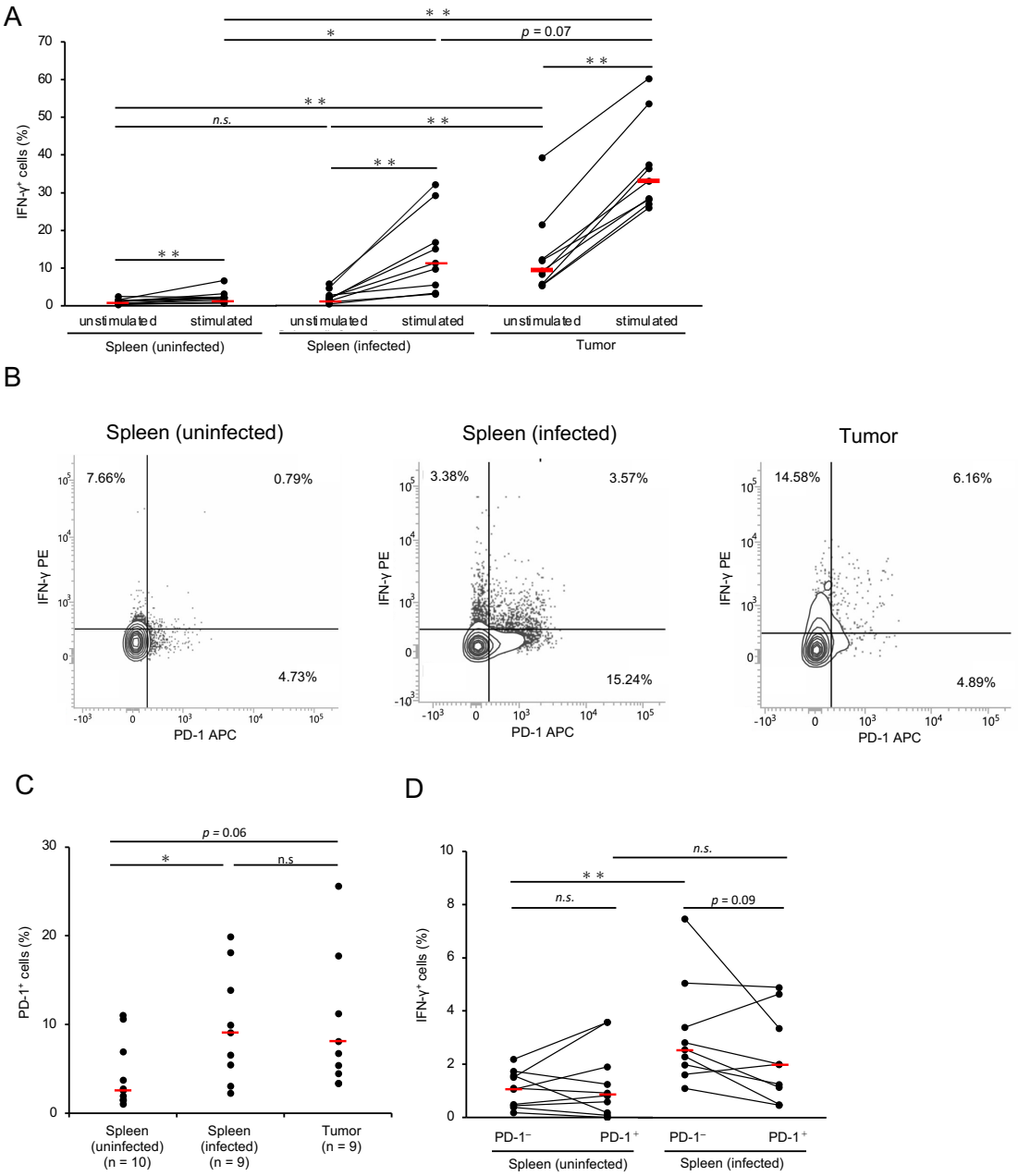

Figure III-6. Expression of interferon-γ (IFN-γ) and PD-1 in CD8$^+$ T cells in MDV-infected chickens

The expression of PD-1 and IFN-γ in the CD8$^+$ T cells was analyzed (control group: n = 10, the spleen of MDV-infected chicken: n = 9, the tumor tissue of MDV-infected chicken: n = 9) (A) The percentages of IFN-γ$^+$ CD8$^+$ T cells in the CD8$^+$ T cell population from spleens and tumor tissues were analyzed after unstimulated and stimulated culture. (B) A representative gating strategy is shown for analyzing CD8$^+$ T cells. (C) The percentages of PD-1$^+$ CD8$^+$ T cells in the CD8$^+$ T cell population from spleens and tumor tissues were analyzed. (D and E) The percentages of IFN-γ$^+$ T cells were compared between PD-1$^+$ CD8$^+$ T cells and PD-1$^-$ CD8$^+$ T cells in the spleen of (D) the control group and (E) the MDV-infected group. Asterisks indicate significant differences (** $p < 0.01$,* $p < 0.05$; Dunn's test (between the groups), Wilcoxon signed-rank sum (within the same individual)).

DISCUSSION

The PD-1/PD-L1 pathway has been shown to exert immunosuppression via T cell exhaustion in many types of tumors and chronic infections (Freeman *et al*., 2000; Ikebuchi *et al*., 2010; Kleffel *et al*., 2015; Maekawa *et al*., 2016). The increased expression of *pd-1* mRNA has also been shown during the pathological stage of MDV-infected chickens (Matsuyama-Kato *et al*., 2012). Additionally, the decreased proportion of $CD8^+$ T cells and γδ T cells observed in Chapters I and II are reminiscent of immunosuppression in the terminal phase of MDV infection. Therefore, in Chapter III, to investigate the involvement of PD-1 in MDV pathogenesis, the protein expression of PD-1 in T cell subsets was analyzed, and the effect of PD-1 expression on the effector function of $CD8^+$ T cells and γδ T cells was evaluated. Flow cytometric analysis revealed an increased proportion of PD-1-expressing $CD4^+$ T cells in MDV-infected chickens. Furthermore, Meq^+ $CD4^+$ T cells displayed significantly higher PD-1 expression than Meq^- $CD4^+$ T cells. In tumor tissues, higher proportions of $CD8^+$ T cells and γδ T cells expressed IFN-γ compared with those in the spleens of both uninfected and infected chickens. In the $CD8^+$ T cell population, the proportion of IFN-γ^+ cells in PD-1^- cells in the spleens of infected chickens was higher than that of uninfected chickens, whereas no difference was detected in the proportion of IFN-γ^+ cells in PD-1^+ cells between the infected and uninfected groups. In γδ T cell populations, the proportion of IFN-γ^+ cells in tumor tissues did not change following mitogen stimulation. Furthermore, no significant difference in the proportion of IFN-γ^+ γδ T cells in the spleens of infected chickens was observed, regardless of PD-1 expression, whereas the proportion of IFN-γ^+ γδ T cells was higher in PD-1^+ cells in the spleens in the uninfected group. Collectively, these findings suggest that tumor cells exhibit a PD-1-expressing phenotype, while PD-1 expression in $CD8^+$ T cells and γδ T cells is associated with diminished immune response during MD development.

The proportion of PD-1-expressing cells was significantly higher in Meq^+ $CD4^+$ T cells than in Meq^- $CD4^+$ T cells, suggesting that MDV-transformed cells elevate PD-1 expression. Two possible mechanisms may account for this observation. The first hypothesis is that MDV preferentially transforms $CD4^+$ T cells expressing PD-1. In humans and mice, activated T cells display high PD-1 expression (Raimondi *et al*., 2006), and MDV-transformed cells express CD25, a marker of T-cell activation (Burgess and Davison, 2002). These observations raise the possibility that MDV selectively establishes latency in activated PD-1^+ $CD4^+$ T cells and subsequently transforms them. An alternative explanation is that MDV-transformed cells may respond to soluble factors from immune

cells in the tumor microenvironment, and then express PD-1. For instance, IFN-γ is a potent inducer of PD-1 expression in both humans and mice (Keir *et al*., 2008), and previous analyses have shown a positive correlation between *pd-1* and *ifn-γ* mRNA levels in tumor lesions from MDV-infected chickens (Matsuyama-Kato *et al*., 2012). In this chapter, the proportion of IFN-γ-expressing $CD8^+$ T cells and γδ T cells was higher in tumor tissues than in the spleens from uninfected and infected chickens, suggesting that PD-1 expression in transformed cells is triggered by cytokines such as IFN-γ in the tumor microenvironment. Consequently, high PD-1 expression in MDV-transformed $CD4^+$ T cells may reflect the pre-transformation phenotype or the factors in the tumor microenvironment. Additionally, PD-1 expression might give an advantage to tumor cells. MDV-transformed T cells possess a phenotype resembling Treg cells that express mTGF-β. In murine models of chronic lymphocytic choriomeningitis virus infection, Treg cells with elevated PD-1 expression can suppress $CD8^+$ T cell proliferation and cytokine production via the PD-1/PD-L1 interaction (Park *et al*., 2015). PD-1 expressed on MDV-transformed $CD4^+$ T cells may contribute to impaired cytokine production by $CD8^+$ T cells. Further studies are required to clarify the role of PD-1 in the immune evasion by transformed cells.

Under unstimulated conditions with mitogen, no significant difference was detected in the proportions of IFN-γ-expressing $CD8^+$ T cells in the spleens of uninfected and infected chickens. In contrast, following mitogen stimulation, the proportion of IFN-γ^+ $CD8^+$ T cells was increased in the spleens of infected chickens and was significantly higher than that in uninfected chickens. Previous studies have shown that MDV-transformed cells downregulate MHC class I expression, facilitating evasion from effector T-cell recognition (Morimura *et al*., 1996). Moreover, $CD8^+$ T cells in MDV-infected chickens exhibit reduced responsiveness to TCR-mediated stimulation (Morimura *et al*., 1996). The stimulation used in this chapter, PMA and ionomycin, bypasses the TCR signaling pathway and directly activates NF-κB in T cells. This suggests that $CD8^+$ T cells with impaired responsiveness to TCR-mediated stimulation could still produce IFN-γ after stimulation with PMA and ionomycin. Taken together, these findings suggest that a subset of $CD8^+$ T cells in the spleens of MDV-infected chickens can still produce cytokines but fails to recognize tumor cells via the TCR, which likely explains why IFN-γ expression in $CD8^+$ T cells in infected chickens remained comparable to that in uninfected chickens under unstimulated conditions.

Consistent with a previous study that *pd-1* mRNA expression is elevated in $CD8^+$ T cells of MDV-infected chickens (Parvizi *et al*., 2010), flow cytometric analysis in this chapter demonstrated an increased proportion of PD-1-expressing $CD8^+$ T cells in both

the spleen and tumor tissues of chickens with MD. Furthermore, in the spleen of the infected group, the proportion of IFN-γ-expressing cells in PD-1^{-} CD8^{+} T cells was higher than in uninfected groups, suggesting an expansion of CD8^{+} T cells specific to infected and/or transformed cells. In contrast, no difference was observed in the proportion of IFN-γ–expressing cells in PD-1^{+} CD8^{+} T cells in the spleens between uninfected and infected chickens. These findings suggest that PD-1 expression is associated with diminished IFN-γ production in CD8^{+} T cells in chickens with MD. Further studies, including the response of CD8^{+} T cells to viral antigens, such as cytokine production and PD-1 expression, are necessary to elucidate the mechanisms underlying the reduced function in CD8^{+} T cells.

A previous research has shown that supernatants from cultured splenocytes of MDV-infected chickens can suppress IFN-γ expression in γδ T cells (Matsuyama-Kato *et al*., 2023a). In the present analysis, the proportion of IFN-γ^{+} γδ T cells in tumor tissues was not increased following mitogen stimulation, whereas the stimulation enhanced IFN-γ production in γδ T cells from the spleens. These observations suggest that the function of γδ T cells could be profoundly impaired by components of the tumor microenvironment. In the spleens of uninfected chickens, PD-1^{+} γδ T cells displayed a significantly higher proportion of IFN-γ-expressing cells compared to PD-1^{-} γδ T cells, indicating that some PD-1-expressing γδ T cells in uninfected chickens possess an IFN-γ-producing phenotype. In contrast, in the spleens of chickens with MD, no increase in IFN-γ expression was detected in PD-1^{+} γδ T cells relative to PD-1^{-} γδ T cells, suggesting impaired function of PD-1^{+} γδ T cells in chickens with MD. For a more comprehensive understanding of the PD-1/PD-L1 pathway in MDV pathogenesis, the development of antibodies targeting PD-1 ligands, such as PD-L1, followed by expression analyses, would be valuable. Additionally, in humans and mice, exhausted γδ T cells co-express other immune checkpoint molecules, including cytotoxic T-lymphocyte–associated protein 4 and lymphocyte-activation gene 3, alongside PD-1. Further investigation of the expression of other immune checkpoint molecules on γδ T cells would be important for elucidating their role in MD pathogenesis.

SUMMARY

Highly virulent MDV field strains have been shown to induce immunosuppression in chickens. In the experimental infections described in Chapter II, rRB-1B_Meq-infected chickens tended to reduce the numbers of $CD8^+$ T cells and γδ T cells in both the spleen and thymus. Given that the PD-1/PD-L1 axis has previously been proposed to be involved in MDV pathogenesis, Chapter III aimed to investigate the expression of PD-1 in $CD4^+$, $CD8^+$, and γδ T cell subsets in the spleen and tumor tissues of chickens with MD and its association with IFN-γ expression in each T cell subset.

Flow cytometric analysis demonstrated an increased proportion of PD-1-expressing $CD4^+$ T cells, the primary targets of MDV tumorigenesis, in both the spleen and tumor tissues of chickens with MD. In $CD4^+$ T cells, the proportion of PD-1^+ cells was higher in Meq-positive cells than in Meq-negative cells. In the spleens of chickens with MD, increased proportions of PD-1^+ cells within $CD8^+$ T cells and γδ T cells were observed relative to uninfected controls. Notably, the proportion of IFN-γ-producing PD-1^+ $CD8^+$ T cells was not increased in the spleens of chickens with MD. Furthermore, under the condition with mitogen stimulation, IFN-γ^+ cells in the γδ T cell populations within tumor tissues remained unchanged. In the spleens of chickens with MD, no difference was detected in the proportion of IFN-γ-producing γδ T cells between PD-1^+ and PD-1^- cells, although in uninfected chickens, the PD-1^+ cells exhibited a higher proportion. These results suggest that PD-1-expressing $CD8^+$ T cells and γδ T cells exhibit functional impairment following MD onset, potentially contributing to MDV-induced immunosuppression. These findings provide novel insights into MDV pathogenesis and the immune response in infected chickens.

CONCLUSION

Marek's disease virus (MDV) causes Marek's disease (MD), characterized by malignant lymphomas, immunosuppression, and neurological disorders, such as leg paralysis and torticollis. The development of effective attenuated vaccines has substantially reduced the incidence of MD to date. However, the increased virulence of field MDV strains has led to vaccine breaks, with MD cases reported in vaccinated flocks worldwide. Meq, MDV oncoprotein, harbors polymorphisms and insertion/deletion sequences that are shared with field strains depending on their virulence. Experimental infections with rMDV demonstrated that the amino acid sequence of Meq can influence MDV virulence. However, the molecular mechanisms by which Meq alters MDV virulence, and the specific amino acid residues involved in this mechanism, remain poorly understood. The present study examined the relationship between the amino acid sequences in Meq and MDV virulence, and explored the mechanisms contributing to immunosuppression in MDV pathogenesis.

In Chapter I, to investigate the mechanisms underlying the increased virulence by the insertion in the transactivation domain of Meq, the effect of the insertion on Meq function and the processes of disease development were analyzed in details. Reporter assays demonstrated that the insertion enhanced transactivation activity on several promoters related to oncogenesis. The insertion also increased Meq protein stability, potentially resulting in the elevated transactivation activity. Infection with a recombinant MDV (rMDV) based on RB-1B, a very virulent MDV strain, carrying the insertion in Meq (rRB-1B_L-Meq) led to early expansion of mTGF-β–expressing $CD4^+$ T cells, a characteristic phenotype of MDV-transformed cells. However, flow cytometric analysis of tumor lesions showed no substantial differences in cellular composition between rRB-1B_L-Meq- and rRB-1B_Meq-infected chickens. Transcriptome profiling revealed similar gene expression patterns in the two infected-groups, but Gene Ontology (GO) enrichment analyses of differentially expressed genes identified distinct biological signatures. Tumors from rRB-1B_L-Meq–infected chickens exhibited enrichment in immune-related GO terms, such as "T cell proliferation" and "chemotaxis". These results suggest that the insertion does not alter Meq transcriptional targets but accelerates tumorigenesis by increasing protein stability and enhancing transactivation function (Fig. 3).

In Chapter II, amino acid polymorphisms in the basic region of Meq were examined, focusing on the combination at positions 71 and 77 found in the attenuated vaccine strain CVI988 (Meq71/77) and the combination at positions 77 and 80 identified in recent

isolates with high virulence in Asia, Africa, and Europe (Meq77/80). Reporter assays demonstrated that most amino acid substitutions at positions 71, 77, and 80 in the basic region into RB-1B-Meq reduced transcriptional regulatory activity. In experimental infections, chickens challenged with an RB-1B-based rMDV encoding Meq71/77 (rRB-1B_Meq71/77) displayed no MD signs and showed no expansion of Meq^+ cells. Moreover, histopathological analysis confirmed the absence of MD-associated lesions. In contrast, rRB-1B_Meq77/80 infection resulted in reduced mortality and tumor incidence, but it caused unexpected clinical signs, including open-mouth breathing, different from those in rRB-1B encoding native RB-1B-Meq. In addition, in the later phase of infection, Meq^+ cells were maintained at low levels, accompanied with a significant increase in $CD8^+$ T cell populations. Intriguingly, histopathological analysis identified hyperplasia in the bronchus-associated lymphoid tissues of the lungs. These findings indicate that the combination of two specific polymorphisms in the basic region of Meq markedly reduce Meq-mediated transcriptional regulation and MDV virulence, and potentially alter clinical manifestations.

In Chapter III, the potential involvement of the PD-1/PD-L1 axis in MDV pathogenesis was examined by assessing PD-1 expression in $CD4^+$, $CD8^+$, and gamma-delta (γδ) T cell subsets within the spleen and tumor tissues of chickens with MD, along with its association with IFN-γ production in each subset. Flow cytometric analysis demonstrated elevated proportions of PD-1^+ cells across all three T cell populations in chickens with MD. In $CD4^+$ T cells, the proportion of PD-1^+ cells was higher in Meq-positive cells than in Meq-negative cells, suggesting that high proportion of MDV-transformed cells expresses PD-1. In $CD8^+$ T cells, the proportion of IFN-γ-producing cells was not increased in PD-1^+ cells of the spleens of chickens with MD. Under culture conditions of mitogen stimulation, IFN-γ expression in γδ T cells from tumor tissues remained unchanged, regardless of PD-1 expression. In addition, in the spleens of chickens with MD, no significant difference was observed in the proportion of IFN-γ–producing γδ T cells between PD-1^+ and PD-1^- subsets, whereas in uninfected chickens, the PD-1^+ subset showed a higher proportion. These findings suggest that PD-1-expressing $CD8^+$ and γδ T cells exhibit impaired effector function following the onset of MD, potentially contributing to MDV-induced immunosuppression.

This study shows that amino acid polymorphisms in the basic region are important determinants of MDV virulence. In addition, insertion in the transactivation domain appear to enhance MDV virulence by increasing the stability and transcriptional regulatory capacity of Meq. The mechanisms that differences in amino acid sequences in the basic region influence MDV virulence may differ from those of the transactivation

domain, and further investigation is required to elucidate how the amino acid sequences of Meq cause differences in the virulence. Additionally, analyses in the relationship between PD-1 expression and their IFN-γ production in cells possessing effector functions, such as $CD8^+$ T cells and γδ T cells, showed a potential role of the PD-1/PD-L1 axis in immunosuppression in MD pathogenesis. Collectively, these findings provide insights into the mechanisms underlying enhanced MDV virulence and its survival strategies in the field, as well as practical implications for the development of more effective vaccines and the prediction of regional shifts in MDV virulence, thereby supporting improved disease control.

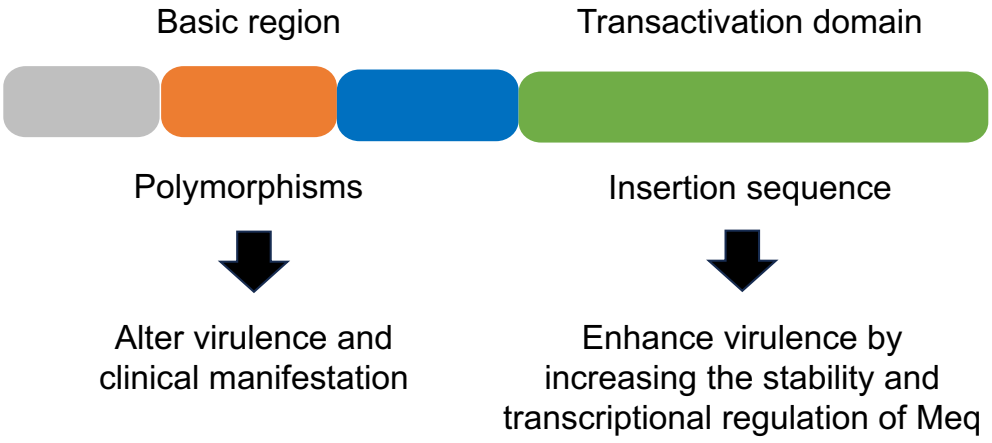

Figure 3. Schematic representation of the effects of mutations in Meq
Polymorphisms in the basic region alter virulence and clinical manifestations. Insertion sequence enhances virulence by increasing protein stability and transcriptional regulation activity of Meq.

ACKNOWLEDGEMENT

I would like to express my deepest appreciation to Dr. Kazuhiko Ohashi, Dr. Satoru Konnai, Dr. Shiro Murata, Dr. Tomohiro Okagawa, and Dr. Naoya Maekawa, Laboratory of Infectious Diseases, Department of Disease Control, Faculty of Veterinary Medicine, Hokkaido University, for their continuous, mentoring, supporting, guidance, assistance, and encouragement during this work.

I owe a deep debt of gratitude to Dr. Yoshihiro Sakoda, Laboratory of Infectious Diseases, Department of Disease Control, Faculty of Veterinary Medicine, Hokkaido University, and Dr. Takashi Kimura, Laboratory of Comparative Pathology, Department of Clinical Sciences, Faculty of Veterinary Medicine, Hokkaido University, for their valuable advice on the experiments and critical review of the manuscripts.

I would like to express my sincere appreciation to Dr. Aoi Kurokawa, National Institute of Animal Health, National Agriculture and Food Research Organization, for their comprehensive supervision on histological analyses, kindly providing the anti-Meq and anti-pp38 antibodies, and helpful suggestions.

I am deeply grateful to Dr. Benedikt B. Kaufer, Institute of Virology, Freie Universität Berlin; Dr. Nikolaus Osterrieder, Tierärztliche Hochschule Hannover; and Dr. Mark S. Parcells, Department of Animal and Food Sciences, University of Delaware, for kindly providing the BAC plasmid of MDV and for their valuable suggestions on the research.

Sincere special thanks are extended to all my colleagues in Laboratory of Infectious Diseases, Department of Disease Control, Faculty of Veterinary Medicine, Hokkaido University, for their kind help and warm friendship.

I am very thankful to the Japan Society for the Promotion of Science (JSPS) for the fellowship that supported the current study. I would like to express my sincere condolences on the death of the experimental animals used for this thesis.

I would like to express my deepest appreciation to my family and friends for their encouragement and dedicated support of my education and research.

REFERENCES

Abdul-Careem MF, Hunter BD, Lee LF, Fairbrother JH, Haghighi HR, Read L, Parvizi P, Heidari M, Sharif S. Host responses in the bursa of Fabricius of chickens infected with virulent Marek's disease virus. *Virology*. 2008 Sep 30;379(2):256-65.

Abdul-Careem MF, Javaheri-Vayeghan A, Shanmuganathan S, Haghighi HR, Read LR, Haq K, Hunter DB, Schat KA, Heidari M, Sharif S. Establishment of an aerosol-based Marek's disease virus infection model. *Avian Dis.* 2009 Sep;53(3):387-91.

Ajithdoss DK, Liao Y, Reddy SM, Lupiani B. Marek's Disease Virus (MDV) Meq oncoprotein plays distinct roles in tumor incidence, distribution, and size. *Viruses.* 2025 Feb 14;17(2):259.

Ajithdoss DK, Reddy SM, Suchodolski PF, Lee LF, Kung HJ, Lupiani B. In vitro characterization of the Meq proteins of Marek's disease virus vaccine strain CVI988. *Virus Res.* 2009 Jun;142(1-2):57-67.

Anobile JM, Arumugaswami V, Downs D, Czymmek K, Parcells M, Schmidt CJ. Nuclear localization and dynamic properties of the Marek's disease virus oncogene products Meq and Meq/vIL8. *J Virol.* 2006 Feb;80(3):1160-6.

Baaten BJ, Staines KA, Smith LP, Skinner H, Davison TF, Butter C. Early replication in pulmonary B cells after infection with Marek's disease herpesvirus by the respiratory route. *Viral Immunol.* 2009 Dec;22(6):431-44.

Bacon LD, Witter RL, Silva RF. Characterization and experimental reproduction of peripheral neuropathy in White Leghorn chickens. *Avian Pathol.* 2001 Oct;30(5):487-99.

Baigent SJ, Kgosana LB, Gamawa AA, Smith LP, Read AF, Nair VK. Relationship between levels of very virulent MDV in poultry dust and in feather tips from vaccinated chickens. *Avian Dis.* 2013 Jun;57(2 Suppl):440-7.

Barrow AD, Burgess SC, Baigent SJ, Howes K, Nair VK. Infection of macrophages by a lymphotropic herpesvirus: a new tropism for Marek's disease virus. *J Gen Virol*. 2003 Oct;84(Pt 10):2635-45.

Bavananthasivam J, Alqazlan N, Alizadeh M, Matsuyama-Kato A, Astill J, Kulkarni RR, Sharif S. The regulatory microenvironment in feathers of chickens infected with very virulent Marek's disease virus. *Viruses.* 2022 Jan 9;14(1):112.

Berthault C, Larcher T, Härtle S, Vautherot JF, Trapp-Fragnet L, Denesvre C. Atrophy of primary lymphoid organs induced by Marek's disease virus during early infection is associated with increased apoptosis, inhibition of cell proliferation and a severe B-lymphopenia. *Vet Res.* 2018 Mar 27;49(1):31.

Bertzbach LD, van Haarlem DA, Härtle S, Kaufer BB, Jansen CA. Marek's disease virus infection of natural killer cells. *Microorganisms*. 2019 Nov 20;7(12):588.

Bonneville M, O'Brien RL, Born WK. Gammadelta T cell effector functions: a blend of innate programming and acquired plasticity. *Nat Rev Immunol.* 2010 Jul;10(7):467-78.

Boodhoo N, Behboudi S. Differential virus-specific IFN-Gamma producing T cell responses to Marek's disease virus in chickens with B19 and B21 MHC haplotypes. *Front Immunol.* 2022a Jan 13;12:784359.

Boodhoo N, Behboudi S. Marek's disease virus-specific T cells proliferate, express antiviral cytokines but have impaired degranulation response. *Front Immunol.* 2022b Sep 15;13:973762.

Boodhoo N, Kamble N, Kaufer BB, Behboudi S. Replication of Marek's disease virus is dependent on synthesis of *de novo* fatty acid and prostaglandin E_2. *J Virol*. 2019 Jun 14;93(13):e00352-19.

Brown AC, Baigent SJ, Smith LP, Chattoo JP, Petherbridge LJ, Hawes P, Allday MJ, Nair V. Interaction of MEQ protein and C-terminal-binding protein is critical for induction of lymphomas by Marek's disease virus. *Proc Natl Acad Sci U S A.* 2006 Feb 7;103(6):1687-92.

Burgess SC, Davison TF. Identification of the neoplastically transformed cells in Marek's disease herpesvirus-induced lymphomas: recognition by the monoclonal antibody AV37. *J Virol*. 2002 Jul;76(14):7276-92.

Burgess SC, Young JR, Baaten BJ, Hunt L, Ross LN, Parcells MS, Kumar PM, Tregaskes CA, Lee LF, Davison TF. Marek's disease is a natural model for lymphomas overexpressing Hodgkin's disease antigen (CD30). *Proc Natl Acad Sci U S A*. 2004 Sep 21;101(38):13879-84.

Calnek, B. W. Pathogenesis of Marek’s disease virus infection. *Marek’s disease*. Pages 25–55, Springer Berlin Heidelberg, Berlin, Heidelberg. 2001

.

Chacón RD, Sánchez-Llatas CJ, L Pajuelo S, Diaz Forero AJ, Jimenez-Vasquez V, Médico JA, Soto-Ugaldi LF, Astolfi-Ferreira CS, Piantino Ferreira AJ. Molecular characterization of the *meq* oncogene of Marek's disease virus in vaccinated Brazilian poultry farms reveals selective pressure on prevalent strains. *Vet Q.* 2024 Dec;44(1):1-13.

Chang KS, Lee SI, Ohashi K, Ibrahim A, Onuma M. The detection of the meq gene in chicken infected with Marek's disease virus serotype 1. *J Vet Med Sci*. 2002 May;64(5):413-7.

Chen D, Guo Y, Jiang J, Wu P, Zhang T, Wei Q, Huang J, Wu D. γδ T cell exhaustion: Opportunities for intervention. *J Leukoc Biol.* 2022 Dec;112(6):1669-76.

Churchill AE, Biggs PM. Herpes-type virus isolated in cell culture from tumors of chickens with Marek's disease. II. Studies in vivo. *J Natl Cancer Inst.* 1968 Oct;41(4):951-6.

Conradie AM, Bertzbach LD, Bhandari N, Parcells M, Kaufer BB. A common live-attenuated avian herpesvirus vaccine expresses a very potent oncogene. *mSphere.* 2019 Oct 9;4(5):e00658-19.

Conradie AM, Bertzbach LD, Trimpert J, Patria JN, Murata S, Parcells MS, Kaufer BB. Distinct polymorphisms in a single herpesvirus gene are capable of enhancing virulence and mediating vaccinal resistance. *PLoS Pathog.* 2020 Dec 11;16(12):e1009104.

Deng X, Li X, Shen Y, Qiu Y, Shi Z, Shao D, Jin Y, Chen H, Ding C, Li L, Chen P, Ma Z. The Meq oncoprotein of Marek's disease virus interacts with p53 and inhibits its transcriptional and apoptotic activities. *Virol J*. 2010 Nov 26;7:348.

Deng Q, Shi M, Li Q, Wang P, Li M, Wang W, Gao Y, Li H, Lin L, Huang T, Wei P. Analysis of the evolution and transmission dynamics of the field MDV in China during the years 1995-2020, indicating the emergence of a unique cluster with the molecular characteristics of vv+ MDV that has become endemic in southern China. *Transbound Emerg Dis.* 2021 Nov;68(6):3574-87.

Engel AT, Selvaraj RK, Kamil JP, Osterrieder N, Kaufer BB. Marek's disease viral interleukin-8 promotes lymphoma formation through targeted recruitment of B cells and CD4+ CD25+ T cells. *J Virol*. 2012 Aug;86(16):8536-45.

Faiz NM, Cortes AL, Guy JS, Fletcher OJ, Cimino T, Gimeno IM. Evaluation of factors influencing the development of late Marek's disease virus-induced immunosuppression: virus pathotype and host sex. *Avian Pathol*. 2017 Aug;46(4):376-85.

Faiz NM, Cortes AL, Guy JS, Reddy SM, Gimeno IM. Differential attenuation of Marek's disease virus-induced tumours and late-Marek's disease virus-induced immunosuppression. *J Gen Virol*. 2018 Jul;99(7):927-36.

Fiddaman SR, Dimopoulos EA, Lebrasseur O, du Plessis L, Vrancken B, Charlton S, Haruda AF, Tabbada K, Flammer PG, Dascalu S, Marković N, Li H, Franklin G, Symmons R, Baron H, Daróczi-Szabó L, Shaymuratova DN, Askeyev IV, Putelat O, Sana M, Davoudi H, Fathi H, Mucheshi AS, Vahdati AA, Zhang L, Foster A, Sykes N, Baumberg GC, Bulatović J, Askeyev AO, Askeyev OV, Mashkour M, Pybus OG, Nair V, Larson G, Smith AL, Frantz LAF. Ancient chicken remains reveal the origins of virulence in Marek's disease virus. *Science*. 2023 Dec 15;382(6676):1276-81.

Freeman GJ, Long AJ, Iwai Y, Bourque K, Chernova T, Nishimura H, Fitz LJ, Malenkovich N, Okazaki T, Byrne MC, Horton HF, Fouser L, Carter L, Ling V, Bowman MR, Carreno BM, Collins M, Wood CR, Honjo T. Engagement of the PD-1 immunoinhibitory receptor by a novel B7 family member leads to negative regulation of lymphocyte activation. *J Exp Med*. 2000 Oct 2;192(7):1027-34.

Fukuchi K, Sudo M, Lee YS, Tanaka A, Nonoyama M. Structure of Marek's disease virus DNA: detailed restriction enzyme map. *J Virol.* 1984 Jul;51(1):102-9.

Gessler M, Poustka A, Cavenee W, Neve RL, Orkin SH, Bruns GA. Homozygous deletion in Wilms tumours of a zinc-finger gene identified by chromosome jumping. *Nature*. 1990 Feb 22;343(6260):774-8.

Ghalyanchilangeroudi A, Hosseini H, Nazarpak HH, Molouki A, Dezfoulian O, Morshed R. Molecular Characterization and Phylogenetic Analysis of Marek's Disease Virus in Iran. *Avian Dis*. 2022 Oct;66(3):1-5.

Gimeno IM. Marek's disease vaccines: a solution for today but a worry for tomorrow? *Vaccine.* 2008 Jul 18;26 Suppl 3:C31-41.

Gimeno IM, Schat KA. Virus-induced immunosuppression in chickens. *Avian Dis*. 2018 Sep;62(3):272-85.

Gimeno IM, Witter RL, Hunt HD, Lee LF, Reddy SM, Neumann U. Marek's disease virus infection in the brain: virus replication, cellular infiltration, and major histocompatibility complex antigen expression. *Vet Pathol*. 2001 Sep;38(5):491-503.

Gurung A, Kamble N, Kaufer BB, Pathan A, Behboudi S. Association of Marek's Disease induced immunosuppression with activation of a novel regulatory T cells in chickens. *PLoS Pathog.* 2017 Dec 21;13(12):e1006745.

Hao X, Li S, Li J, Yang Y, Qin A, Shang S. An anti-tumor vaccine against Marek's disease virus induces differential activation and memory response of γδ T cells and CD8 T cells in chickens. *Front Immunol.* 2021 Feb 15;12:645426.

Ikebuchi R, Konnai S, Sunden Y, Onuma M, Ohashi K. Molecular cloning and expression analysis of bovine programmed death-1. *Microbiol Immunol.* 2010 May;54(5):291-8.

Jones D, Lee L, Liu JL, Kung HJ, Tillotson JK. Marek disease virus encodes a basic-leucine zipper gene resembling the fos/jun oncogenes that is highly expressed in lymphoblastoid tumors. *Proc Natl Acad Sci U S A.* 1992 May 1;89(9):4042-6.

Kamble N, Gurung A, Kaufer BB, Pathan AA, Behboudi S. Marek's disease virus modulates T cell proliferation *via* activation of cyclooxygenase 2-dependent prostaglandin E2. *Front Immunol.* 2021 Dec 22;12:801781.

Keir ME, Butte MJ, Freeman GJ, Sharpe AH. PD-1 and its ligands in tolerance and immunity. *Annu Rev Immunol.* 2008;26:677-704.

Kleffel S, Posch C, Barthel SR, Mueller H, Schlapbach C, Guenova E, Elco CP, Lee N, Juneja VR, Zhan Q, Lian CG, Thomi R, Hoetzenecker W, Cozzio A, Dummer R, Mihm MC Jr, Flaherty KT, Frank MH, Murphy GF, Sharpe AH, Kupper TS, Schatton T. Melanoma cell-intrinsic PD-1 receptor functions promote tumor growth. *Cell.* 2015 Sep 10;162(6):1242-56.

Kozako T, Yoshimitsu M, Fujiwara H, Masamoto I, Horai S, White Y, Akimoto M, Suzuki S, Matsushita K, Uozumi K, Tei C, Arima N. PD-1/PD-L1 expression in human T-cell leukemia virus type 1 carriers and adult T-cell leukemia/lymphoma patients. *Leukemia.* 2009 Feb;23(2):375-82.

Kozdruń W, Styś-Fijoł N, Czekaj H, Piekarska K, Niczyporuk JS, Stolarek A. Occurrence of Marek's disease in poland on the basis of diagnostic examination in 2015-2018. *J Vet Res*. 2020 Dec 1;64(4):503-07.

Kumar P, Dong H, Lenihan D, Gaddamanugu S, Katneni U, Shaikh S, Tavlarides-Hontz P, Reddy SM, Peters W, Parcells MS. Selection of a recombinant Marek's disease virus in vivo through expression of the Marek's EcoRI-Q (Meq)-encoded oncoprotein: characterization of an rMd5-based mutant expressing the Meq of strain RB-1B. *Avian Dis*. 2012 Jun;56(2):328-40.

Kurokawa A, Yamamoto Y. Development of monoclonal antibodies specific to Marek disease virus-*Eco*RI-Q (Meq) for the immunohistochemical diagnosis of Marek disease using formalin-fixed, paraffin-embedded samples. *J Vet Diagn Invest*. 2022 May;34(3):458-64.

Lee SM, Oh H. Association of PD-L1 positivity with Epstein Barr virus infection and microsatellite instability in gastric carcinomas with lymphoid stroma. *Sci Rep*. 2024 Dec 28;14(1):30932.

Lee SI, Takagi M, Ohashi K, Sugimoto C, Onuma M. Difference in the meq gene between oncogenic and attenuated strains of Marek's disease virus serotype 1. *J Vet Med* Sci. 2000a Mar;62(3):287-92.

Lee LF, Wu P, Sui D, Ren D, Kamil J, Kung HJ, Witter RL. The complete unique long sequence and the overall genomic organization of the GA strain of Marek's disease virus. *Proc Natl Acad Sci U S A*. 2000b May 23;97(11):6091-6.

Levitskaya J, Sharipo A, Leonchiks A, Ciechanover A, Masucci MG. Inhibition of ubiquitin/proteasome-dependent protein degradation by the Gly-Ala repeat domain of the Epstein-Barr virus nuclear antigen 1. *Proc Natl Acad Sci U S A.* 1997 Nov 11;94(23):12616-21.

Levy AM, Gilad O, Xia L, Izumiya Y, Choi J, Tsalenko A, Yakhini Z, Witter R, Lee L, Cardona CJ, Kung HJ. Marek's disease virus Meq transforms chicken cells via the v-Jun transcriptional cascade: a converging transforming pathway for avian oncoviruses. *Proc Natl Acad Sci U S A*. 2005 Oct 11;102(41):14831-6.

Levy AM, Izumiya Y, Brunovskis P, Xia L, Parcells MS, Reddy SM, Lee L, Chen HW, Kung HJ. Characterization of the chromosomal binding sites and dimerization partners of the viral oncoprotein Meq in Marek's disease virus-transformed T cells. *J Virol*. 2003 Dec;77(23):12841-51.

Li S, Yang J, Zhu Y, Ji X, Wang K, Jiang S, Luo J, Wang H, Zheng W, Chen N, Ye J, Meurens F, Zhu J. Chicken DNA sensing cGAS-STING signal pathway mediates broad spectrum antiviral functions. *Vaccines (Basel).* 2020 Jul 9;8(3):369.

Liu JL, Kung HJ. Marek's disease herpesvirus transforming protein MEQ: a c-Jun analogue with an alternative life style. *Virus Genes*. 2000;21(1-2):51-64.

Liu JL, Lee LF, Ye Y, Qian Z, Kung HJ. Nucleolar and nuclear localization properties of a herpesvirus bZIP oncoprotein, MEQ. *J Virol*. 1997 Apr;71(4):3188-96.

Liu JL, Teng M, Zheng LP, Zhu FX, Ma SX, Li LY, Zhang ZH, Chai SJ, Yao Y, Luo J. Emerging hypervirulent Marek's disease virus variants significantly overcome protection conferred by commercial vaccines. *Viruses*. 2023 Jun 25;15(7):1434.

Lupiani B, Lee LF, Cui X, Gimeno I, Anderson A, Morgan RW, Silva RF, Witter RL, Kung HJ, Reddy SM. Marek's disease virus-encoded Meq gene is involved in transformation of lymphocytes but is dispensable for replication. *Proc Natl Acad Sci U S A.* 2004 Aug 10;101(32):11815-20.

Maekawa N, Konnai S, Okagawa T, Nishimori A, Ikebuchi R, Izumi Y, Takagi S, Kagawa Y, Nakajima C, Suzuki Y, Kato Y, Murata S, Ohashi K. Immunohistochemical analysis of PD-L1 expression in canine malignant cancers and PD-1 expression on lymphocytes in canine oral melanoma. *PLoS One*. 2016 Jun 8;11(6):e0157176.

Marek, J. Multiple Nervenentzündung (Polyneuritis) *bei Hühnern. Dtsch. Tierärztl. Wochenschr*. 1907, 15, 417–21.

Markowski-Grimsrud CJ, Schat KA. Cytotoxic T lymphocyte responses to Marek's disease herpesvirus-encoded glycoproteins. *Vet Immunol Immunopathol.* 2002 Dec;90(3-4):133-44.

Matsuyama-Kato A, Boodhoo N, Raj S, Abdul-Careem MF, Plattner BL, Behboudi S, Sharif S. The tumor microenvironment generated by Marek's disease virus suppresses interferon-gamma-producing gamma delta T cells. *Vet Microbiol*. 2023a Oct;285:109874.

Matsuyama-Kato A, Iseki H, Boodhoo N, Bavananthasivam J, Alqazlan N, Abdul-Careem MF, Plattner BL, Behboudi S, Sharif S. Phenotypic characterization of gamma delta (γδ) T cells in chickens infected with or vaccinated against Marek's disease virus. *Virology*. 2022 Mar;568:115-25.

Matsuyama-Kato A, Murata S, Isezaki M, Kano R, Takasaki S, Ichii O, Konnai S, Ohashi K. Molecular characterization of immunoinhibitory factors PD-1/PD-L1 in chickens infected with Marek's disease virus. *Virol J.* 2012 May 21;9:94.

Matsuyama-Kato A, Shojadoost B, Boodhoo N, Raj S, Alizadeh M, Fazel F, Fletcher C, Zheng J, Gupta B, Abdul-Careem MF, Plattner BL, Behboudi S, Sharif S. Activated chicken gamma delta T cells are involved in protective immunity against Marek's disease. *Viruses.* 2023b Jan 19;15(2):285.

Meijerink N, van Haarlem DA, Velkers FC, Stegeman AJ, Rutten VPMG, Jansen CA. Analysis of chicken intestinal natural killer cells, a major IEL subset during embryonic and early life. *Dev Comp Immunol.* 2021 Jan;114:103857.

Mescolini G, Lupini C, Felice V, Guerrini A, Silveira F, Cecchinato M, Catelli E. Molecular characterization of the meq gene of Marek's disease viruses detected in unvaccinated backyard chickens reveals the circulation of low- and high-virulence strains. *Poult Sci.* 2019 Aug 1;98(8):3130-37.

Morimura T, Ohashi K, Kon Y, Hattori M, Sugimoto C, Onuma M. Apoptosis and CD8-down-regulation in the thymus of chickens infected with Marek's disease virus. *Arch Virol.* 1996;141(11):2243-9.

Motai Y, Murata S, Sato J, Nishi A, Maekawa N, Okagawa T, Konnai S, Ohashi K. Characterization of a very short Meq protein isoform in a Marek's disease virus strain in Japan. *Vet Sci.* 2024 Jan 20;11(1):43.

Murata S, Hashiguchi T, Hayashi Y, Yamamoto Y, Matsuyama-Kato A, Takasaki S, Isezaki M, Onuma M, Konnai S, Ohashi K. Characterization of Meq proteins from field isolates of Marek's disease virus in Japan. *Infect Genet Evol.* 2013 Jun;16:137-43.

Murata S, Okada T, Kano R, Hayashi Y, Hashiguchi T, Onuma M, Konnai S, Ohashi K. Analysis of transcriptional activities of the Meq proteins present in highly virulent Marek's disease virus strains, RB1B and Md5. *Virus Genes.* 2011 Aug;43(1):66-71.

Murata S, Yamamoto E, Sakashita N, Maekawa N, Okagawa T, Konnai S, Ohashi K. Research Note: Characterization of S-Meq containing the deletion in Meq protein's transactivation domain in a Marek's disease virus strain in Japan. *Poult Sci.* 2021 Nov;100(11):101461.

Mwangi WN, Smith LP, Baigent SJ, Beal RK, Nair V, Smith AL. Clonal structure of rapid-onset MDV-driven CD4+ lymphomas and responding CD8+ T cells. *PLoS Pathog*. 2011 May;7(5):e1001337.

Nair V. Latency and tumorigenesis in Marek's disease. *Avian Dis*. 2013 Jun;57(2 Suppl):360-5.

Okada T, Takagi M, Murata S, Onuma M, Ohashi K. Identification and characterization of a novel spliced form of the meq transcript in lymphoblastoid cell lines derived from Marek's disease tumours. *J Gen Virol*. 2007 Aug;88(Pt 8):2111-20.

Park HJ, Park JS, Jeong YH, Son J, Ban YH, Lee BH, Chen L, Chang J, Chung DH, Choi I, Ha SJ. PD-1 upregulated on regulatory T cells during chronic virus infection enhances the suppression of CD8+ T cell immune response via the interaction with PD-L1 expressed on CD8+ T cells. *J Immunol.* 2015 Jun 15;194(12):5801-11.

Parvizi P, Andrzejewski K, Read LR, Behboudi S, Sharif S. Expression profiling of genes associated with regulatory functions of T-cell subsets in Marek's disease virus-infected chickens. *Avian Pathol.* 2010 Oct;39(5):367-73.

Patria JN, Jwander L, Mbachu I, Parcells L, Ladman B, Trimpert J, Kaufer BB, Tavlarides-Hontz P, Parcells MS. The *Meq* genes of Nigerian Marek's disease virus (MDV) field isolates contain mutations common to both European and US high virulence strains. *Viruses*. 2024 Dec 31;17(1):56.

Perumbakkam S, Hunt HD, Cheng HH. Differences in CD8αα and cecal microbiome community during proliferation and late cytolytic phases of Marek's disease virus infection are associated with genetic resistance to Marek's disease. *FEMS Microbiol Ecol.* 2016 Dec;92(12):fiw188.

Qian Z, Brunovskis P, Rauscher F 3rd, Lee L, Kung HJ. Transactivation activity of Meq, a Marek's disease herpesvirus bZIP protein persistently expressed in latently infected transformed T cells. *J Virol*. 1995 Jul;69(7):4037-44.

Raimondi G, Shufesky WJ, Tokita D, Morelli AE, Thomson AW. Regulated compartmentalization of programmed cell death-1 discriminates CD4+CD25+ resting regulatory T cells from activated T cells. *J Immunol.* 2006 Mar 1;176(5):2808-16.

Read AF, Baigent SJ, Powers C, Kgosana LB, Blackwell L, Smith LP, Kennedy DA, Walkden-Brown SW, Nair VK. Imperfect vaccination can enhance the transmission of highly virulent pathogens. *PLoS Biol.* 2015 Jul 27;13(7):e1002198.

Renz KG, Cooke J, Clarke N, Cheetham BF, Hussain Z, Fakhrul Islam AF, Tannock GA, Walkden-Brown SW. Pathotyping of Australian isolates of Marek's disease virus and association of pathogenicity with meq gene polymorphism. *Avian Pathol*. 2012;41(2):161-76.

Rispens BH, van Vloten H, Mastenbroek N, Maas JL, Schat KA. Control of Marek's disease in the Netherlands. II. Field trials on vaccination with an avirulent strain (CVI 988) of Marek's disease virus. *Avian Dis*. 1972 Apr;16(1):126-38.

Sabsabi MA, Kheimar A, You Y, von La Roche D, Härtle S, Göbel TW, von Heyl T, Schusser B, Kaufer BB. Unraveling the role of γδ T cells in the pathogenesis of an oncogenic avian herpesvirus. *mBio*. 2024 Aug 14;15(8):e0031524.

Sato J, Murata S, Yang Z, Kaufer BB, Fujisawa S, Seo H, Maekawa N, Okagawa T, Konnai S, Osterrieder N, Parcells MS, Ohashi K. Effect of insertion and deletion in the Meq protein encoded by highly oncogenic Marek's disease virus on transactivation activity and virulence. *Viruses*. 2022 Feb 14;14(2):382.

Schat KA. History of the first-generation Marek's disease vaccines: The science and little-known facts. *Avian Dis*. 2016 Dec;60(4):715-24.

Shamblin CE, Greene N, Arumugaswami V, Dienglewicz RL, Parcells MS. Comparative analysis of Marek's disease virus (MDV) glycoprotein-, lytic antigen pp38- and transformation antigen Meq-encoding genes: association of meq mutations with MDVs of high virulence. *Vet Microbiol.* 2004 Sep 8;102(3-4):147-67.

Sharma JM, Witter RL, Coulson BD. Development of cell-mediated immunity to Marek's disease tumor cells in chickens inoculated with Marek's disease vaccines. *J Natl Cancer Inst.* 1978 Nov;61(5):1273-80.

Spatz SJ, Petherbridge L, Zhao Y, Nair V. Comparative full-length sequence analysis of oncogenic and vaccine (Rispens) strains of Marek's disease virus. *J Gen Virol.* 2007 Apr;88(Pt 4):1080-96.

Srivastava R, Dervillez X, Khan AA, Chentoufi AA, Chilukuri S, Shukr N, Fazli Y, Ong NN, Afifi RE, Osorio N, Geertsema R, Nesburn AB, Wechsler SL, BenMohamed L. The herpes simplex virus latency-associated transcript gene is associated with a broader repertoire of virus-specific exhausted CD8+ T cells retained within the trigeminal ganglia of latently infected HLA transgenic rabbits. *J Virol*. 2016 Mar 28;90(8):3913-28.

Teng M, Zheng LP, Li HZ, Ma SM, Zhu ZJ, Chai SJ, Yao Y, Nair V, Zhang GP, Luo J. Pathogenicity and pathotype analysis of Henan isolates of Marek's disease virus reveal long-term circulation of highly virulent MDV variant in China. *Viruses.* 2022 Jul 27;14(8):1651.

Tischer BK, von Einem J, Kaufer B, Osterrieder N. Two-step red-mediated recombination for versatile high-efficiency markerless DNA manipulation in Escherichia coli. *Biotechniques.* 2006 Feb;40(2):191-7.

Tischer BK, Kaufer BB. Viral bacterial artificial chromosomes: generation, mutagenesis, and removal of mini-F sequences. *J Biomed Biotechnol.* 2012;2012:472537.

Trimpert J, Groenke N, Jenckel M, He S, Kunec D, Szpara ML, Spatz SJ, Osterrieder N, McMahon DP. A phylogenomic analysis of Marek's disease virus reveals independent paths to virulence in Eurasia and North America. *Evol Appl.* 2017 Sep 3;10(10):1091-101.

Tulman ER, Afonso CL, Lu Z, Zsak L, Rock DL, Kutish GF. The genome of a very virulent Marek's disease virus. *J Virol*. 2000 Sep;74(17):7980-8.

Umthong S, Dunn JR, Cheng HH. Depletion of CD8αβ^{+} T cells in chickens demonstrates their involvement in protective immunity towards Marek's disease with respect to tumor incidence and vaccinal protection. *Vaccines (Basel).* 2020 Sep 24;8(4):557.

Vychodil T, Conradie AM, Trimpert J, Aswad A, Bertzbach LD, Kaufer BB. Marek's disease virus requires both copies of the inverted repeat regions for efficient *in vivo* replication and pathogenesis. *J Virol.* 2021 Jan 13;95(3):e01256-20.

Wajid SJ, Katz ME, Renz KG, Walkden-Brown SW. Prevalence of Marek's disease virus in different chicken populations in Iraq and indicative virulence based on sequence variation in the ecoRI-q (meq) gene. *Avian Dis.* 2013 Jun;57(2 Suppl):562-8.

Wajid SJ, Walkden-Brown SW, Vanselow BA, Islam AF, Renz KG. *In vivo* characterisation of two Australian isolates of Marek's disease virus including pathology, viral load and neuropathotyping based on clinical signs. *Aust Vet J.* 2015 Jul;93(7):240-7.

Wannaratana S, Prakairungnamthip D, Tunterak W, Charoenvisal N, Limpavithayakul K, Areeraksakul P, Sasipreeyajan J, Thontiravong A. Pathogenicity and transmissibility of Marek's disease virus isolated from chickens in Thailand. *Poult Sci.* 2025 Jul 3;104(10):105519.

Wannaratana S, Tunterak W, Prakairungnamthip D, Sasipreeyajan J, Thontiravong A. Genetic characterization of Marek's disease virus in chickens in Thailand reveals a high genetic diversity of circulating strains. *Transbound Emerg Dis.* 2022 Nov;69(6):3771-79.

Witter RL, Calnek BW, Buscaglia C, Gimeno IM, Schat KA. Classification of Marek's disease viruses according to pathotype: philosophy and methodology. *Avian Pathol.* 2005 Apr;34(2):75-90.

Yamagami S, Sato J, Motai Y, Maekawa N, Okagawa T, Konnai S, Ohashi K, Murata S. Genomic characteristics and distinctive genetic polymorphisms of Marek's disease virus strains circulating in Japan. *J Vet Med Sci.* 2025 May 15;87(5):517-31.

Yu ZH, Teng M, Luo J, Wang XW, Ding K, Yu LL, Su JW, Chi JQ, Zhao P, Hu B, Zhang GP, Liu JX. Molecular characteristics and evolutionary analysis of field Marek's disease virus prevalent in vaccinated chicken flocks in recent years in China. *Virus Genes*. 2013 Oct;47(2):282-91.

Zhuang X, Zou H, Shi H, Shao H, Ye J, Miao J, Wu G, Qin A. Outbreak of Marek's disease in a vaccinated broiler breeding flock during its peak egg-laying period in China. *BMC Vet Res*. 2015 Jul 23;11:157.

SUMMARY IN JAPANESE

和文要旨

マレック病ウイルス（Marek's disease virus, MDV）は、悪性リンパ腫、免疫抑制、脚麻痺や斜頸などの神経症状を特徴とするマレック病（MD）を引き起こす。弱毒化生ワクチンの開発・普及により、MD の発生は制御されてきたが、野外株の病原性増強に伴い、近年ワクチン接種鶏における MD の発症例 (ワクチンブレイク) が世界各地で報告されている。MDV のオンコプロテインである Meq は、$CD4^+$ T 細胞の形質転換に必須であり、病原性に応じて多型や挿入／欠失配列を有することが知られている。実際に、実験感染により Meq のアミノ酸多型が病原性に変化させることが示された。しかし、その詳細な分子機構や関与するアミノ酸残基については十分に解明されていない。そこで本研究では、Meq のアミノ酸配列と MDV の病原性との関係を解析し、病態形成に関与する分子機構を明らかにすることを目的とした。

第 I 章では、Meq の転写活性化調節領域内の挿入配列が病原性を増強する分子機構を解析した。挿入配列が、Meq タンパク質の安定性を向上させ、さらに、レポーターアッセイにより、MDV の腫瘍化に関連するプロモーター活性を増強することを明らかにした。RB-1B 株由来の L-Meq を持つ組換え MDV（rRB-1B_L-Meq）を使った感染試験では、MDV の腫瘍細胞と同じ表現型である mTGF-β 発現 $CD4^+$T 細胞の早期増殖が観察され、腫瘍形成の加速が示唆された。一方で、フローサイトメトリー解析では、腫瘍内の細胞構成に顕著な差は認められず、さらに RNA-sequencing 解析でも腫瘍組織のトランスクリプトームが強い正の相関が示唆された。これらの結果から、挿入配列は転写標的を変化させず、Meq の安定性と転写活性化能を向上させることで腫瘍形成を促進させることが示唆された。

第 II 章では、Meq の塩基性領域のアミノ酸多型に着目し、ワクチン株 CVI988 に認められる 71 番目と 77 番目のアミノ酸多型の組み合わせ（Meq71/77）、および近年のアジア、アフリカ、ヨーロッパ分離株に共通する 77 番目と 80 番目の組み合わせ（Meq77/80）を解析した。レポーターアッセイでは、これらの塩基性領域に認められるアミノ酸置換が、Meq の転写調節能を低下させることが確認された。さらに、これらの配列を導入した組換え MDV（rRB-1B_Meq71/77、rRB-1B_Meq77/80）を用いた感染実験において、rRB-1B_Meq71/77 感染鶏では MD の発症や Meq 陽性細胞の増殖が観察されず、さらに病理学的検査においても MD の発生を示す所見は認められなかった。一方、rRB-1B_Meq77/80 感染では死亡率および腫瘍発生率が低下したものの、開口呼吸などの RB-1B-Meq を持つ組換え

MDV とは異なる症状を呈し、病理学的解析により気管支関連リンパ組織の過形成が認められた。これらの結果から、塩基性領域における 2 つのアミノ酸配列の組み合わせにより、Meq の転写調節能や MDV の病原性が変化し、さらには病態の表現型にも影響を及ぼす可能性が示された。

第 III 章では、上述の感染実験の病態後期に観察された $CD8^+$ T 細胞および gamma-delta (γδ) T 細胞の減少への PD-1/PD-L1 経路による免疫抑制の関与を検討した。MD 発症鶏の脾臓および腫瘍組織内で、$CD4^+$、$CD8^+$、γδ T 細胞いずれにおいても PD-1 陽性細胞の割合が増加していた。特に $CD4^+$ T 細胞では Meq 陽性細胞で PD-1 発現が高かった。PD-1 陽性 $CD8^+$ T 細胞では IFN-γ 産生能の亢進が認められなかった。腫瘍組織由来の γδ T 細胞では刺激培養後も IFN-γ 産生上昇が観察されなかった。さらに、非感染鶏の脾臓由来の γδ T 細胞では PD-1 陰性細胞に比べ、PD-1 陽性細胞に IFN-γ が高発現していたが、MD 発症鶏の脾臓由来の γδ T 細胞では、PD-1 陽性および陰性細胞間における IFN-γ 産生の差が認められなかった。これらの結果は、PD-1 陽性 T 細胞の機能不全による MD の病態後期の免疫抑制への関与を示唆している。

本研究は Meq の転写活性化調節領域における挿入配列がタンパク質安定性と転写活性化能を増強し MDV の病原性を高めること、塩基性領域のアミノ酸多型が病原性や病態を変化させること、さらに PD-1/PD-L1 経路が MDV の免疫抑制に関与することを明らかにした。これらの成果は、MDV の病原性進化や免疫回避機構に関する理解を深め、将来的な高病原性株の出現予測や、より効果的なワクチン開発に貢献する重要な知見である。